NASA CR 129045

ANALYSIS OF FLIGHT TEST

TRANSITION AND TURBULENT HEATING DATA

PART I - BOUNDARY LAYER TRANSITION RESULTS

(NASA-CR-129045) ANALYSIS OF FLIGHT TEST TRANSITION AND TURBULENT HEATING DATA. PART 1: BOUNDARY LAYER TRANSITION RESULTS Final A. Martellucci, et al (General Electric Co.) Nov. 1972 83 p CSCL 20D G3/12

N73-12287

Unclas 48276

A. Martellucci
B. L. Maguire
R. S. Neff

DEC 1972
RECEIVED
NASA STI FACILITY
INPUT BRANCH

GENERAL ELECTRIC COMPANY
PHILADELPHIA, PA.

PRECEDING PAGE BLANK NOT FILMED

FOREWORD

The present report is one of a series of two which define the post flight evaluation of a series of ballistic flight test boundary layer transition and turbulent heating data. Part I presents the results of the boundary layer transition investigation. Part II presents the results of the turbulent heating investigation (NASA CR 130251).

These reports document the work performed under Contract No. NASW-2234, for the period June 1971 through October 1972. The investigation was conducted for National Aeronautics and Space Administration Headquarters Division with Mr. Alfred Gessow as the NASA technical monitor.

The authors wish to express their appreciation to the following General Electric Company personnel; Dr. F. Alyea, Mr. A. Birnbaum, Mr. T. Harper, Dr. C. Kyriss, and Ms. E. Storer.

The authors also wish to express their appreciation to Dr. M. Morkovin for his helpful discussion and comments pertaining to the transition data analysis and formulations.

TABLE OF CONTENTS

Section		Page
1	INTRODUCTION	1
2	GENERAL COMMENTS ON BOUNDARY LAYER TRANSITION	3
	2.1 Summary Correlations	3
	2.2 Phenomenological Correlations	3
	2.2.1 Effect of Ablation/Transpiration	4
	2.2.2 Nose Cap Bluntness	6
	2.2.3 Angle of Attack	6
3	FLIGHT DATA COMPILATION AND EVALUATION	9
	3.1 Angle of Attack	10
	3.2 Post Flight Trajectory	10
	3.3 Vehicle Geometry	10
	3.4 On-Board Sensors	11
	3.5 Redundant Transition Altitude Sensors	11
4	PERTINENT CHARACTERISTICS OF THE SELECTED VEHICLES	13
5	ANALYTIC TECHNIQUE DESCRIPTION	15
6	DATA EVALUATION PROCEDURE AND RESULTS	17
7	ATTEMPTED CORRELATIONS OF BOUNDARY LAYER TRANSITION FLIGHT TEST DATA	21
	7.1 Frustum Data and Correlations	21
	7.2 Local Properties in the Nosetip Region	23
8	IDENTIFICATION OF FUNDAMENTAL PARAMETERS AFFECTING BOUNDARY LAYER TRANSITION	27
9	CONCLUSIONS	31
10	REFERENCES	33
11	TABLES	37
12	FIGURES	59

LIST OF FIGURES

Figure		Page
1	Effect of Frustum Ablation on Transition Location	59
2	Effect of Nose Blowing on Transition Progression (N_2 Injectant)	60
3	Local Transition Reynolds Number Variation with Bluntness	61
4	Local Transition Reynolds Number Variation with Bluntness	62
5	Effect of Nose Bluntness on Transition Location	63
6	Variation of Transitional Flow Period with Path Angle	64
7	Geometric Details - Vehicle T03	65
8	Post Flight Trajectory - Vehicle T03	66
9	Angle of Attack Variation with Altitude	67
10	Boundary Layer Transition History - Vehicle T03	68
11	Computed Nose Tip Shapes During Re-entry	69
12	Measured and Predicted Ablation Histories (Sta. 55.86)	70
13	Axial Distribution of Vehicle Wall Temperature - Vehicle T03	71
14	Axial Distribution of Mass Addition Rate - Vehicle T03	72
15	Flight Data Correlation Using Frustum Parameters; R_{es} vs. M_e	73
16	Flight Data Correlation Using Frustum Parameters (R_{θ_s} vs M_e)	74
17	Effect of Unit Reynolds Number on Flight Vehicle Transition	75
18	Summary Type Correlation; $Re_{\infty D}$ vs. R_{N_0}/R_B	76
19	Flight Data Using Wall Gas Enthalpy Correlation Parameters	77
20	Flight Data Correlation Using Frustum Parameters; m_L vs. Re_s	78
21	Definition of Terminology	79
22	Flight Data Correlation Using Nose Parameters; $\bar{m}_{2R_{N'}}$ vs. $Re_{\infty R_{N'}}$	80
23	Flight Data Correlation Using Nose Parameters; $\bar{m}$ vs. Re_s @ $2R_{N'}$	81
24	Flight Data Correlation Using Nose Parameters ~ $\bar{m}_{2R_{N'}}$ vs. $\Delta S/R_{N_{eff}}$	82
25	Flight Data Correlation Using Nose Parameters ~ $\dot{m}/\dot{m}_b$ vs. $Re_{s_{2R_{N'}}}$	83
26	Flight Data Correlation Using Nose Parameters ~ $\bar{m}$ vs. R_{e_θ} @ $2R_{N'}$	84
27	Flight Data Correlation Using Nose Parameters ~ $\bar{m}_{2R_{N'}}$ vs. $\Delta S/\delta_{2R_{N'}}$	85
28	Effect of Nose Ablation on Flight Vehicle Transition	86
29	Typical Vehicle History of $\bar{m}$ vs. R_{e_s} @ $2R_{N'}$	87
30	"Flight Transition Data" - Bluntness Effect	88

LIST OF TABLES

Table		Page
1	GE-RESD Development of Re-Entry Vehicle Systems	37
2	Methods of Transition Onset Detection	38
3	Sphere-Cone R/V Transition Altitude	39
4A	Vehicle Selection - Transition Study	40
4B	Vehicle Selection - Transition Study	41
4C	Vehicle Selection - Transition Study	42
4D	Vehicle Selection - Transition Study	43
5	Comparison of Local Properties from ENSBL/VIZAAD	44
6	Free Stream Properties at Transition Altitude	45
7A	Calculated Local Flow Properties on the Frustum	47
7B	Calculated Local Flow Properties on the Frustum	49
8	Correlation Attempts Based on Frustum Conditions	51
9A	Calculated Local Flow Properties in the Nose Region	53
9B	Calculated Local Flow Properties in the Nose Region	55
10	Correlation Attempts Based on Nose Tip Conditions	57

NOMENCLATURE

A	Area
C_p	Pressure coefficient
D	Base Diameter
H_o	Total enthalpy
h	Altitude
h_w, h_r	Enthalpy, wall and recovery, respectively
L	Length
M	Mach number
M_w	Molecular weight of injectant
$\dot{m}$	Integrated mass flow $\int (\rho v)_w \, dA_s$
$\bar{\dot{m}}$	Normalized mass ratio $\dot{m}/(\rho u)_\infty A_{ref}$
P	Pressure
$\dot{q}$	Heat transfer rate
R	Body radius
R_N	Nose radius
R_{N_o}	Unablated nose radius
$R_{N_{eff}}$	Stagnation region nose radius
R_N'	Ablated nose equivalent spherical radius
R_e	Local unit Reynolds number
R_{e_∞}	Free stream unit Reynolds number
S	Wetted length
ΔS	Incremental wetted length
S_T	Stanton number $\dot{q}/(\rho u)_\infty (H_o - h_w)$
T	Temperature

NOMENCLATURE (Continued)

u_e	Local edge velocity
U	Velocity
v_w	Injectant velocity, normal to wall
x	axial coordinate
α	angle of attack
γ_E	re-entry path angle from horizontal
δ	boundary layer thickness
δ^*	boundary layer displacement thickness
θ	boundary layer momentum thickness
θ_c	cone half angle
λ_∞	$(\rho v)_w / (\rho u)_\infty$
λ	$\bar{m}\,(M_{w_{air}}/M_{w_{inj}})^K$ where K is any number
μ	viscosity
ρ	density
ϕ	meridian angle

SUBSCRIPTS

B	base
e	conditions at boundary layer edge
E	conditions at re-entry ($h \approx 75 - 90$ km)
L	properties at length $x = L$
$2R_N'$	properties at length $x = 2R_N'$
S	wetted length
T_r	properties at the transition onset point
w	properties at wall
ref	reference properties (see Figure 21)
∞	free stream conditions
b.l.	boundary layer

ACRONYMS

HEAT SHIELD MATERIALS

ATJ, (ATJ-S) - Graphite (Union Carbide)

BE - beryllium

CC - carbon-carbon

CP - carbon-phenolic

G - graphite

PG - phenolic-graphite

PR - phenolic refrasil

PYRO G - pyrolytic graphite

SP - silica-phenolic

QP - quartz phenolic

3DQP - 3-D quartz phenolic

TFE - Teflon

PROGRAMS

ABLE - Ablating Boundary Layer Equilibrium program

ENSBL - Equilibrium Non-Similar Boundary Layer program

FLOWFIELD - Method of Characteristics program

REKAP - REaction Kinetics Ablation Program

RESEP II - Transient Nose Shape Change Program

VIZAAD - Viscous Interaction Zero Angle-of-Attack Drag program

SECTION 1

INTRODUCTION

One of the most important considerations in the optimization of re-entry vehicle design is the application of a realistic criterion for transition from laminar to turbulent boundary layer flows. For example, the thickness of the thermal protection system, and in fact, the selection of the surface materials, are strongly dependent upon the transition altitude and the time the vehicle is exposed to transitional-turbulent heating. Also, trajectory optimization of a vehicle system is sensitive to such phenomena as nose tip transition effects on nose shape change, heat shield surface ablation anomalies, and the induced pressure and shear stress due to transition progression over the surface. Obviously, improved vehicle performance and/or lighter vehicle weights could be achieved if a more accurate transition altitude could be determined. Clearly, this requires that methods exist within the aerospace community to accurately predict the transition altitude for future civilian and military re-entry systems.

The transition process can be characterized by a series of stages, beginning in the fully laminar boundary layer. The process is initiated by the onset of instabilities or waves, which is followed by the occurrence of intermittent turbulent eddies and an increase of intermittency until the turbulent eddies appear continuous. An increase in the turbulent intensity is followed by a decrease in the intensity, and, finally, the attainment of fully-developed turbulence, in which the turbulence intensity is essentially constant with increasing Reynolds number. The complexity of this fluid dynamic process has, to date, precluded the development of definitive analytical models to describe this phenomena or to predict the location of transition for re-entry vehicles[1].

Since analytic techniques for predicting the location of boundary layer transition are not available, vehicle designers must rely upon correlations of flight test data for the prediction of the altitude where boundary layer transition is to occur. The data correlations can generally be divided into two categories, one based on aerodynamic parameters related to free stream conditions and initial geometries[2] (here referred to as "Summary Correlations"), and the other related to the local fluid properties which exist at the boundary layer edge, at the transition point[3,4,5,6] (here referred to as "Phenomenological Correlations"). This latter approach should consider the actual vehicle geometry at transition onset and presupposes that accurate analytic techniques are available for local property prediction. In previous studies no accounting has been made for vehicle geometric changes due to ablation or for the influence of the ablative products on the boundary layer properties.

This report presents the results of an investigation wherein a consistent and accurate re-evaluation has been conducted of the vast body of Air Force sponsored ballistic flight test boundary layer transition data. Prior to the initiation of this study, the

data had not been scrutinized in detail, on a post flight basis, to properly account for: (1) design versus the actual vehicle trajectory, (2) nose shape change, (3) vehicle attitude at transition onset, (4) the ablation mass addition history, (5) the accuracy of the reported transition altitudes, etc., and their collected effects on the local properties. The current study attempted to account for these effects and to accurately establish a set of fifty-five (55) data points which have been correlated to provide design guidelines for future analytical and experimental studies.

The flight test programs from which these data were obtained are, in general, classified. Specific information pertaining to details and the identification of the vehicles selected for this study are contained in a classified addendum to this report*. Also contained are detailed listings of the computer inputs necessary to define the local properties at the transition altitude for each vehicle.

---

*General Electric Co. TIS 72SD253, December, 1972.
Requests for copies of this addendum must be approved by AF/SAMSO, El Segundo, Calif.

SECTION 2

GENERAL COMMENTS ON BOUNDARY LAYER TRANSITION

Explicit analytic methods suitable for predicting the occurrence of boundary layer transition and the properties of the flow while it is transiting from a laminar to a turbulent state have eluded the fluid dynamicist since transition was "discovered". As a consequence, the approaches currently employed by vehicle designers for the transition altitude are generally based on flight test empirical correlations or ground test observations. These correlations can be divided into two broad classes, one based on the macroscopic behavior of vehicles, which will be termed "Summary Correlations," the second based upon detailed flow properties at the transition point and the flow history to this point. These latter correlations are termed "Phenomenological Correlations." Some comments concerning each of these types of correlations follow.

2.1 SUMMARY CORRELATIONS

The summary correlations are usually generated for equivalent classes of vehicles which have similar heat shield materials, nose radii, cone angles, etc. An example of a correlation of this type was presented recently by McCauley[2]. In this approach, flight data are correlated using free stream and preflight shape parameters. The data are grouped into classes by the heat shield, the cone angle, and the vehicle's initial nose radius as parameters. If a reasonable set of information from "similar" vehicles exist, then a design correlation can be formulated from these data which could "accurately" be used for flight predictions within the range of the prior data. The shortcomings of these correlations arise when vehicles are designed and flown for heat shield materials for which no data exist, or when the geometry parameters (cone angle, nose radius, and shape) are such that extrapolations are required. Although there is a place for these correlations to aid in vehicle design, fundamental studies dealing with the details of the phenomena are required for future vehicle systems.

2.2 PHENOMENOLOGICAL CORRELATIONS

Phenomenological correlations are those that are based on flight or ground test data and are involved with local flow parameters. Many correlations of this type have been developed and virtually each aerospace concern has its own favorite[3,5,6]; however, it can safely be said that, when sufficient flights are included, data exist that will violate each current correlation. This indicates that all the parameters that affect transition are not known for each flight test point, and/or the existing correlations may not contain some important parameters which affect transition.

To remedy this situation, a large number of ground based investigations have been performed over the past several years; each to establish the influence of some particular parameters on the onset and propagation of transition or on local flow properties. Although, in general, one does not get quantitative agreement between flight test transition data and ground test, the ground test studies are extremely useful in establishing trends and a basic understanding of the problem. The following comments are provided to indicate, based on these ground test results, how various phenomena — heat shield and nose tip ablation, nose bluntness, angle of attack — influence the location of transition. These observations coupled with the flight data analyses performed in this study have lead to a re-orientation of our thinking about the transition phenomena and the myriad of phenomenological correlations which depend upon the definition of local properties on the conical frustum. As will become evident in this report, and as one expects, the occurrence of transition near the end of the conical frustum is dependent upon disturbances generated near the nose tip and, thus, cannot be adequately correlated by local properties on the frustum, at the transition station.

2.2.1 EFFECT OF ABLATION/TRANSPIRATION

2.2.1.1 Frustum Ablation

Virtually all of the high performance ballistic re-entry vehicles have an ablating heat shield and/or an ablating nose. Various heat shield materials have been flown which range from the low temperature ablators, like Teflon and the epoxies, which emit rather large quantities of mass into the boundary layer, to the high temperature ablators, of the carbon class, which emit relatively small quantities of mass. In the determination of the local properties on the vehicle, the resultant vehicle shape change and the mass added into the boundary layer must be accounted for. The induced viscous effects due to the addition of the ablative products in the boundary layer is a subject that has been analyzed and reported by Fannelop[7], Mann[8], and Hayasi[9]. Many of the phenomenological correlations have not accounted for the effects of mass addition on the local properties, which could be important to the basic understanding of the problem.

It is of interest to note that recent ground test data[10] have shown that ablation from the frustum (simulated by injection) apparently does not have a first order effect on frustum transition. Shown in Figure 1 are heat transfer data obtained on a 5° half angle cone at Mach 8 for three values of the mass injection parameter (which was uniform over the porous elements). One will note that frustum ablation did not affect the location and extent of the transition zone on the model, to first order. It should also be noted that these mass injection rates bracket those encountered in flight for current heat shield materials. The relevance of these data to the ultimate transition correlation developed are discussed in Section 8.

Another facet of the effects of ablation is the surface roughness resulting during reentry. Each heat shield material has its own peculiar characteristics in this accord. Materials such as Teflon, which sublimes, maintain a relatively smooth surface. The carbons, which char, generally maintain a degree of smoothness although the char possesses some small roughness. On the other hand, materials such as the 3-D quartz phenolics could develop a rough surface. If this material is on the nose, where the boundary layers are thin, one would expect to see this roughness influence the transition altitude. However, on the frustum, the thickening boundary layers tend to alleviate the problem somewhat. Thus, one should weigh these data carefully in comparison to non-ablating, Teflon, or carbon heat shields. If one is trying to investigate the influence of roughness on transition in ground test facilities, care must be exercised in the simulation since the normal injection velocities associated with the ablating process tend to reduce the effect of the roughness on the fluid mechanical properties.

One last item of importance pertaining to the effects of ablation on transition measurements is the evaluation of the "wall properties." The enthalpy of the gaseous mixture adjacent to the wall is strongly affected by the gases emitted into the boundary layer during ablation. For correlations concerned with the gas enthalpy adjacent to the wall, the chemistry of the ablative products must be considered and not the pure air enthalpy that would result from the wall temperature.

2.2.1.2 Nose Tip Ablation/Transpiration

The use of a transpiration cooled nose or an ablating nose configuration is a subject that has received considerable attention over the past decade. There have been several studies conducted for both ground and flight tests, where the influence of a nose transpirant on the onset and propagation of downstream transition have been investigated. It has been shown by Dunavant and Everhart[11] and by Martellucci and Laganelli[12] in ground test studies that the injection of a gaseous transpirant (Nitrogen) from the nose cap destabilizes the boundary layer on the frustum. The injection of helium was found to stabilize the frustum boundary layer. Furthermore, the effect of the transpirant on transition is more pronounced at zero or small angle of attack than at larger angles of attack ($\alpha \rightarrow \theta_C$), due to cross flow. Shown in Figure 2 are the transition results measured at AEDC by Martellucci and Laganelli[12] for a 4° half angle cone. Although a transpiring system was used in these tests, it also can be considered to be simulating ablation from the nose. It is evident that blowing or ablation from the nose, which implies the introduction of a disturbance element, clearly affects transition. Therefore, in transition data correlations, mass injection from the nose must be considered a fundamental parameter, independent of whether the mass was transpired or ablated into the boundary layer.

2.2.2 NOSE CAP BLUNTNESS

The effect of spherical nose bluntness on boundary layer transition has been delineated by Stetson and Rushton[13] and Softley[14], Figures 3 and 4, respectively. These investigations have differentiated between "small" and "large" bluntness transition regimes including a bluntness reversal effect, wherein increasing R_N from the sharp case caused the transition location to move aft, until further increases in R_N moved transition forward toward the nose. Recently obtained data at Mach 8 on a 5° cone[10], corroborated these trends, wherein slight changes in the nose radius had a first order effect on the transition location, Figure 5. This contrasts with the negligible effect of frustum ablation on transition location which was measured for this same model, Figure 1.

That these regimes are germane to re-entry vehicle boundary layer transition development has been demonstrated by the NASA flown Re-entry F vehicle. Re-entry F was a 5° half-angle, 13-foot long sphere cone with a 0.1-inch radius ATJ-S nose cap and a beryllium frustum. Flight test transition data have recently been finalized for this experiment by Wright and Zoby[15]. The previously discussed "bluntness reversal" effect noted in ground experiments was also evident in the flight data ($M_\infty = 20$), thus lending credence to this bluntness concept. It is thus important to recognize this "bluntness" effect in the evaluation of ground and flight test transition data for purposes of transition correlation development.

Another facet of the effects of nose bluntness on flight test transition correlation development is the influence of laminar nose blunting on local properties. During re-entry, not only does the nose of the vehicle recede but in addition, the shape changes. The significance of this effect varies, depending upon the trajectory flown, the nose material selected, and the initial bluntness of the vehicle. For vehicles with bluntness ratios of $R_N/R_B \approx 0.04 \rightarrow 0.20$, the nose shape has a marked effect on the local properties which must be accounted for in phenomenological correlations.

2.2.3 ANGLE OF ATTACK

The influence of angle of attack on the location and shape of a transition front has been established in numerous ground test programs[13,16-19]. Because of the paucity of detailed 3-D flight data, it is difficult to determine the sensitivity of the transition front and progression to angle of attack effects. At best, one can only establish whether the transition location is forward on the lee or windward side.

Ground test results have shown that the transition front is strongly distorted at small angles of attack[13,16] (i.e., $\alpha \approx 1\text{-}2°$). Generally, the transition location moves forward on the leeward side and slightly aft on the windward ray. In addition, the coupling of bluntness with angle of attack further distorts the transition front shape. An example of the sensitivity of the transition front shape to bluntness and angle of

3

attack, as presented in Reference 12, may be found in Figure 2. The rather extreme sensitivity for small α is evident from this figure.

To obtain the maximum usability from flight data, it is desirable to analyze a flight vehicle at several altitudes as the transition front is moving forward over the various sensors. However, because of the dynamic loads associated with the traversal of this moving front, re-entry vehicles generally experience a momentary divergence in angle of attack. This will occur even though the angle of attack at transition onset at the vehicle base may be small. Furthermore this divergence will occur on vehicles with non-ablative and ablative heat shields. Available data indicate that the magnitude of the divergence tends to be related to the magnitude with which the heat shield ablates. Because of the uncertain quantitative influence of angle of attack on transition location and local properties, transition progression for these cases would be suspect for ballistic vehicle transition correlations.

SECTION 3

FLIGHT DATA COMPILATION AND EVALUATION

The Department of Defense has sponsored a myriad of ballistic re-entry vehicle flight test programs through the various governmental agencies. Each vehicle system, and sometimes each vehicle, has specific test objectives. In order to meet these various objectives, the test vehicles are generally instrumented with on-board sensors. For many of these flights, the altitude at which the boundary layer flow transits from laminar to transitional-turbulent flow can be deduced from a variety of these sensors. It is the objective of this study to compile the data from these flights and to evaluate the boundary layer transition phenomena.

The significance of boundary layer transition in the design and in the performance of a vehicle depends upon its size, shape, and trajectory. For example, the material selection and the thickness of the heat protection system are strongly influenced by the transition altitude and the time the vehicle is exposed to the more severe transitional-turbulent flow environment (Figure 6). For the majority of the DOD flown flights, which re-enter with relatively steep path angles, the vehicles experience transitional boundary layer flows for only 2-3 seconds and turbulent flows for 15-20 seconds. Therefore, the exact altitude at which transition occurs is not generally critical to the mission design, and consequently, the transition data available from these vehicles has never been fully exploited. That is, the data exist in the raw data form but analysis of local properties to further our understanding of transition onset were never really justified. However, flights at low path angles experience transition for long time periods, and consequently, require detailed knowledge of this regime to insure an adequate heat shield design.

On the basis of this wealth of existing yet unanalyzed flight test data, the current study was undertaken. A summary of some of the major programs for sphere-cone vehicles that GE-RESD has been involved in, up through the Re-entry F program, may be found in Table 1. Through its involvement as a prime contractor in these programs, GE-RESD had on hand the Flight Evaluation Reports (FER) which document the data from each flight and also had in its files data from other aerospace contractor's flight test programs. These reports form the data base for the current study from which the phenomena which affect the flight test transition locations can be ascertained.

This literature search yielded some two hundred flight data reports. These reports were then screened for those vehicles which had transition data which met the following requirements:

(1) Small angle of attack at transition onset, that is $\alpha / \theta_c \lesssim 0.1$

(2) Post flight trajectory reconstruction

(3) Simple sphere-cone geometry; no biconics, overlays, flares, etc.

(4) On-board sensors

(5) Redundant transition altitude sensors.

From this search, fifty-five (55) vehicles were selected, forty (40) which met these criteria and fifteen (15) which departed from them in one or more areas. The significance of each of the parameters listed above will be discussed.

3.1 ANGLE OF ATTACK

As noted in Section 2.2.3, large asymmetries in the shape of the transition front occur even at small angle-of-attack (i.e., $\alpha \approx 1-2°$). Depending upon the rate with which transition traverses the vehicle surface, these α asymmetries may give rise to an error or scatter in transition correlations. Minimizing the angle of attack at transition onset to some small value, which is somewhat arbitrary (i.e., $\alpha / \theta_c \lesssim 0.1$), would tend to eliminate this source of scatter. Thus the "base line" correlations only contain data which meet this criteria. Additional data were considered which violate this criteria to establish the sensitivity of the resultant correlations to spurious angle-of-attack effects which are inherent in all flight data.

3.2 POST FLIGHT TRAJECTORY

The evaluation of the local properties at the wall and the boundary layer edge at the transition point, necessitates an accurate definition of the free stream conditions and the actual ablated geometry of the vehicle, both of which are trajectory dependent. However, as a result of anomalous booster behavior and the subsequent separation of the re-entry vehicle from the booster, the entry conditions may vary considerably from the preflight design value. From atmospheric entry until impact, the vehicle passes through an altitude range of approximately 100 km or 330,000 feet. Consequently, the density and the unit Reynolds number of the free stream through which the vehicle flies cover several orders of magnitude. The density of the free stream and the velocity of the vehicle governs the nature of the interaction of the fluid with the vehicle. This information, coupled with the re-entry path angle and angle of attack history of the vehicle, determines the wall temperature and the ablation response of the vehicle nose and heat shield and, thus, has a direct bearing on transition occurrence.

3.3 VEHICLE GEOMETRY

Flight tests have the stigma that several parameters are all varying simultaneously. One such complication arises due to the geometry of the configuration. The selection of axisymmetric configurations at zero angle of attack provides, in essence, a two-dimensional correlation that is free of cross flow influences. Furthermore, the selection of simplified geometries such as spherically blunted cones affords a correlation that is not predominately influenced by geometry as could be the case if conically flared or cone-cylinder-flare type vehicles were considered.

3.4 ON-BOARD SENSORS

For small vehicles, (like decoys), flight data generally consists of off-board measurements such as radar deduced ballistic coefficients. Other data, such as frequency of oscillation, can also be obtained from which angle of attack histories can be inferred; however, these data are less accurate and consequently less reliable. For larger vehicles, on-board measurements are made in addition to the usual radar coverage. These measurements are obtained from rate gyros, lateral and axial accelerometers, forebody and base pressure sensors, ablation rate sensors, thermal differential sensors or in-depth thermal sensors, etc. It is from these instrumented flights that the definition of the experimental test conditions can best be ascertained. Therefore, a basic requirement for the selection criteria is that the vehicle possess sufficient on-board aerothermodynamic instrumentation to reconstruct the experimental test conditions and to define transition location.

3.5 REDUNDANT TRANSITION ALTITUDE SENSORS

There are several means of detecting transition onset for both flight and ground test, as noted in Table 2. The various techniques do not measure the same point in the transitional flow process, because each instrument or technique is sensitive to a different characteristic of the flow. In fact, at any vehicle station, boundary layer transition is a gradual phenomenon and may occur over an altitude range of as much as 10 km. Beginning with fully laminar, it progresses through a series of stages, i.e., onset of instabilities or waves, occurrence of intermittent turbulent eddies, increase of intermittency until the turbulent eddies appear continuous, increase in the turbulent intensity followed by a decrease in the intensity, and, finally, the attainment of fully-developed turbulence in which the turbulent intensity is essentially constant with increasing Reynolds number. Hence, the definition of the occurrence of transition as a single discrete event must be arbitrary and be based upon identification of onset as one of the above events. As long as the criterion used is consistent and is based on a readily measured phenomenon, or its ramification on a measurable parameter, any of the above stages might be selected to define boundary layer transition. However, from a vehicle design approach, the phase of transition which coincides with some phenomenon of practical interest, such as the relatively sharp increase in the measured surface heat transfer rate, is probably the most useful criterion and was the one relied upon more heavily in the correlations to be presented in this report.

It should be noted that several of the techniques employed in flight test can only be used to detect transition onset at the base. The techniques referred to here are items 2 and 3 of Table 2. Each of these techniques measure some peculiarity which reflects the change of boundary layer state as transition occurs at the vehicle base. Furthermore, each of these techniques cannot distinguish whether the vehicle is at angle of attack, nor is its sensitivity to error due to angle of attack known. The average altitude of occurrence which results from these measurements, as noted in Table 3, can sometimes be in considerable disagreement. The measurement techniques which can

provide a more detailed measure of localized transition motion along the frustum utilize thermal or acoustic sensors. However, re-entry vehicles are generally instrumented to measure the occurrence of transition onset at the base and the available data along the frustum are somewhat sketchy. As a result, the emphasis in this study will be on transition onset near the vehicle base. If transition progression data were available which met the requirements, and if sensors in the frustum exist, these data were also considered.

SECTION 4

PERTINENT CHARACTERISTICS OF THE SELECTED VEHICLES

From the roughly two hundred vehicles that were reviewed, forty (40) were found to meet all of the criteria that were described in Section 3. This constitutes the base-line set for the correlation. These are coded by a letter with a two digit system such as BXX, CXX, etc. (see Table 4). An additional fifteen (15) vehicles were selected which have one or more factors which separate them from the base line set. These factors can include one or more of the following: (a) an angle of attack at transition onset, $\alpha/\theta_c \geq 0.1$, (b) a Teflon boot over the basic vehicle nose cone which creates a geometric abnormality, and (c) a nose material which could ablate into a roughened state. These vehicles were coded by the same letter system but with a three digit system, BXXX.

The fifty-five selected vehicles were divided into four letter categories which delineate the frustum heat shield material.* These categories are defined here as:

(1) The non-ablators with a beryllium heat shield-coded here as B.

(2) Carbon class heat shields - coded as C. These include phenolic graphite (PG), carbon phenolic (CP), and carbon-carbon (CC).

(3) Silica class heat shields - coded as S. These include phenolic refrasil (PR), silica phenolic (SP) and tapewound silica phenolic (TWSP), and tape-wound quartz phenolic (TWQP) and three dimensional quartz phenolic (3DQP).

(4) Low temperature ablators - coded as T, the Teflon materials.

Coincidentally, the ablation rate of each material class increases going from B to T, alphabetically. Of the fifty-five vehicles selected, twenty-six were flown by GE and twenty-nine were flown by other Aerospace Contractors.

Table 4 also serves to show a comparison of the chosen vehicles with those selected by McCauley[2] and Stuerke, et al[20] for use in their correlative schemes. The 37 vehicles utilized by McCauley were correlated using free stream parameters and the vehicle geometry. The results of these "summary type" correlations are useful for trend development but not for a basic understanding of the transition phenomena, such as is desired here. The 15 vehicles selected by Stuerke for his detailed evaluation and correlation overlap with the current study for only 10 of these cases. It should

*As will be shown later, it became obvious that this classification by frustum material was misleading, and a coding by the nose material would have been more appropriate.

be noted however, that in Reference 20, the nose shape was considered to be spherical in all cases (i.e., the ablated shape resulting from laminar flow ablation was not considered). Furthermore, the ablation rate from the nose was not considered. As noted in Section 2.2 this could result in significant differences in local properties, depending on the bluntness ratio.

Within each heat shield material class there are vehicles which have the same geometric characteristics; however, the nose materials differ. One such example of this is vehicle B-14 which has a SP nose ($h_{Tr} \approx 27$ KM), and B-15 which has an ATJ-S nose ($h_{Tr} \approx 16.5$ KM). It is evident from these data that the nose material apparently does affect the transition altitude. One can postulate many reasons for this, such as through its effect on local properties (i.e., through boundary layer entrainment and the subsequent aerodynamic effective shape change) or through an effect of the gaseous ablative constituents on the boundary layer stability, etc. Another point of interest is the repeatibility of data as is noted from B-13 and B-15 which have similar nose materials, re-entry conditions, and geometries. This was assuring.

From the documents which contain the flight data pertinent to each vehicle, details concerning the reconstruction of the experiment down through the transition altitude were extracted. This information and the procedure used to analyze the data are contained in Section 6. The following section (Section 5) contains a description of the analytic techniques that were utilized in this study.

SECTION 5

ANALYTIC TECHNIQUE DESCRIPTION

Several computer programs were available at GE/RESD to define the local boundary layer edge properties. These programs include both detailed numerical solutions of the governing equations and semi-empirical engineering solutions. These include:

1. Inviscid Zero Yaw Flow Field Program (Flow Field)[21]--Numerical solution of inviscid shock layer for axisymmetric bodies to provide shock shape and surface pressure as input to the boundary layer programs.
2. Equilibrium Non-Similar Boundary Layer Program (ENSBL)[22]--Numerical solution of boundary layer equations to define local viscous properties and profiles in laminar and turbulent flow.
3. Viscous Interaction Zero Angle of Attack Drag Program (VIZAAD)[23]--Engineering methods to determine local boundary layer edge properties for axisymmetric bodies with or without surface ablation.
4. Ablating Boundary Layer Equilibrium Program (ABLE)[24]--Solution of reaction-chemistry and mass conservation equations to provide surface heat transfer and rate of surface recession for use in REKAP program.
5. Reaction Kinetics Ablation Program (REKAP)[25]--Numerical solution of the heat conduction equation to define in-depth material response and mass loss for use in ENSBL and VIZAAD.
6. Combined Thermochemical and Thermomechanical Response in Nosetips (RESEP II)[26]--Engineering method to determine thermochemical shape change of ablative nose tips throughout re-entry which is used as input to FLOW FIELD and VIZAAD to define local boundary layer properties.

This system of computer codes provided the local boundary layer properties along the entire vehicle length in laminar, transitional, and turbulent flow for the flight test vehicles defined in Section 4.0. The local properties used in developing transition correlations, therefore, included the effects of nose shape change (RESEP II), surface mass loss (ABLE/REKAP), and inviscid-viscous interaction (FLOW FIELD and ENSBL/VIZAAD).

SECTION 6

DATA EVALUATION PROCEDURE AND RESULTS

The procedure and techniques that were employed to evaluate the local flow properties on the vehicle involved the following logic:

1. Data extraction from the Flight Evaluation Reports (FER)
2. Computation of the vehicle nose shape change
3. Determination of the frustum ablation characteristics
4. Calculation of the inviscid flow field
5. Viscous property definition which includes the effect of shape change and ablation
6. Real gas ablative product determination

A summary of the details involved in each of these steps, along with some sample results, is presented below.

Data Extraction from the FER

The following data were extracted from each flight report:

A. Geometry details

B. Heat shield material and thickness (including any antennae)

C. Substrate material and thickness

D. Trajectory information (time, velocity, altitude)

- on the beryllium and carbon vehicles the data are required to impact or vehicle demise*
- on the phenolics and Teflon vehicles data are required down through transition

E. Angle-of-attack history

*For the turbulent heating task, the nose shape change is required for altitudes well below the vehicle transition onset altitude. The ablative heat shield vehicles are not suitable for this task because of the blockage effects of ablation on the heat transfer (see Vol. II).

F. A listing of the aerothermodynamic instrumentation and location

G. Altitude of transition as deduced from each sensor or data system

H. Nose recession data and any other shape change data

An example of information extracted for vehicle T03 is contained in Figures 7 through 10.

Evaluation of Nose Shape Change

With the trajectory and heat shield characteristics known, the RESEP program[26] was utilized to deduce the vehicle's nose shape change as a function of altitude.* Some typical results of this computation for vehicles C03 and B13 may be found in Figure 11.

Frustum Ablation Characteristics

For vehicles with ablation from the frustum, such as the carbons, the phenolics, and the Teflon vehicles, the REKAP program[25] was used in addition to the RESEP program[26]. The former program provides the wall temperature, surface recession, and mass loss rate as a function of time. Some typical results of this analysis for vehicle T03 are shown in Figure 12 to 14 for surface recession, wall temperature, and ablation rate distributions, respectively.

Inviscid Flow Field

For the resultant vehicle shape, at the frustum transition altitude(s), the surface pressure distribution and the bow shock shape were determined from the flow field program[21]. These inviscid properties are required inputs to the viscous codes for local property definition.

Viscous Property Determination

The local properties in the boundary layer at a prescribed point in the trajectory (i.e., the transition altitude for the transition study, or a lower altitude for the turbulent heating investigation) were determined with the VIZAAD program. The results of this program were then used to develop "phenomenological" correlations. Since this is an engineering type program, sporadic checks on its accuracy were made with the ENSBL program [22] which is finite difference computer code. A

*It should be noted that calculations were not made for each vehicle but computations were made for sets with a common γ_E, R_N and material.

typical comparison of the results of ENSBL with VIZAAD for two stations on a vehicle of the B03 class is shown in Table 5. As a result of these occasional checks with ENSBL, wherein good agreement was noted, the use of the VIZAAD program results was justified.

The inputs required for these viscous computer programs are:

A. Vehicle shape

B. Shock shape

C. Pressure distribution

D. Ablation rate distribution

E. Wall temperature distribution

F. Free stream conditions

Real Gas Ablative Product Determination

The last step in the local property determination cycle is the computation of the enthalpy of the gaseous mixture at the vehicle surface which is made with the ABLF program[24]. The inputs required to this program are the heat shield material constituents, the local flow environment such as the pressure and temperature, the wall temperature and the wall gasification rates which are the results of the REKAP program [25].

SECTION 7

ATTEMPTED CORRELATIONS OF BOUNDARY LAYER TRANSITION FLIGHT TEST DATA

Viscous computations of local properties along the length of the vehicle were performed for each of the fifty-five flight test cases at the measured transition altitude. Free stream conditions, at the transition altitude are defined in Table 6. From the computed local flow properties, a large number of parameters, both frustum and nose tip related, have been analyzed in an attempt to identify the critical parameters which affect transition, and to develop, if possible, a flight test transition correlation.

7.1 FRUSTUM DATA AND CORRELATIONS

The calculated local flow properties at the transition onset location on the vehicle frustum are tabulated in Table 7. Using these data, a number of correlations, both traditional and innovative, were attempted. Table 8 lists the twenty-two (22) correlation parameters which were evaluated using the local properties on the frustum. As will be discussed below, none of the parameters based on frustum local properties appeared to order all the data. Limited subsets did indicate trends, but as more flight data were added, the scatter in the correlations increased. In effect, no correlation was achieved. Some examples of these local property transition data in the form of transition correlations, currently in vogue, are discussed below.

One attempted local property transition correlation utilized the local wetted length Reynolds number at the transition location, Re_s, versus local edge Mach number, Me[4], as shown in Figure 15. The considerable scatter, when a large number of flight test points are included, is obvious.

Several aerospace contractors[26-28] are employing transition correlations based on the local momentum thickness Reynolds number, Re_θ, and local edge Mach number, Me, as shown in Figure 16. In particular, Philco-Ford[28] has developed for the Low Recession Nose Tip (LORN) program, the following expression for transition location,

$$Re_\theta = 275\, e^{(.135\ Me)}$$

Philco-Ford utilizes this expression for nose tip transition. However, the data on which this correlation is based is from frustum flight test data for vehicles with graphite nosetips. From the data spread shown in Figure 16 for the same or similar vehicles (Symbols □, ▽, ◇) the usefulness of a transition criterion based on Re_θ with Me must be questioned.

Another correlation, which is currently being used by NASA on the Space Shuttle program, was developed by McDonnell-Douglas (MDAC)[20] which states that:

$$\frac{Re_{\theta}/Me}{(Re/ft)^{0.2}} = f(\delta) = \text{function at the flow direction}$$

For the vehicles used in this study $f(\delta) = 10$. This correlation was developed from a limited set of flight data (12 vehicles). For the 55 vehicles considered in the current study, the variation of Re_{θ}/Me with the local unit Reynolds number, Re/ft, is shown in Figure 17. The line of the MDAC correlation is also shown. It is quite evident from these data that there is no unit Reynolds number effect nor do the parameters correlate the data. To further clarify this point, those vehicles with a beryllium frustum are shown as filled symbols. This subset of 17 vehicles clearly shows a lack of unit Reynolds number effect. It should be noted that the viscous calculations employed in the present study yielded local properties which agreed quite well with the MDAC calculations for the same flights. Thus, the apparent discrepancy between MDAC's correlation and the present data points is not due to differences in calculating local properties but rather increased scatter due to the increase in the number of flights analyzed.

Figure 18 is an example of a summary type correlation; RN_0/R_B, the preflight bluntness ratio, versus $Re_{\infty D}$, the free stream Reynolds number based on the vehicle base diameter at the measured transition altitude. McCauley[2] has proposed this correlation for various sets of vehicles. The classification of vehicles into individual sets is based on similar heat shield materials and vehicle geometry parameters. While this type correlation may be useful to design an additional vehicle of the same class, it does not provide information which can be interpolated or extrapolated to a new design problem. In reality, the data in Figure 18 indicate that even within a single class of vehicles, i.e., the 8° half angle ATJ/Pr (◇), the scatter is sufficient to invalidate the correlation.

The wall gas enthalpy correlation of Berkowitz, et al[6] is shown in Figure 19. Although the beryllium heat shield data are nominally ordered by local edge Mach number, no consistent correlation appears to exist between the beryllium and Teflon heat shield vehicles. In addition, the history of transition data along the surface for vehicle B01, in itself violates this correlation. That is, during re-entry, the edge Mach number at the transition station continually decreases, while the local Reynolds number at transition initially increases then decreases (this is the bluntness reversal effect noted by Steston & Rushton[13] and Softley[14]). This is denoted in Figure 19 by the arrows on the data point in the upper right.

There have been numerous studies relative to the effects of frustum ablation on frustum transition, the most recent of which is an experimental study by Stalmach, et al[29]. In this study heat transfer data were obtained in the LTV facility on a 12°

half angle porous cone which was nominally 9.5 inches long and had a non-porous nose which was 0.38 inches long. Stalmach concluded from the results of his measurements that for a given mass injection rate, the transition location was sensitive to the injection distribution. The transition Reynolds numbers were significantly greater when the injection distribution was constant than when the distribution decreased rapidly with distance from the apex. Although these results apparently contradict previous studies(10-12), closer inspection of the data indicate that for Stalmach's tests, the porous region near the nose probably affects transition and not the frustum per se. Nevertheless, for the flight data analyzed herein, attempts were made to establish whether the transition data would correlate with any integrated blowing (ablation) parameter. In Figure 20, the integrated blowing parameter, $\dot{m}/\dot{m}_{ref}$ to the transition location is plotted against the local wetted length Reynolds number. It was evident that neither these parameters nor any frustum ablation parameter would order the data.

Thus it can be stated that, no correlation based upon local properties on the frustum was acceptable in terms of data scatter and general usefulness.

7.2 LOCAL PROPERTIES IN THE NOSETIP REGION

As discussed in Section 2.2, ground test data have indicated the importance of nose tip disturbances in effecting transition, while frustum conditions as simulated by mass addition appeared to have a second order influence. The flight data itself as tabulated in Table 4 show that within a class of vehicles as defined by geometry and heat shield material, transition altitudes vary widely. In particular, cases B12 and B13, two vehicles with identical geometry and frustum heat shield material and similar flight histories but with nosetip materials with significantly different properties, had transition altitudes that differed by 15 Km. On the other hand, cases P04 and T04, vehicles with identical geometry, flight histories and nose tip material, but very different frustum heat shield materials, had transition altitudes within 2 Km. From these flight results and the ground test observations, an investigation of possible correlations based on local properties in the nose tip region was undertaken.

The viscous computations of local properties on the frustum, at the transition onset sensor location, also provide the local properties along the entire length of the vehicle. Information similar to that used in the attempts to correlate the flight data with frustum local properties, was tabulated for a fixed location in the nose region, $X = 2R_N'$ in Table 9. Here R_N' is the equivalent spherical (ablated) nose radius at the transition altitude.

Figure 21 defines the terminology used for the correlations attempted with nose related parameters. All local properties were assessed at $X = 2R_N'$. The selection of $2R_N'$, although arbitrary, was made for the sake of consistency, since

the vehicles had nose sections of varying lengths. The need was for a station which would reflect the nose shape change/recession due to ablation, a station which was on the cone, and thus, in a relatively constant pressure region, and yet not a station so far removed from the nose region as to constitute another frustum point. The sensitivity of the most successful correlation to the choice of a 2 R_N' station as opposed to R_N' or 3-4 R_N' will be discussed in Section 8.

Other length parameters defined in Figure 21, which were used in the correlation attempts, are R_{Neff} and ΔS. R_{Neff} is the effective radius of curvature in the stagnation region. For most of the vehicles, (i.e., those with $h_{tr} \gtrsim 30$ Km), $R_{Neff} \approx R_N'$. However if the vehicle underwent transition at a relatively low altitude, such as cases C03 and C04, the laminar flow heating caused a blunting of the vehicle resulting in $R_{Neff} > R_N'$. The length, ΔS, is defined as the wetted length between $X = 2\ R_N'$, the station at which the local properties were evaluated, and $X = X_{TR}$, the location of the frustum transition sensor whose response determined the transition onset altitude.

Table 10 lists the various correlations attempted using the calculated local properties at 2 R_N'. Since ground test data had shown the importance of nose mass addition(12), a number of correlations were attempted using the mass loss parameter, $\bar{\dot{m}}$, for $0 \leq X \leq 2 R_N'$

The initial attempt was to plot the normalized ablation rate $\bar{\dot{m}}$ (see Figure 21) versus the free stream Reynolds number based on R_N' (Figure 22). It was apparent from this set that the data appeared to be somewhat ordered by nose tip related parameters. The vehicles in the blunt class (data points in the lower right) did not appear to correlate well, however, so other local property parameters were sought. One such parameter was the local wetted length Reynolds number at 2 R_N' (Figure 23). In this format, all of the data appeared ordered, and, in addition, it was further noted that the sharp vehicles were clustered in the upper left and the blunt towards the lower right. Thus it was apparent that a length parameter existed which might further order the data. This parameter was ultimately found to be $\Delta S/R_{Neff}$. A cross plot of $\bar{\dot{m}}$ with $\Delta S/R_{Neff}$ is shown in Figure 24. All of the data appear to be ordered by nose tip material (i.e. Teflon versus graphite). The correlation presented in Figures 23 and 24 will be discussed in detail in Section 8.

Attempts were made to establish more fundamental parameters reflecting characteristic boundary layer parameters. The first of these was to normalize the ablative mass loss with the boundary layer mass flow at the 2 R_N' station. This is shown in Figure 25. This evidently does not help. Another attempt was to base the Reynolds number (Figure 23) on the momentum thickness at the 2 R_N' station. This is shown in Figure 26, and once again, this does not improve the correlation. A third attempt was made to normalize the wetted length by the viscous layer thickness at the 2 R_N station. The variation of $\bar{\dot{m}}$ with $\Delta S/\delta_{2R_N'}$ is shown in

Figure 27. At this point, it was concluded that the parameters defined in Figures 23 and 24 best characterized the transition phenomena. A detailed description of this correlation and its implication to the transition phenomena and also its agreement with ground test data trends is contained in the following section.

SECTION 8

IDENTIFICATION OF FUNDAMENTAL PARAMETERS AFFECTING BOUNDARY LAYER TRANSITION

As mentioned earlier, it was evident that the nose, or some facet thereof, has a definite effect on the location of transition. From a direct observation of the raw flight data (vehicles B12 and B13), for the same trajectory and entry conditions, a 15 kilometer difference in transition altitude was noted. It was felt, at the initiation of this study that the difference would possibly be accounted for in local properties on the frustum if the nose ablation effects were accounted for. However, as noted in Section 7.1, it became apparent that no combination of frustum related parameters (i.e., properties at the transition onset point) correlate the data. Limited subsets of data appear to correlate, however, as more data are added to these "correlations," they tend to disappear in the scatter. Many examples of this are contained in the prior section. Since our objective was to find and isolate primary factors affecting transition location, and not to provide pseudo-design correlations, these attempts were deemed as unsatisfactory.

With this de-emphasis of free stream related parameters and knowledge of the apparent sensitivity of the nose (these conclusions are applicable to both the flight data and ground test results) the search for nose tip parameters began. Our obvious first attempts were to investigate those frustum related parameters which had limited success on data subsets. As discussed in Section 7.2, the majority of these did not order the data. Yet, it was obvious that the nose was the forcing function affecting transition. Guided by the parameters used in the ground test programs of References 11 and 12, and by the theoretical analyses of Mack[30] (stability theory) and Donaldson[31] (invariant modeling), the parameters that were isolated were the non-dimensional mass loss rate of a sector of the nose tip, $\bar{\dot{m}}$, and the local wetted length Reynolds number at the end of this sector, R_{es} at 2 R_N' (Figure 21). Both of these parameters were evaluated at the altitude where transition occurs on the frustum and can be viewed as the forcing functions or measures of the disturbance introduced into the boundary layer. A third parameter is required, namely, the distance from this point (i.e., the value of the wetted length S at 2 R_N') to the location of transition on the frustum, ΔS.

The variation of $\bar{\dot{m}}$ with R_{es} for all of the vehicles analyzed* (with the exception of B09 where $\bar{\dot{m}} \equiv 0$) is shown in Figure 28. It is evident from this figure that all of the data are ordered/correlated into two sets. What the data in the lower set (labeled Graphitic nose) have in common is that the nose material is fabricated of some graphitic material,

*Caution should be exercised when using data from vehicles with silica noses because of (1) the uncertainty of the vaporization rate relative to the total mass loss rate, and (2) the general paucity of data analyzed which precludes a definitive trend.

independent of the frustum material of the vehicle. The vehicles of the upper set have a Teflon nose; independent of the frustum material. That is, the transition data are apparently correlated by a nose related parameter, independent of whether the frustum is beryllium, phenolic refrasil, carbon phenolic, or Teflon. For example, one fundamental parameter that varies from one line to the other is the molecular weight, M_w, of the gaseous ablative products of the nose material. For the graphite case, $M_w \approx 28$ and for Teflon, $M_w \approx 50-70$.

These findings are somewhat contrary to our original thinking (and I might add to that of the aerospace community at large). What this analysis of flight test boundary layer transition data has revealed is that frustum effects are apparently of second order. This finding is not to be construed as a general rule, applicable for all flight data. As pointed out by Morkovin [1], more than one type of instability mechanism can exist. In the data set collected, virtually all of the vehicles had ablating noses and, as a result, the transition process was dominated by the nose region ablative process.

As such, for this data set, the frustum effects were apparently of second order. However as the ablation rate from the nose diminishes, or as transition approaches the nose other factors can become important and may indeed dominate the process. Factors such as the frustum wall temperature (or enthalpy), or roughness could then be important and become first order effects as has been observed in many ground test experiments.

Another interesting facet is evident from the presentation of results of Figure 28. The data are further ordered, along each nose tip correlating line (i.e., graphites and Teflon), by the length to the transition point on the frustum, ΔS, normalized by the effective stagnation point radius, $R_{N_{eff}}$. The lines drawn from lower left to upper right represent points of constant $\Delta S/R_{N_{eff}}$ for both Teflon and Graphite noses. Thus all the relatively sharp nosed vehicles are clustered in the upper left (i.e., large $\Delta S/R_{N_{eff}}$) and the blunt vehicle are at the lower right (i.e., small $\Delta S/R_{N_{eff}}$).

In summary, for the data set considered in this study (i.e., the fifty-four vehicles), the parameters represented in Figure 28 (namely, $\bar{m}$, $R_{es_{2R_N}}$, $\Delta S/R_{N_{eff}}$) order the flight test transition data whereas all others described in Section 7 have failed. The significance of the parameters described in this correlation can be stated as follows; some characteristic of the ablating nose is creating a disturbance in the boundary layer. This disturbance applifies such that at a distance ΔS downstream the turbulence in the boundary layer grows so that the sensible heating to the surface departs from the laminar level. The parameters that have been isolated here characterize this disturbance. The Reynolds number represents some critical Reynolds number, while the injectant rate $\bar{m}$ and a property of the gaseous constituents, say the molecular weight

of the ablative products, represents a measure of the disturbance*. The conclusions and correlation developed with the flight data are in complete agreement with the trends observed in ground test pertaining to the sensitivity of transition to nose effects, and the insensitivity to frustum effects such as ablation.

After the initial effort was completed, resulting in the data collection of Table 4, some additional flight data on an ATJ nose-beryllium frustum vehicle with a 22° half cone angle was brought to the authors attention.[32] These data were also analyzed in the same manner as discussed earlier and the results are presented in Figure 28 (labeled with the 22). The multiple points correspond to transition movement along the frustum. One will note that excellent agreement with the resultant correlation is also noted. Hence, it can be stated that this ordering of the data is not restricted to slender cones as the original data collection would imply.

The obvious question arises as to how one uses this correlation to establish the transition altitude of a vehicle, or the movement of transition along a vehicle. The altitude variation of the nose related parameters, $\bar{m}$, R_{es}, $R_{N_{eff}}$ must be determined with the techniques described in Section 5. For the typical vehicle, this variation is shown in Figure 29. As the vehicle re-enters the earth's atmosphere, the ablation of the nose begins and increases monatonically with decreasing altitude down through peak heating which generally occurs below the "transition" altitude. The apparent peaking in the parameter $\bar{m}$ occurs because the denominator (i.e., $(\rho u)_\infty A_{ref}$) increases at a faster rate thereby causing the reversal of trend. As a result, the altitude variation of $\bar{m}$ with R_{es} becomes nominally parallel to the correlating level of Figure 28 (i.e., either the curve labeled graphite or Teflon depending on the nose material). When the critical length is reached (i.e., the value of ΔS corresponding to the vehicle length), then transition will occur at the vehicle base. To further map transition movement along the vehicle simply requires one to continue mapping the points along this trajectory variation as ΔS decreases. Thus, the cross lines of $\Delta S/R_{N_{eff}}$ become the lines of critical importance to obtaining a transition altitude at a particular vehicle station.

One question pertaining to this correlation which should be clarified pertains to the arbitrary selection of a representative nose length, $2R_N'$. That is, is this length critical to the correlation? Or would the length R_N' or $3\text{-}5R_N'$ have been more significant? As mentioned earlier, this length was selected to represent that region of the nose where the disturbances that affect transition are introduced. It was evident that frustum effects should be de-emphasized, yet some character of the vehicle cone angle was felt to be important in these results. For some limited points, this effect

*It is recognized that these specific parameters, $\bar{m}$, $\dot{R}_{es_{2R_N}}$, $\Delta S/R_{N_{eff}}$, may not be the final ones. That some nose parameters are fundamental to identify transition is, however, undeniable.

was investigated for $\ell = R_N'$ and $3 R_N'$ and the result is that the lines corresponding to the Graphite and Teflon noses are not affected. All points in the nose region lie along these two lines.

It is of interest to note that vehicle bluntness effects are intrinsic to the resultant correlation and need not be treated in any special manner. That this statement is valid can best be illustrated by presenting the flight data in the format R_{es} versus $R_{e_\infty N}$ (Figure 30). The data fairing through the data of Stetson and Rushton[13] is repeated from Figure 3. One will note that the data set includes both sharp and blunt classes of vehicles.

To summarize our findings, it was found that boundary layer transition on the frustum of re-entry vehicles can be correlated with nose tip related parameters which represent disturbance elements ($\dot{m}$, $R_{es_{2R_N'}}$), coupled with a length parameter ($\Delta S/R_{N_{eff}}$) which is required for this disturbance to affect a change in the laminar boundary layer state. Although specific parameters were isolated to develop a correlation, one can state quite basically that boundary layer transition for re-entry vehicles is dependent on the entry conditions (i.e., the trajectory), which effect $\dot{m}$, R_{es}, $R_{N_{eff}}$, the initial radius of the nose and the material with which it is fabricated which also affects $\bar{\dot{m}}$, R_{es}, $R_{N_{eff}}$, and the size (length) of the vehicle, ΔS. All of these facets are required to develop the correlating parameters.

SECTION 9

CONCLUSIONS

The results of the analysis of fifty-five ballistic flight vehicles indicate that frustum transition of re-entry vehicles appears to be nose tip dominated. Frustum related parameters and materials apparently have a second order effect on transition. This implies that local viscous parameters on the frustum should not correlate flight test transition data, and in fact, they do not. Specific parameters relative to the nose tip have been identified as the apparent dominant factors that characterize the transition phenomena and a correlation of the flight test data has been presented. This finding is not to be construed as a general rule, applicable for all flight data. As the ablation rate from the nose diminishes, or as transition approaches the nose other factors can become important and may indeed dominate the process.

SECTION 10

REFERENCES

1. Morkovin, M.V., "Critical Evaluation of Transition From Laminar to Turbulent Shear Layers with Emphasis on Hypersonically Travelling Bodies", AFFDL-TR-68-149 (March 1969).

2. McCauley, W., "The Reynolds Number Realm of Boundary Layer Transition As Obtained from Re-Entry Flight Test Data", Classified Proceedings of the Strategic Missile Sciences Meeting AERL 71-1062, Vol. 2, Annapolis, Md., pp 295-312, (May 1971).

3. Timmer, H.G., Arne, C. L., Stokes, T.R., Jr., and Tang, H.H., "Ablation Dynamics for Slender Re-Entry Bodies", Vol. I Theoretical Analyses and Results, AFFDL-TR-70-27, MdDonnell-Douglas Corp., Santa Monica, Calif. (May 1970).

4. Berkowitz, A.M. and Stewart J.D., "Detection and Correlation of Transition Data", Boundary Layer Transition Study Group Meeting, Air Force Rpt. BSD-TR-67-213, Vol. 1, pp 3-1 to 3-61 (Aug. 1967).

5. Kohrs, R., Pannabecker, C., Pattay, S. and Wells, D., "The Determination of Hypersonic Drag Coefficients for Cones, Biconics, and Triconics", AVMSD-0316-67-CR, AVCO Corporation Wilmington, Mass. (March 1967).

6. Berkowitz, A., Martellucci, A. and Kryiss, C., "General Electric Transition Technology Development", Vol. II Proceedings of the Boundary Layer Transition Workshop held 3-5 Nov. 1971, Air Force Report No. TOR-0172(528616-16)-5, pp. 3-1 to 3-60 (Dec. 1971).

7. Fannelop, T.K., "Displacement Thickness for Boundary Layers with Surface Mass Transfer", AIAA Journal, Vol. 4, No. 6, pp 1142-1147 (June 1966).

8. Mann, W. M., Jr. "Effective Displacement Thickness for Boundary Layers with Surface Mass Transfer", AIAA Journal, Vol. 1, No. 5, pp. 1181-1182 (May 1963).

9. Hayasi, N., "Displacement Thickness of the Boundary Layer with Blowing", AIAA Journal, Vol. 3, No. 12, pp. 2348-2349 (Dec. 1965).

10. General Electric Company, "STREET-G Contract — Hypersonic Cone Boundary Layer Experiment", Unpublished Data - 1972.

11. Dunavant, J.C. and Everhart, P.E., "Exploratory Heat Transfer Measurements at Mach 10 on a 7.5° Total-Angle Cone Downstream of a Region of Air and Helium Transpiration Cooling", NASA TND-5554, (December 1969).

12. Martellucci, A. and Laganelli, A., "Downstream Effects of Gaseous Injection Through a Porous Nose", TIS 71SD218, General Electric Co., Philadelphia, Pa. (February 1971).

13. Stetson, K.F. and Rushton, G.H., "Shock Tunnel Investigation of Boundary Layer Transition at M-5.5", AIAA JOURNAL, Vol. 5, No. 5, pp 899-906, (May 1967).

14. Softley, E.J., "Transition of the Hypersonic Boundary Layer on a Cone, Part II Experiment at M=10 and More on Blunt Cone Transition", GE-TIS R67SD14, General Electric Co., Philadelphia, Pa., (October 1968).

15. Wright, R.L. and Zoby, E.V., "Flight Measurements of Boundary Layer Transition on a 5° Half-Angle Cone at a Free Stream Mach Number of 20 (Re-Entry F)", NASA TMX-2253 (May 1971).

16. Martellucci, A. and Neff, R.S., "Influence of Asymmetric Transition on Re-Entry Vehicle Characteristics", Journal of Spacecraft & Rockets, Vol. 8, No. 5, pp. 476-482 (May 1971).

17. DiCristina, V., "Three-Dimensional Laminar Boundary Layer Transition on a Sharp 8° Cone at Mach No. 10", AIAA Paper 69-12 (January 1969).

18. McCauley, W.D., Saydah, A.R. and Bueche, J.F., "Effect of Spherical Roughness on Hypersonic Boundary Layer Transition", AIAA Journal, Vol. 4, No. 12, pp 2142-2148 (December 1969).

19. DeCarlo, J., et al, "Mach 5 to 12 Inlet Development Program, Phase I - Data Report", Technical Report FHR 2817-29-1, Fairchild Hiller Corp., Long Island, New York (1965).

20. Stuerke, D.H., Masek, R.V., Mattox, D.L. and Mockapetris, L., "Correlation of Flight Boundary Layer Transition Data", AFFDL-TR-71-26, McDonnell-Douglas Corporation, St. Louis, Mo. (May 1971).

21. Gravalos, F.G., Edelfelt, I.H. and Emmons, H.W., "The Supersonic Flow About a Blunt Body of Revolution for Gases at Chemical Equilibrium", Proceedings of the 9th Annual Congress of the IAF, Amsterdam, 1958.

22. Rie, H., "The GE-RESD Equilibrium Non-Similar Boundary Layer Program (ENSBL)", TIS 71SD212, General Electric Co., Philadelphia, Pa., (February, 1971).

23. Studerus, C.J. and Dienna, E.A., "Viscous Interaction Zero Angle of Attack Drag (VIZAAD) Program", TIS 64SD292, General Electric Co., Philadelphia, Pa. (November 1964).

24. Fogaroli, R.P. and Brant, D.T., "ABLE Computer Program", TFM 9151-071, General Electric Co., Philadelphia, Pa. (November 1971).

25. Gordon, P., "Analysis of One-Dimensional Heat Conduction Computer Program", TIS R66SD10, General Electric Company, Philadelphia, Pa. (March 1966).

26. Chin, J.H., "Advanced Composites II (RESEP II) - Computer User's Manual", N-16-69-5, Lockheed Missiles and Space Company, Sunnyvale, Calif., (September 1964) Also SAMSO TR-70-16.

27. Strategic Re-Entry Technology Program (STREET A), "Final Report Volume II, Task 7.5 Nosetip Ablation Phenomena", SAMSO-TR-70-247, Vol. II, (November 1970).

28. Philco-Ford Space and Re-Entry Systems Division, "Definition of LORN Boundary Layer Transition Criterion", DR-4517, Philco-Ford, Inc., Newport Beach, Calif.

29. Stalmach, C.J., Jr., Bentin, J.J., Pope, T.C., "A Study of Boundary Layer Transition on Outgassing Cones in Hypersonic Flow", NASA CR-1908 (December 1971).

30. Mack, L.M., "Notes on the Theory of Instability of Incompressible and Compressible Laminar Boundary Layers", Von Karman Institute for Fluid Dynamics, Brussels, Belgium, 1968.

31. Donaldson, C., Sullivan, R.F. and Yates, J.E., "An Attempt to Construct an Analytical Model of the Start of Compressible Transition", Proceedings of the Boundary Layer Transition Workshop, Vol. 4, (November 1971).

32. Sherman, M.M. and Nakamura, T., "Flight Test Measurements of Boundary Layer Transition on a Non-Ablating 22° Cone", AIAA Paper 68-1152, December 3-5, 1968.

TABLE 1. GE-RESD DEVELOPMENT OF RE-ENTRY VEHICLE SYSTEMS

	X	X	X				X	X	X	X	X	X		

X Denotes Applicable to Current Study

TABLE 2. METHODS OF TRANSITION ONSET DETECTION

	Flight Test	Gun Ranges	Wind Tunnel
1. Heat Transfer or Differential Thermal Sensors	X	---	X
2. Drag (Ballistic Coeff.) Accelerometers or Radar Data	X	X	---
3. Base Pressure	X	---	---
4. Pitot Pressure (Surface or Profile)	---	---	X
5. Visual (Schlieren, Shadow-Graph, etc.)	---	X	X
6. Heat Sensitive Paints, Crystals etc.	---	---	X
7. Reflectometers	X	---	---
8. Acoustic Sensors	X	---	X

TABLE 3. SPHERE-CONE R/V TRANSITION ALTITUDE

Nose Material	Heat Shield Material	Nose Radius (m)	Transition Altitude (KM)		
			Base Pressure	Reflectometer	Accel.
ATJ	PR	0.00952	17.4	-	19.8
TFE/CP	PR	0.0127	26.5	26.2	25.9
TFE/CP	PR	0.00952	25.3	26.2	25.1
TFE/CP	CP	0.0127	25.1	24.9	25.9
TFE/CP	R6300	0.0127	23.6	24.4	24.4
TFE/PR	PR	0.00952	26.2	25.3	25.8
CP	PR	0.0127	25.0	25.1	24.6
PR	PR	0.00952	22.6	23.9	24.2
TFE/CP	CP	0.0127	31.4	28.0	28.6
ATJ-S	PR	0.00635	20.1	20.1	20.4

TABLE 4A. VEHICLE SELECTION - TRANSITION STUDY

Frustum - Beryllium

Case	Material		Transition Altitude (KM)	GE/NASA	Stuerke et al (Ref. 20) AF-FDL	McCauley (Ref. 2) Aerospace
	Nose	Frustum				
B01	ATJ	BE	30.48	X	X	X
B02	ATJ	BE	33.38	X	X	X
	ATJ-S	BE				X
	ATJ	BE			X	
B03	ATJ	BE	37.19	X		X
B04	Graph	BE	38.10	X		
	ATJ	BE				X
B05	Graph	BE	38.10	X	X	X
B06	ATJ-S	BE	22.86	X		X
B07	ATJ-S	BE	19.81	X	X	X
B08	ATJ	BE	18.29	X		X
	ATJ-S	BE				X
B09	SS	Inconel	7.38	X	X	
	Steel	Copper			X	
B10	ATJ-S	BE	25.47	X		
B11	SP	BE	28.96	X		
B12	SP	BE	30.48	X		
B13	ATJ	BE	15.24	X		
B14	SP	BE	27.13	X		
B15	ATJ	BE	16.46	X		
B16	SP	BE	27.43	X		
B-101	PG	BE	35.66	X		
B-102	PG	BE	33.83	X		
B-103	PG	BE	33.83	X		

TABLE 4B. VEHICLE SELECTION - TRANSITION STUDY

Frustum - Carbon Class

Case	Material		Transition Altitude (KM)	GE/NASA	Stuerke et al (Ref. 20) AF-FDL	McCauley (Ref. 2) Aerospace
	Nose	Frustum				
C01	PG	PG	22.56	X	X	X
	TFE/ATJ	CP				X
	ATJ	CP				X
	ATJ	CP				X
C02	ATJ	CP	19.51	X		X
	ATJ	CP				X
	ATJ-S	CC + Overlay			X	X
	ATJ-S	CC + Overlay				X
	ATJ-S	CC + Overlay				X
C03	ATJ-S	CC	7.47	X		
C04	ATJ-S	CC	10.97	X		
	3DQP	CP				X
C05	CP	CP	26.21	X		
C06	CP	PG	19.51	X		
	H_2O TCNT	Refract			X	
	H_2O TCNT	CP				
	H_2O TCNT	CP				
C-103	PG	PG	37.19	X		
C-101	CP	CP	26.82	X		
C-102	TFE/CP	CP	32.31	X		

TABLE 4C. VEHICLE SELECTION - TRANSITION STUDY

Frustum - PR, SP, 3DQP

Case	Material		Transition Altitude (KM)	GE/NASA	Stuerke et al (Ref. 20) AF-FDL	McCauley (Ref. 2) Aerospace
	Nose	Frustum				
S01	ATJ	PR	28.35	X		
S02	ATJ	PR	25.0	X		
S03	ATJ	PR	28.96	X		
S04	ATJ	PR	32.31	X		X
	ATJ	PR				X
S05	CP	SP	24.84	X		
S07	SP	TWSP	22.56	X		
S08	ATJ	SP	20.73	X	X	X
S09	ATJ-S	SP	21.03	X		X
	ATJ-S	SP				X
S10	ATJ-S	SP	30.97	X		X
S-101	3DQP	3DQP	27.43	X		X
S-102	3DQP	QP	34.14	X	X	X
S-103	TFE/CP	SP	26.21	X		
S-104	TFE/SP	TWSP	25.30	X		
S-105	TFE/CP	TWCP	23.77	X		
S-106	TFE/CP	TWCP	25.60	X		
S-107	TFE/SP	TWSP	25.91	X		
S-108	ATJ	PR	35.66	X		

TABLE 4D. VEHICLE SELECTION - TRANSITION STUDY

Frustum - Teflon (Low Temp. ABL.)

Case	Material		Transition Altitude (KM)	GE/NASA	Stuerke et al (Ref. 20) AF-FDL	McCauley (Ref. 2) Aerospace
	Nose	Frustum				
T01	Tfe	Tfe	39.62	X		
T02	Tfe	Tfe	31.09	X		X
T03	Tfe	Tfe	36.88	X	X	X
T04	ATJ	Tfe	34.14	X		X
T05	Tfe	Tfe	39.17	X	X	X
T06	Tfe	Tfe	38.71	X		
T07	Tfe	Tfe	38.40	X	X	X
T08	Tfe	Tfe	38.71	X		
T10	ATJ-S	Tfe	28.96	X		X
	ATJ-S	Tfe				X
T-101	Tfe	Tfe	35.05	X		

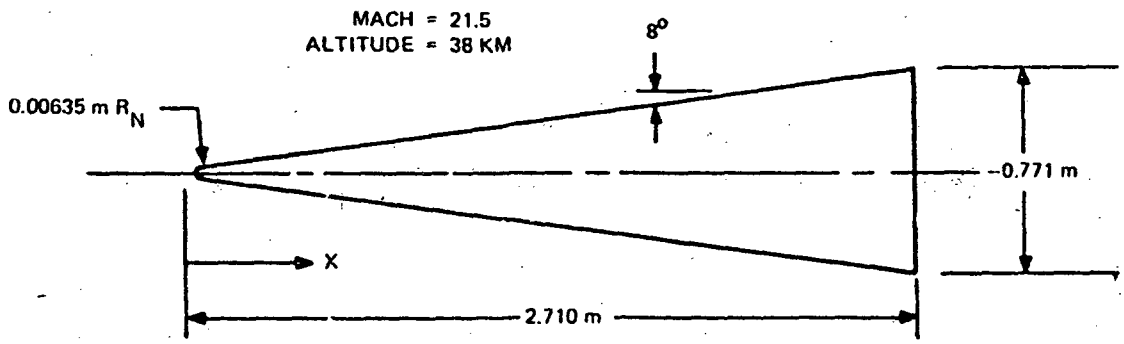

MACH = 21.5

ALTITUDE = 38 KM

	δ m	δ^* m	θ m	Re_s	u_e m/sec	$\dot{q}$ watts/m^2	M_e
x = 1.59 m							
ENSBL	4.27^{-2}	3.35^{-3}	1.50^{-4}	8.92^{+6}	6827.	5.92^{+5}	12.93
VIZAAD	3.84^{-3}	3.26^{-3}	1.73^{-4}	8.10^{+6}	6827.	6.52^{+5}	12.52
x = 2.68 m							
ENSBL	5.46^{-3}	4.24^{-3}	2.01^{-4}	1.43^{+7}	6827.	4.51^{+5}	12.74
VIZAAD	4.94^{-3}	4.21^{-3}	2.16^{-4}	1.40^{+7}	6827.	5.03^{+5}	12.62

TABLE 5. COMPARISON OF LOCAL PROPERTIES FROM ENSBL/VIZAAD

FOLDOUT FRAME 1

U_{∞} x 10^{-4} FT/SEC.

	B01	B02	B03	B04	B05	B06	B07	B08	B09	B10	B11	B12	B13	B14	B15	B
	□	□	□	□	□	□	□	□	Z	□	⊠	⊠	□	⊠	□	
h_t - KM	30.48	33.38	37.19	38.1	38.1	22.86	19.81	18.29	7.38	23.47	28.96	30.48	15.24	27.13	16.46	27
$(P_{\infty}$ x $10^{-3})$ N/M^2	1.094	.726	.422	.372	.372	3.543	5.[illegible]	7.230	38.97	3.222	1.399	1.114	11.6[illegible]	1.843	[illegible]	1
ρ x $10^2)$ - Kg/M^3	1.679	1.691	.807	.529	.529	5.622	9.162	1.629	56.54	5.106	2.162	1.711	15.76	2.874	15.49	2
$(u_{\infty}$ x $10^{-3})$ M/SEC	6.02	6.92	4.[illegible]	6.86	6.85	6.61	5.47	5.71	.964	5.73	4.78	6.00	4.86	6.04	5.10	5
T_{∞} - °K	227.	232.	241.	245.	245.	219.	217.	217.	240.	220.	228.	227.	217.	224.	217.	224
$(R_{e_{\infty}}/M)$ x 10^{-7}	.684	.502	.267	.230	.230	2.58	3.527	6.36	3.60	2.03	.704	.696	6.43	1.187	5.446	1
h_t - KFT	100.	109.5	122.	125	125.	75.	65.	60.	24.2	77.	95.	100.	50.	89.	[illegible]	90
P_{∞} - LB/FT^2	22.86	15.17	8.817	7.769	7.769	73.99	118.9	151.0	814.	67.3	29.2	23.27	243.6	38.5	201.	36.
ρ x 10^3 LBM/FT^3	1.048	.681	.379	.3302	.330	3.51	5.72	7.26	35.3	3.188	1.35	1.066	11.71	1.794	9.67	1.
u_{∞} x 10^{-4} FT/SEC.	1.976	2.27	2.259	2.250	2.247	2.16[illegible]	1.796	1.872	0.323	1.880	1.570	1.970	1.600	1.98	1.675	1.
T_{∞} °R	409.	417.6	434.6	441.	44[illegible]	396.	390.	390.	432.	396.	408.	409.	390.	403.	390.	403.
$(R_{e_{\infty}}/FT)$ x 10^{-6}	2.085	1.529	.815	.7023	.7015	7.[illegible]	10.75	19.39	10.96	6.191	2.146	2.115	19.61	3.619	16.60	3.
$R_{e_{\infty}}$ D x 10^{-6}	4.743	4.023	1.260	2.809	2.104	5.910	8.062	14.54	7.763	7.739	2.862	2.647	24.50	4.524	20.75	4.
M_{∞}	19.91	22.69	22.01	21.87	21.[illegible]	21.25	18.60	19.39	3.17	19.26	15.90	19.26	18.54	20.16	17.36	19.

	S01	S02	S03	S04	S05	S07	S08	S09	S10		S101	S102	S103	S104	S105	S10
	◇	◇	◇	◇	◊	×	◇	◇	◇		⌂	⌂	⌂	⌂	⌂	C
h_t - KM	28.35	25.0	29.96	32.31	24.84	22.56	20.73	21.03	35.97		27.43	34.14	26.21	25.30	23.77	25.
$(P_{\infty}$ x $10^{-3})$ - N/M^2	1.534	2.552	1.400	[illegible]	2.613	3.713	4.932	4.706	.501		1.761	.650	2.118	2.436	3.077	2.
ρ x $10^2)$ KG/M^3	2.377	4.014	2.162	1.292	4.112	5.906	7.977	7.535	.730		2.739	.968	3.314	3.828	4.866	3.
u_{∞} - M/SEC	6.87	7.06	4.92	6.81	6.71	6.46	6.40	6.07	6.32		6.81	6.71	6.77	6.49	6.40	6.
T_{∞} - °K	225.	222.	226.	229.	221.	219.	217.	218.	239.		224.	234.	223.	222.	220.	222.
(Re_{∞}/M) x 10^{-7}	1.114	1.944	1.004	.591	1.904	2.658	3.52	3.202	.300		1.277	.428	1.542	1.712	2.159	1.
h_t - KFT	93.	82.0	95.	106.	81.5	74.	68.0	69.0	118.		90.	112.	86.0	83.	78.	84.
P_{∞} - LB/FT^2	32.04	53.29	29.23	17.74	54.57	77.56	103.0	98.[illegible]	10.[illegible]		36.78	13.58	44.25	50.87	64.26	46.
ρ x 10^3 LBM/FT^3	1.484	2.506	1.350	.8066	2.567	3.657	4.940	4.704	.456		1.710	.6043	2.009	2.39	3.038	2.
u_{∞} x 10^{-4} FT/SEC	2.255	2.314	2.239	2.235	2.20	2.120	2.080	1.990	2.073		2.235	2.200	2.220	2.130	2.10	2.
T_{∞} °R	405.	399.	406.	412.	399.	394.	391.	392.	430.		403.	421.	401.	399.	397.	400.
(Re_{∞}/FT) x 10^{-6}	3.395	5.956	3.061	1.802	5.805	8.102	10.73	9.761	.9165		3.892	1.305	4.70	5.219	6.58	4.
$R_{e_{\infty}}$ D	8.572	15.04	7.729	4.550	6.289	9.777	11.624	10.57	3.642		4.687	4.350	5.092	5.654	7.128	5.
M_{∞}	22.88	23.70	22.68	22.50	22.55	21.78	21.49	20.54	20.36		22.74	21.88	22.67	21.80	21.49	21.

FOLDOUT FRAME 2

TABLE 6. FREE STREAM PROPERTIES AT THE TRANSITION ALTITUDE

214	215	B16		B101	B102/ B103		C01	C02	C03	C04	C05	C06		C101	C102	C103
⊠	⊏	⊠		⊡	⊡		▷	△	▷	▷	◇	▷		◇	◇	◸
7.13	16.46	27.43		35.66	33.83		22.56	19.51	7.47	10.97	26.21	19.51		37.19	26.82	32.31
1.843	9.621	1.761		.523	.640		3.713	5.975	38.486	22.791	2.118	5.975		.422	1.931	.849
2.874	15.49	2.739		.764	1.016		5.906	9.611	55.90	36.68	3.316	9.611		.606	3.011	1.292
6.04	5.19	5.94		6.83	6.54		6.58	5.01	3.06	4.05	6.85	6.04		6.53	6.46	6.71
4.	217.	224.		236.	233.		219.	217.	239.	217.	223.	217.		243.	223.	229.
1.187	5.446	1.114		.339	.140		2.708	3.389	11.09	10.43	1.555	4.078		.265	1.335	.582
9.	54.	90.		117.	111.		74.	64.	24.5	36.	86.	64.		122.	88.	106.
8.5	201.	36.78		10.92	14.20		77.56	124.8	803.8	476.	44.25	124.9		9.818	40.33	17.74
1.794	9.67	1.71		.477	.634		3.687	6.00	34.9	22.9	2.07	6.00		.3786	1.88	.8066
1.98	1.675	1.950		2.24	2.145		2.160	1.645	1.005	1.330	2.240	1.984		2.240	2.12	2.20
1.	399.	402.		429.	420.		394.	390.	431.	390.	401.	390.		437.	402.	412.
1.619	16.60	3.395		1.034	1.338		8.255	10.33	33.8	31.78	4.740	12.43		.8086	4.068	1.774
4.524	20.75	4.244		2.611	3.345		6.109	12.48	46.47	43.70	2.70	9.261				
9.46	17.36	19.94		22.05	21.38		22.19	17.03	9.88	13.76	22.87	20.50		21.82	21.61	22.15

204	S105	S106	S107	S108		T01	T02	T03	T04	T05	T06	T07	T08	T10		T101
◇	◇	◇	◇	◇		○	○	○	▽	○	○	○	○	▽		◇
.30	23.77	25.60	25.91	35.66		39.62	31.09	36.88	34.14	39.17	38.71	38.40	38.71	29.76		35.05
.436	3.077	2.325	2.219	.523		.302	1.017	.440	.650	.322	.342	.357	.342	1.400		.570
.828	4.866	3.646	3.476	.764		.429	1.557	.634	.967	.452	.483	.505	.483	2.162		.839
.49	6.40	6.31	6.22	6.86		6.86	6.89	6.89	6.77	6.64	6.30	6.85	6.86	6.70		6.81
.	220.	222.	222.	236.		219.	226.	242.	234.	248.	247.	246.	247.	226.		237.
.712	2.159	1.585	1.487	.341		.181	.724	.281	1.091	.756	.769	.737	.705	.739		.944
.	76.	84.	85.	117.		130.	102.	121.	112.	123.5	127.	126.	127.	95.		115.
.87	64.26	48.56	46.35	10.92		6.31	21.25	9.20	13.58	6.72	7.146	7.450	7.146	29.23		11.91
.39	3.038	2.276	2.170	.477		.264	.973	.396	.604	.282	.3016	.3155	.3016	1.350		.524
.130	2.10	2.070	2.040	2.25		2.25	2.26	2.260	2.222	2.180	2.067	2.248	2.250	2.197		2.235
.	397.	400.	400.	429.		449.	410.	435.	421.	447.	444.	443.	444.	406.		426.
.219	6.58	4.53	4.532	1.039		.553	2.208	.8567	1.317	.576	.5861	.6687	.640	3.003		1.140
.654	7.128	5.232	4.910	2.623		1.863	5.575	2.163	3.325	2.304	2.344	2.246	2.149	2.252		2.878
.80	21.49	21.17	20.85	22.15		21.67	22.73	22.06	22.09	21.05	20.02	21.81	21.79	22.25		22.09

FOLDOUT FRAME 1

	B01	B02	B03	B04	B05	B06	B07	B08	B09	B10	B11	B12	B13	B14	B15	
	□	□	□	□	□	□	□	□	⧄	□	⊠	⊠	□	⊠	□	
$(R_e/M) \times 10^{-6}$	13.45	11.02	4.92	4.43	4.36	7.00	10.07	15.78	39.11	.643	.336	.272	2.116	.384	1.818	
$(R_e/FT) \times 10^{-6}$	4.10	3.36	1.50	1.35	1.33	2.13	3.07	0.481	11.92	0.196	.1025	.0828	.645	.117	.554	
$(R_{N_0}/R_B \text{ Local}) \times 10^2$	.785	1.7	1.05	.426	.90	4.09	4.09	15.3		33.	32.9	32.9	32.9	33.8	32.0	32
M_e	14.73	12.83	12.00	12.13	11.65	7.81	7.21	3.68	2.91	3.40	3.69	3.78	3.38	3.45	3.43	3
P_e/P_∞	5.75	16.01	15.21	14.85	17.02	9.45	6.87	5.03	1.38	5.18	3.77	5.41	4.11	5.64	4.36	5
ρ_e/ρ_∞	3.149	5.140	4.485	4.512	4.848	1.140	1.058	.262	1.23	.251	.293	.290	.248	.266	.258	.
u_e/u_∞	.995	.989	.987	.988	.986	.958	.955	.766	.969	.736	.813	.763	.754	.740	.752	.
Tw/T_∞	1.235	1.796	1.626	1.361	1.474	2.253	2.359	2.205	1.875	1.919	1.650	1.614	2.82	1.787	2.40	1.
$hw/hr \times 10^2$	1.79	2.03	1.93	1.83	1.79	2.58	4.24	3.20	69.0	2.78	3.60	2.2	5.60	2.44	4.32	2.
$R_{e_\delta} \times 10^{-6}$	49.43	29.13	21.31	18.8	15.55	7.17	10.34	1.45	13.71	.806	.404	.326	2.53	.443	2.36	.
$R_{e_{\delta^*}} \times 10^{-4}$	5.95	3.36	2.79	2.70	2.30	1.00	1.29	.309	1.502	.229	.430	.283	.413	.243	.386	.
$R_{e_{\delta^*}} \times 10^{-4}$	5.40	2.83	2.24	2.25	1.86	.70	.872	.053	.733	.0314	.0692	.0384	.0710	.0318	.0609	.
$R_{e_\theta} \times 10^{-4}$	.177	.146	.134	.126	.113	.0830	.1044	.044	.141	.0332	.0622	.0445	.0519	.0390	.0415	.
$\bar{m} \times 10^3$	○	○	○	○	○	○	○	○	○	○	○	○	○	○	○	(

FOLDOUT FRAME 2

TABLE 7A. CALCULATED LOCAL FLOW PROPERTIES ON THE FRUSTUM

14	B15	B16	B101	B102/B103	C01	C02	C03	C04	C05	C06	C101	C102	C103
1	□	⊠	◻	◻	◸	△	◺	◺	◊	◺	◊	◯	◸
84	1.818	.390	7.447	9.941	8.963	9.974	12.68	8.724	10.86	6.201	5.085	11.06	12.98
17	.554	.119	2.27	3.03	2.732	3.04	3.865	2.659	3.31	1.89	1.55	3.37	3.956
	32.0	32.9	1.72	1.74	5.86	3.67	10.2	10.2	4.29	8.33	.873	3.91	1.84
5	3.43	3.60	12.60	11.15	5.96	8.0	2.84	3.07	9.06	4.92	11.80	8.8	11.2
4	4.36	5.43	15.35	21.34	23.07	3.83	4.578	7.73	16.18	15.49	15.91	17.98	1.28
66	.258	.275	5.031	5.836	1.860	.897	.573	.585	2.507	.990	4.49	3.457	5.877
40	.752	.756	.989	.985	.921	.965	.770	.755	.966	.864	.986	.972	.984
37	2.40	1.638	1.625	1.957	3.358	5.462	6.960	6.667	4.140	8.205	2.288	5.970	2.670
1	4.32	2.25	1.93	2.50									
13	2.36	.468	19.46	20.46	5.3	21.4	9.18	6.316	12.33	4.35	18.0	22.0	25.4
13	.386	.324	2.70	2.54	.762	2.063	1.044	.792	1.55	.748	2.58	2.24	3.79
18	.0609	.0508	2.24	2.03	.421	1.912	.397	.238	1.18	.269	2.12	1.96	3.09
90	.0415	.0506	.119	.131	.1009	.190	.123	.113	.108	.127	.124	.208	.193
	○	○	○	○	.908	.485	.183	.208	.273	.930	.0071	1.8	2.21

FOLDOUT FRAME 1

	S01	S02	S03	S04	S05	S07	S08	S09	S10		S101	S102	S103	S104	S105
	◇	◇	◇	◇	◊	×	◇	◇	◇		⌀	⌀	⌀	⌀	⌀
$(R_e/M) \times 10^{-6}$	20.24	33.89	18.50	13.45	4.888	9.317	16.73	1.378	6.824		6.102	2.283	5.451	7.119	4.331
$(R_e/FT) \times 10^{-6}$	6.17	10.3	5.64	4.10	1.49	2.84	5.10	0.42	2.08		1.86	.696	1.57	2.17	1.32
$(R_{N_0}/R_B \text{ Local}) \times 10^2$	1.75	1.75	1.75	1.75	8.65	6.81	4.02	60.5	.425		7.31	7.57	7.42	5.58	7.5
M_e	12.16	12.12	12.16	12.84	6.23	6.90	7.43	3.17	12.33		8.45	7.98	6.91	7.25	5.64
P_e/P_∞	16.18	17.40	16.0	16.0	18.2	17.1	17.2	10.0	13.2		13.9	16.0	18.4	16.6	16.8
ρ_e/ρ_∞	4.54	4.517	4.563	5.182	1.414	1.665	2.055	.494	4.781		1.883	2.102	1.672	1.861	1.192
u_e/u_∞	.987	.9866	.987	.989	.916	.911	.9052	.730	.989		.965	.960	.941	.952	.896
T_w/T_∞	4.11	5.01	5.42	3.64	7.54	2.264	7.033	8.928	4.884		3.102	2.969	8.229	7.769	8.564
$h_w/h_r \times 10^2$															
$R_{e_S} \times 10^{-6}$	51.85	86.5	47.4	34.6	4.78	9.50	17.0	1.18	29.1		7.90	7.49	5.43	7.63	4.36
$R_{e_3} \times 10^{-4}$	6.09	6.32	5.92	6.92	.879	1.87	1.86	.434	6.58		1.86	1.66	1.17	1.22	.764
$R_{e_{\delta^*}} \times 10^{-4}$	5.12	5.66	5.05	5.90	.438	.922	1.22	.082	5.65		1.06	.926	.634	.768	.374
$R_{e_\theta} \times 10^{-4}$	.279	0.310	.270	.298	.133	.269	.180	.062	.266		.234	.219	.158	.156	.112
$\bar{m} \times 10^3$	1.49	.608	1.66	3.9	1.34	3.38	.698	1.03	4.18		4.74	4.36	3.36	1.73	1.69

FOLDOUT FRAME 2

TABLE 7B. CALCULATED LOCAL FLOW PROPERTIES ON THE FRUSTUM

S102	S103	S104	S105	S106	S107	S108	T01	T02	T03	T04	T05	T06	T07	T08	T10		T101
♂	♂	♂	♂	♂	♂	♂	○	○	○	▽	○	○	○	○	▽		♂
[illegible]	5.151	7.119	4.331	3.775	7.447	7.152	3.314	16.21	6.463	9.416	3.478	3.773	4.002	3.871	12.63		8.661
.696	1.57	2.17	1.32	1.15	2.27	2.18	1.01	4.94	1.97	2.87	1.06	1.15	1.22	1.18	3.85		2.64
.57	7.42	5.58	7.5	7.5	5.73	1.75	0.94	1.75	1.75	1.75	1.06	1.06	1.14	1.13	4.09		1.75
.98	6.91	7.28	5.64	5.99	7.54	12.3	11.80	12.83	12.70	12.52	11.68	11.64	11.90	11.80	12.47		13.73
.0	18.4	16.8	16.8	16.0	15.5	15.9	14.9	16.3	15.7	15.6	14.1	12.9	14.9	15.0	9.57		15.6
.192	1.672	1.861	1.192	1.305	2.032	4.885	4.167	5.118	5.151	4.98	4.29	4.343	4.374	4.344	2.985		5.153
.960	.941	.952	.896	.914	.956	.988	.987	.989	.989	.988	.986	.987	.987	.987	.988		.989
.969	8.229	7.769	8.564	7.125	7.750	4.709	4.01	4.39	4.14	4.28	4.027	4.054	4.063	4.054	4.433		4.225
							-.392	-.382	-.385	-.40	-.418	-.465	-.391	-.393	-.406		-.396
.49	5.43	7.63	4.36	3.86	7.91	18.4	11.1	41.1	16.5	24.1	14.6	16.1	15.8	15.3	12.5		22.0
.66	1.17	1.22	.764	.796	1.43	5.70	3.56	10.40	6.36	4.74	4.75	11.3	4.26	4.70	4.54		7.88
.926	.634	.768	.374	.413	.952	4.84	2.94	8.73	5.32	3.96	3.90	9.46	3.65	3.87	3.82		5.95
.219	.158	.136	.112	.110	.139	.247	.174	.479	.277	.207	.217	.491	.201	.222	.279		.346
.36	3.36	1.73	1.69	2.52	1.87	6.53	7.12	6.54	9.64	3.02	7.27	17.7	6.40	7.36	8.8		9.0

TABLE 8. CORRELATION ATTEMPTS BASED ON FRUSTUM CONDITIONS

	Re_∞	$Re_{\infty L}$	$Re_{\infty D}$	$Re_{\infty R'_N}$	$(Re_S)_L$	$(Re)_L$	$(Re_{\delta^*})_L$	$(Re_\theta)_L$	$(Re_\theta/M_e)_L$
ALTITUDE		X				X			
Re_∞				X	X	X			
$Re_{\infty L}$				X	X				
$Re_{\infty D}$							X		
$Re_{\infty R'_N}$	X	X			X	X			
$(Re_S)_L$	X	X		X					
Re_L	X			X					17
$(Re_{\delta^*})_L$									X
$(Re_\theta)_L$									X
$(Re_\theta/Me)_L$						17			
R_{N_o}/R_B			18		X	X			
M_e					15		X	16	
h_w/h_r					19				
P_e									X
P_∞									X
$\bar{m}_L$					20				
$\Delta S/R_{N_o}$					X				

N. B. Numbers in Table refer to Figure number in text which shows correlation attempt.

FOLDOUT FRAME 1

	B01	B02	B03	B04	B05	B06	B07	B08	B09	B10	B11	B12	B13	B14	B15	B16
	□	□	□	□	□	□	□	□	⊘	□	⊠	⊠	□	⊠	□	⊠
$(R_N' \times 10^2)$ -m	.268	.661	.631	.253	.454	.488	.50	1.713	.0244	5.968	5.767	5.764	5.715	5.742	5.968	5.773
$(R_{N_{eff}} \times 10^2)$ -m	.472	.844	.741	.424	.622	1.097	.768	1.713	.0244	5.968	6.462	6.462	5.715	6.462	5.968	6.462
$(S \times 10^2)$ -m	.719	1.768	1.646	.671	1.189	1.317	1.347	4.450	.0616	18.29	14.72	14.69	14.63	14.72	15.24	14.78
$(R_e/m) \times 10^{-6}$	.456	.306	.180	.170	.168	1.327	2.455	2.676	20.06	1.060	.706	.448	4.254	.687	3.543	.670
$R_N' - FT$	.0088	.0217	.0207	.0083	.0149	.016	.0166	.0562	.0008	.1958	.1892	.1891	.1875	.1884	.1958	.1884
$R_{N_{eff}} - FT$	.0155	.0277	.0243	.0139	.0204	.036	.0252	.0562	.0008	.1958	.212	.212	.1875	.212	.1958	.212
$S - FT$	.0236	.058	.054	.022	.039	.0432	.0442	.146	.002	.600	.483	.482	.480	.483	.500	.485
$R_e/FT \times 10^{-5}$	1.390	.934	.548	.518	.513	4.044	7.482	8.158	16.15	3.230	2.153	1.365	12.97	2.093	10.80	2.041
$R_{e_s} \times 10^{-4}$	.328	.542	.296	.114	.200	1.747	3.037	11.91	1.223	19.38	10.4	6.58	62.24	10.11	54.0	9.9
$R_{e_\delta} \times 10^{-2}$	1.696	1.868	1.348	.901	1.108	2.20	4.968	8.240	4.892	.258	40.69	22.80	25.94	27.83	25.38	28.37
$R_{e_{\delta^*}} \times 10^{-1}$	3.350	2.092	1.381	1.404	1.342	4.812	11.75	10.69	21.22	7.687	60.71	22.93	42.0	26.96	37.91	28.74
$R_{e_\theta} \times 10^{-1}$	2.141	1.961	1.655	1.310	1.939	1.832	2.544	5.564	.6115	12.37	54.47	35.16	17.57	39.56	17.99	41.64
M_e	2.734	2.78	2.63	2.815	2.76	2.60	2.61	2.65	2.16	2.77	2.76	2.67	2.64	2.61	2.63	2.63
$\bar{m} \times 10^2$	2.18	1.36	1.65	2.28	1.72	.80	.785	.255	0	.08	.194	.178	.09	.127	.06	.136
$\dot{m}/\dot{m}_{bl}$	.175	.161	.146	.108	.111	.223	.254	.184	0	.08	.15	.21	.110	.206	.110	.207
$\bar{m}$ max $\times 10^2$	2.37	1.68	2.01	2.73	2.13	.897	.862	.283	0	.09	.238	.217	.10	.139	.110	.163
$\bar{m}$ stag $\times 10^2$	2.30	1.68	2.01	2.71	2.09	.895	.852	.283	0	.09	.152	.142	.07	.009	.08	.105

FOLDOUT FRAME

TABLE 9A. CALCULATED LOCAL FLOW PROPERTIES IN THE NOSE REGION

2	B13	B14	B15	B16	B101	B101 102	C01	C02	C03	C04	C05	C06	C101	C102	C03
4	5.715	5.742	5.968	5.773	.631	.640	.716	.707	1.247	1.246	.652	.991	.448	1.335	.637
2	5.715	6.462	5.968	6.462	.585	.844	.963	.707	2.256	1.841	1.006	1.390	.639	1.500	.878
1	14.63	14.72	15.24	14.78	1.676	1.737	1.914	1.890	3.414	3.38	1.759	2.643	1.189	3.438	1.792
18	4.254	.687	3.543	.670	.225	.295	1.531	2.037	13.65	9.222	.847	2.501	.185	1.216	.355
91	.1875	.1884	.1958	.1894	.0207	.0210	.0235	.0232	.0409	.0407	.0214	.0325	.0147	.0438	.0209
2	.1845	.212	.1958	.212	.0192	.0277	.0316	.0232	.074	.0604	.033	.0456	.0213	.0492	.0288
2	.480	.483	.500	.485	.055	.057	.0628	.062	.112	.111	.0577	.0867	.039	.1128	.0588
5	12.97	2.093	10.80	2.041	.676	.898	4.666	6.210	41.61	28.1	2.582	7.624	.564	3.706	1.081
	62.24	10.11	54.0	9.9	.372	.512	2.93	3.55	46.6	31.2	1.49	6.61	.220	4.18	.636
	25.94	27.83	25.38	28.37	1.075	1.706	4.036	7.638	27.05	19.95	3.563	5.718	1.528	23.24	1.816
	42.0	26.90	37.91	28.74	1.325	2.209	5.786	19.87	107.8	52.43	4.622	9.454	1.963	16.42	2.246
	17.5	39.56	17.99	41.64	1.174	1.495	2.33	4.130	—	—	1.120	3.194	1.455	37.43	1.719
	2.64	2.61	2.63	2.63	2.76	2.69	2.54	2.77	2.39	2.48	2.70	2.58	2.81	3.23	2.74
3	.09	.127	.06	.136	1.38	1.60	.755	.968	.0544	.087	1.0	.41	2.43	3.45	4.18
	.110	.206	.110	.207	.181	.187	.256	.254	—	.231	.188	.232	.138	.177	.173
1	.10	.139	.110	.163	1.64	2.00	.968	.909	.058	.104	1.25	.498	2.88	3.62	1.62
1	.07	.009	.08	.105	1.64	1.99	.963	.881	.054	.094	1.25	.492	2.80	3.56	1.62

FOLDOUT FRAME 1

	S01	S02	S03	S04	S05	S07	S08	S09	S10	S101	S102	S103	S104	S105	S106	S
	◇	◇	◇	◇	◊	×	◇	◇	◇	ó	ó	ó	ó	ó	ó	(
$(R_x' \times 10^2)$ - m	.661	.668	.661	.652	1.247	1.259	.689	3.64	.265	1.314	3.880	1.341	1.[illegible]	1.359	1.337	1.(
$(R_{x_{eff}} \times 10^2)$ - m	.844	.668	.844	.520	1.524	1.355	1.015	3.81	.338	1.271	3.81	1.408	.951	1.512	1.463	1.(
$(S \times 10^2)$ - m	1.768	1.780	1.768	1.737	3.273	3.261	1.890	9.540	.707	3.392	10.1	[illegible].42	2.59	3.48	3.47	2.(
$(R_e/M) \times 10^{-6}$	.645	1.319	.594	.345	1.087	1.543	1.884	1.792	.556	.837	.284	1.148	1.378	1.507	1.422	1.3
R_x' - FT	.0217	.0219	.0217	.0214	.0409	.0413	.0226	.1195	.0087	.0431	.1273	.0416	.0331	.0446	.0442	.(
$R_{x_{eff}}$ - FT	.0277	.0219	.0277	.0302	.050	.0346	.0333	.125	.0111	.0417	.125	.0462	.0312	.0496	.0480	.0
S - FT	.058	.0584	.058	.057	.1074	.1070	.062	.3130	.0232	.1113	.3314	.1123	.085	.1143	.1140	.0
$(R_e/FT) \times 10^{-5}$	1.966	4.020	1.812	1.053	3.314	4.706	5.741	5.463	1.694	2.550	0.867	3.500	4.200	4.593	4.33	4.0
$R_{e_s} \times 10^{-4}$	1.140	2.348	1.054	0.60	3.37	5.036	3.56	17.10	.393	2.838	2.872	3.93	5.57	5.25	4.94	3.4
$R_{e_t} \times 10^{-2}$	2.811	13.76	2.645	1.495	5.104	17.22	2.779	9.331	6.268	15.47	11.70	15.75	19.74	20.00	22.30	21.0
$R_{e_t}^* \times 10^{-2}$	.346	1.823	.327	.197	.4345	1.609	.594	1.022	1.035	1.232	.929	1.044	1.456	1.488	1.715	2.0
$R_{e_\theta} \times 10^{-2}$	.249	1.855	.232	.139	.459	2.159	.0518	.754	4.975	2.54	1.925	2.466	3.219	3.075	3.477	4.2
M_e	2.58	2.73	2.60	2.67	2.57	2.67	2.52	2.54	3.77	2.86	2.82	3.09	3.14	2.94	3.28	3.1
$\bar{m} \times 10^2$	1.21	2.07	1.33	1.35	.340	.158	.786	.186	3.66	.236	.218	2.83	3.54	2.56	3.05	3.7
$\dot{m}/m_{bl}$	.201	.121	.216	.210	.105	.192	.343	.161	.049	.152	.200	.230	.187	.242	.203	.14
$\bar{m}$ max $\times 10^2$	1.47	2.12	1.64	1.61	.396	.158	.810	.228	3.92	.237	.218	2.90	3.44	2.62	3.17	3.89
$\bar{m}$ stag $\times 10^2$	1.47	1.49	1.64	1.61	.390	.147	.810	.228	3.48	.195	.209	2.84	3.31	2.53	3.13	3.54

FOLDOUT FRAME 2

TABLE 9B. CALCULATED LOCAL FLOW PROPERTIES IN THE NOSE REGION

S103	S104	S105	S106	S107	S108	T01	T02	T03	T04	T05	T06	T07	T08	T10	T101
○	○	○	○	○	◇	○	○	○	▽	○	○	○	○	▽	○
.7.1	1.009	1.359	1.347	1.006	.631	.457	.863	.786	.640	.640	.768	.640	.640	.469	.802
408	.951	1.512	1.463	1.058	.585	.640	.558	.768	.920	.893	.716	.893	.893	.686	.774
42	2.59	3.48	3.47	2.59	1.706	1.189	2.225	2.030	1.707	1.707	1.969	1.707	1.707	1.253	2.322
348	1.378	1.507	1.422	1.342	.218	.771	.822	.483	.273	.649	.565	.702	.668	.554	.655
0416	.0531	.0446	.0442	.0330	.0207	.015	.0283	.0258	.021	.021	.0252	.0210	.0210	.0154	.0263
0462	.0312	.0496	.0480	.0347	.0192	.0210	.028	.0252	.0302	.0293	.0285	.0292	.0293	.0225	.0254
1123	.085	.1143	.1140	.085	.056	.039	.073	.0[illegible]	.056	.056	.0646	.056	.056	.0411	.0762
500	4.200	4.593	4.33	4.091	.664	2.351	2.507	1.473	.832	1.979	1.721	2.139	2.098	1.689	1.997
03	5.57	5.25	4.94	3.477	.372	.917	1.83	.825	.466	1.108	1.112	1.198	1.175	.694	1.522
75	19.74	20.00	22.30	21.07	1.082	11.36	19.05	10.14	1.315	14.62	10.84	14.01	14.14	2.398	14.82
44	1.456	1.488	1.715	2.056	.133	.850	1.257	.863	.171	1.076	1.050	.986	1.001	.368	1.216
66	3.219	3.075	3.477	4.206	.119	2.389	3.552	2.083	.150	2.955	2.[illegible]52	2.794	2.782	.168	2.898
9	3.14	2.94	3.28	3.19	2.77	5.91	3.[illegible]	4.03	2.77	5.60	5.01	5.54	5.59	2.70	4.56
3	3.54	2.56	3.05	3.76	1.37	15.2	6.31	7.82	1.39	13.0	14.0	11.3	11.8	1.61	8.65
30	.187	.242	.203	.146	.178	.110	.133	.149	.192	.0982	.180	.100	.100	.206	.114
0	3.44	2.62	3.17	3.89	1.67	15.81	6.33	8.53	1.67	13.65	14.16	11.83	12.36	1.77	9.05
4	3.31	2.53	3.13	3.54	1.67	14.87	5.79	8.42	1.67	12.57	12.49	10.89	11.38	1.69	8.85

TABLE 10. CORRELATION ATTEMPTS BASED ON NOSE TIP CONDITIONS

	$(Re_S)_{2R'_N}$	$Re_{2R_N'}$	$\bar{\dot{m}}_{2R_N'}$	$\bar{\dot{m}}_{stag}$	$\bar{\dot{m}}_{max}$	$\lambda_{k=1}$	$\lambda_{k=2.5}$	$(\dot{m}/\dot{m}_{bl})_{2R'_N}$
ALTITUDE			X	X	X	X		
Re_∞				X				
Re_{R_B}			X					
$Re_{\infty R_N}$			22			X		
Re_{S_L}	X		X		X			
Re_L		X						
$(Re_{\delta^*})_L$			X			X		
$(Re_\theta)_L$			X			X		
$(Re_\theta/M_e)_L$			X					
$Re_{S_{2R'_N}}$			23				X	25
$Re_{2R'_N}$								X
$(Re_\theta)_{2R'_N}$			26					
$(Re_\theta/M_e)_{2R'_N}$			X					
R_N/R_B					X			
$\Delta S/R'_N$	X		X				X	X
$\Delta S/R'_{N_{eff}}$	X		24					
$\Delta S/\delta_{2R'_N}$			27					X
$\Delta S/\theta_{2R'_N}$	X							
$(Re_{\delta^*})_{2R'}$			X					

N.B. Numbers in Table refer to Figure number in text which shows correlation

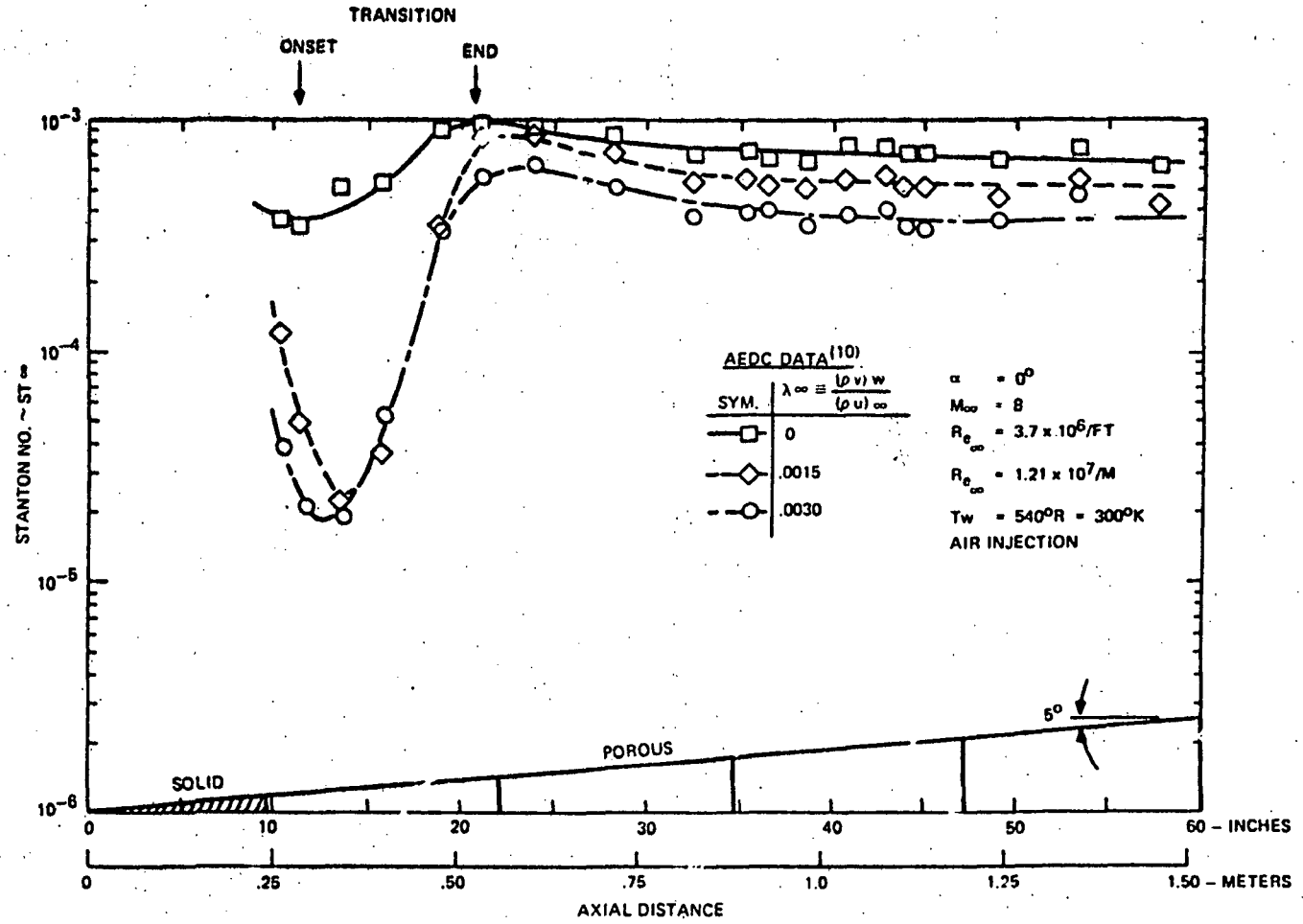

Figure 1. Effect of Frustum Ablation on Transition Location

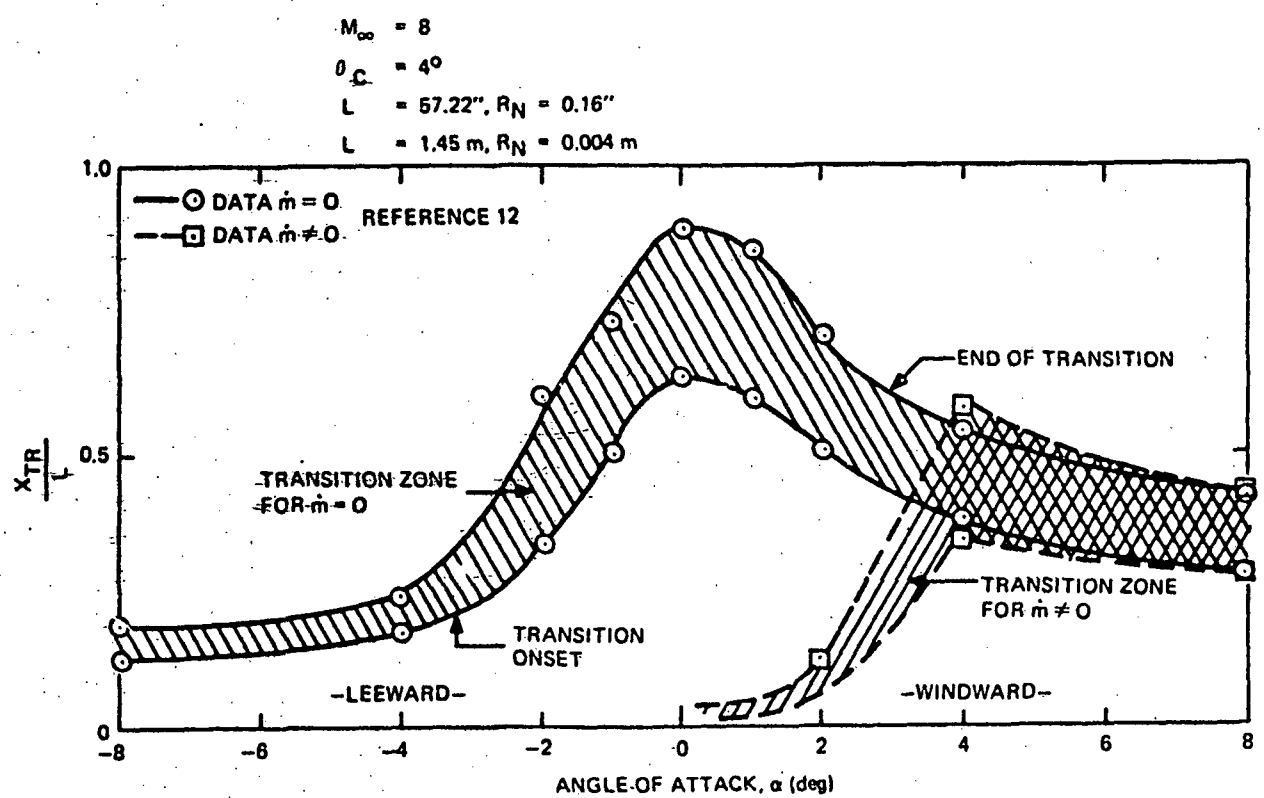

Figure 2. Effect of Nose Blowing on Transition Progression (N_2 Injectant)

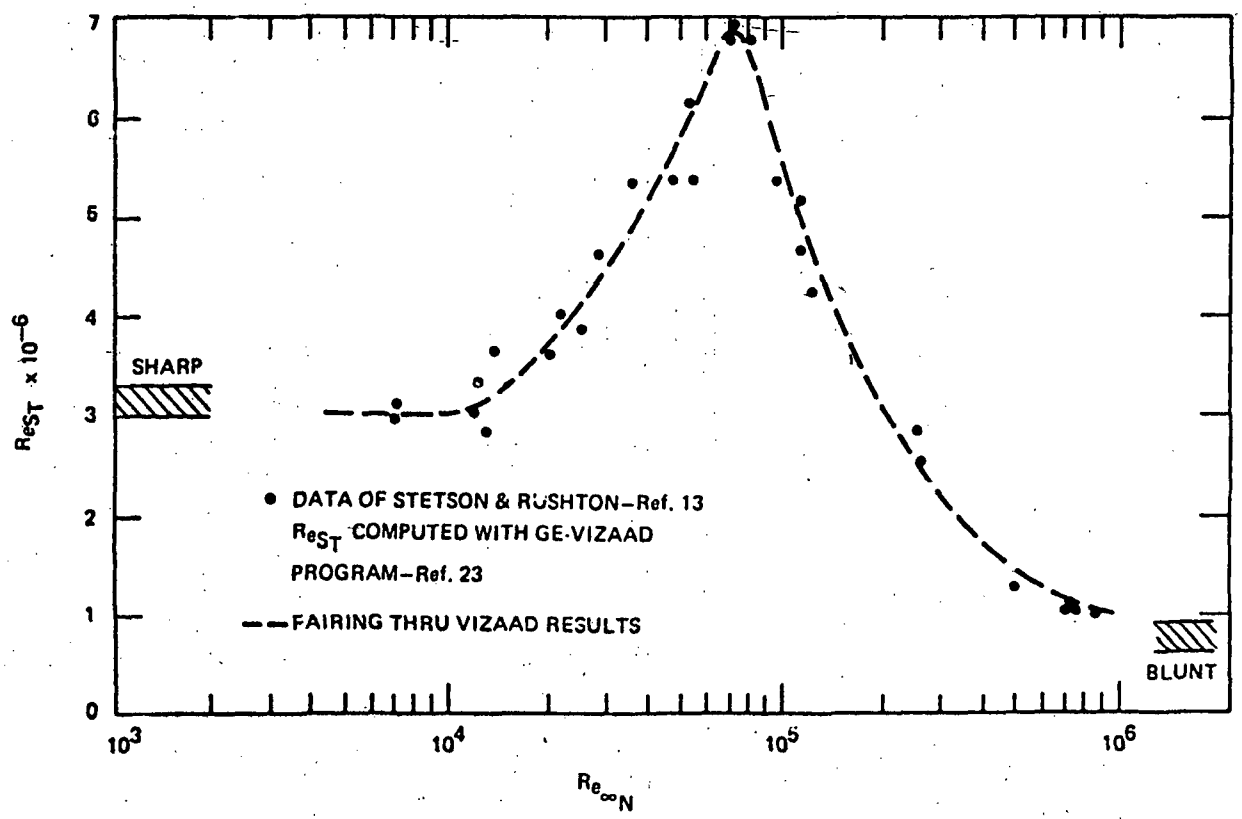

Figure 3. Local Transition Reynolds Number Variation with Bluntness

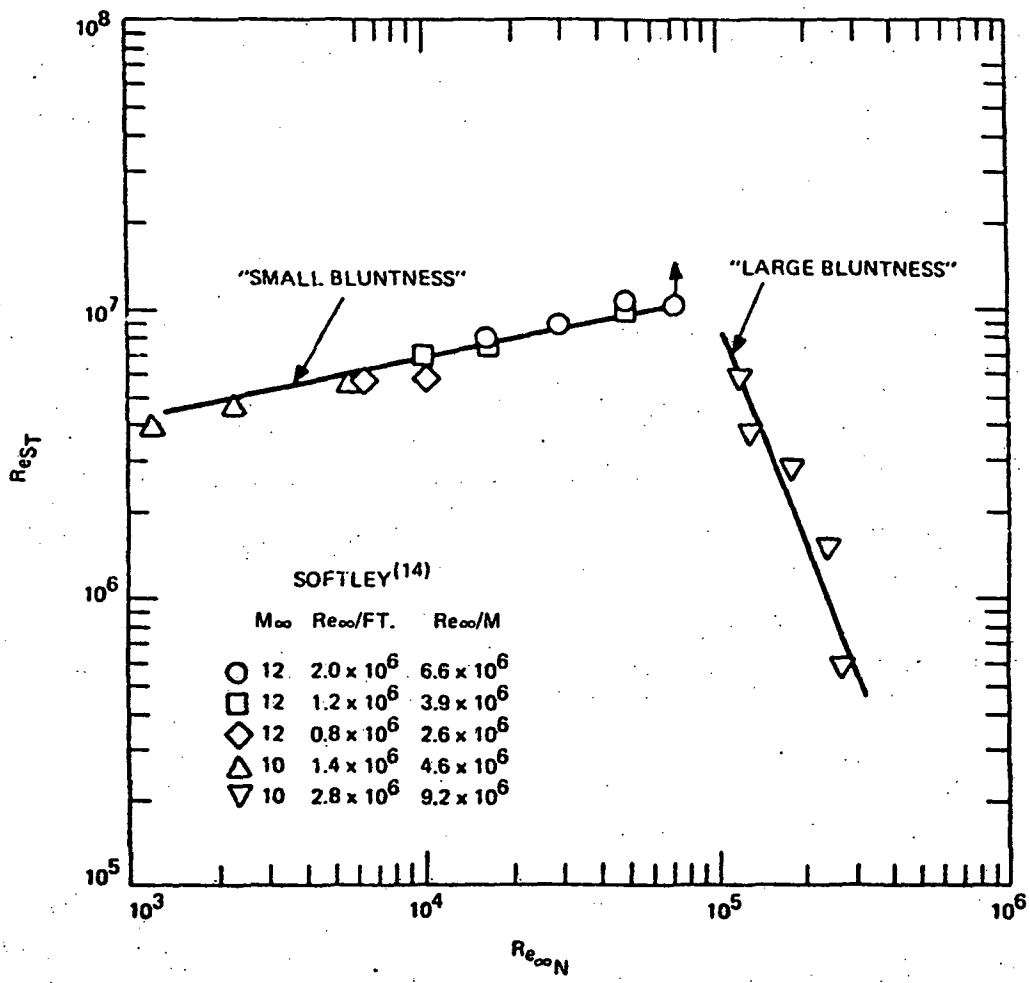

Figure 4. Local Transition Reynolds Number Variation with Bluntness

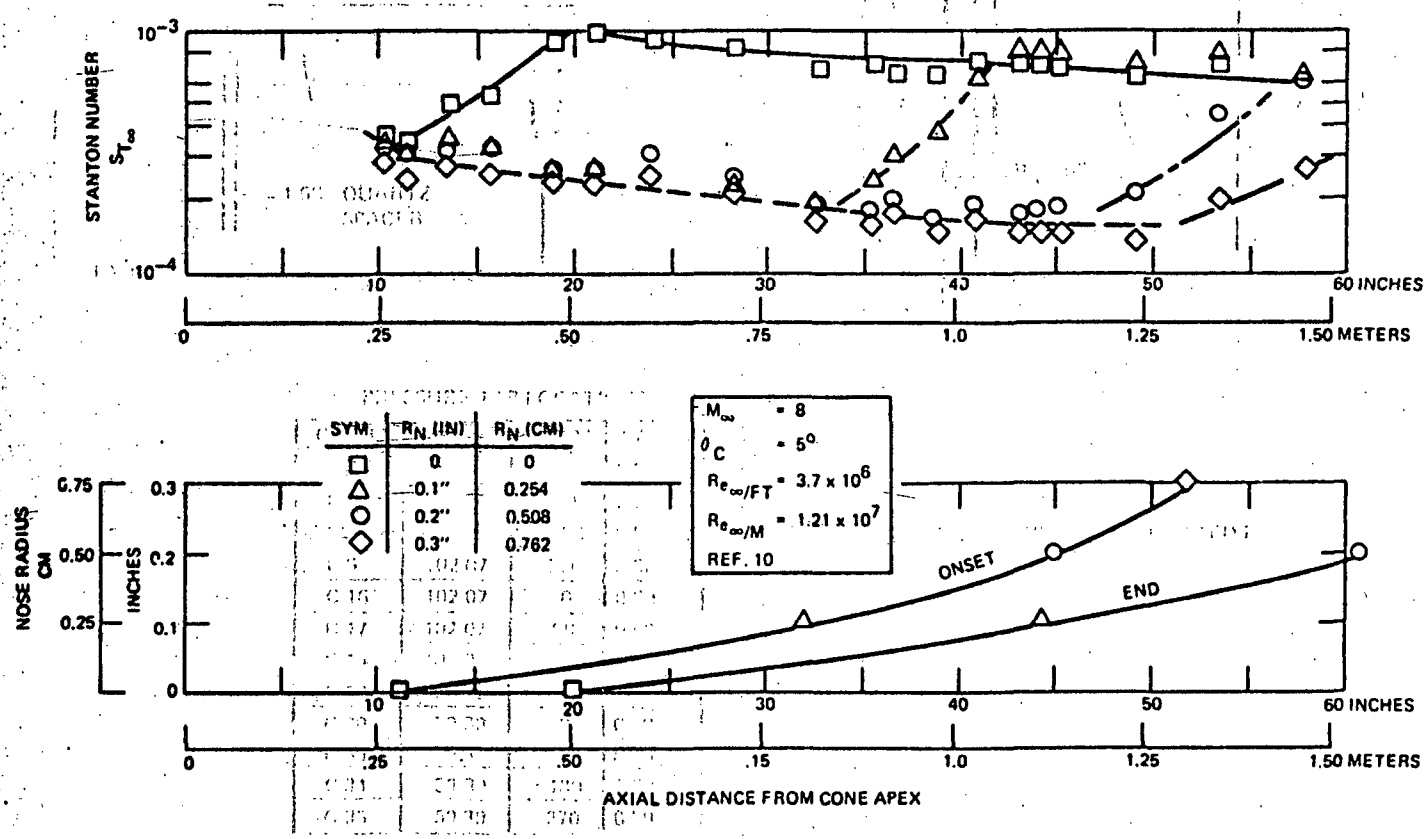

Figure 5. Effect of Nose Bluntness on Transition Location

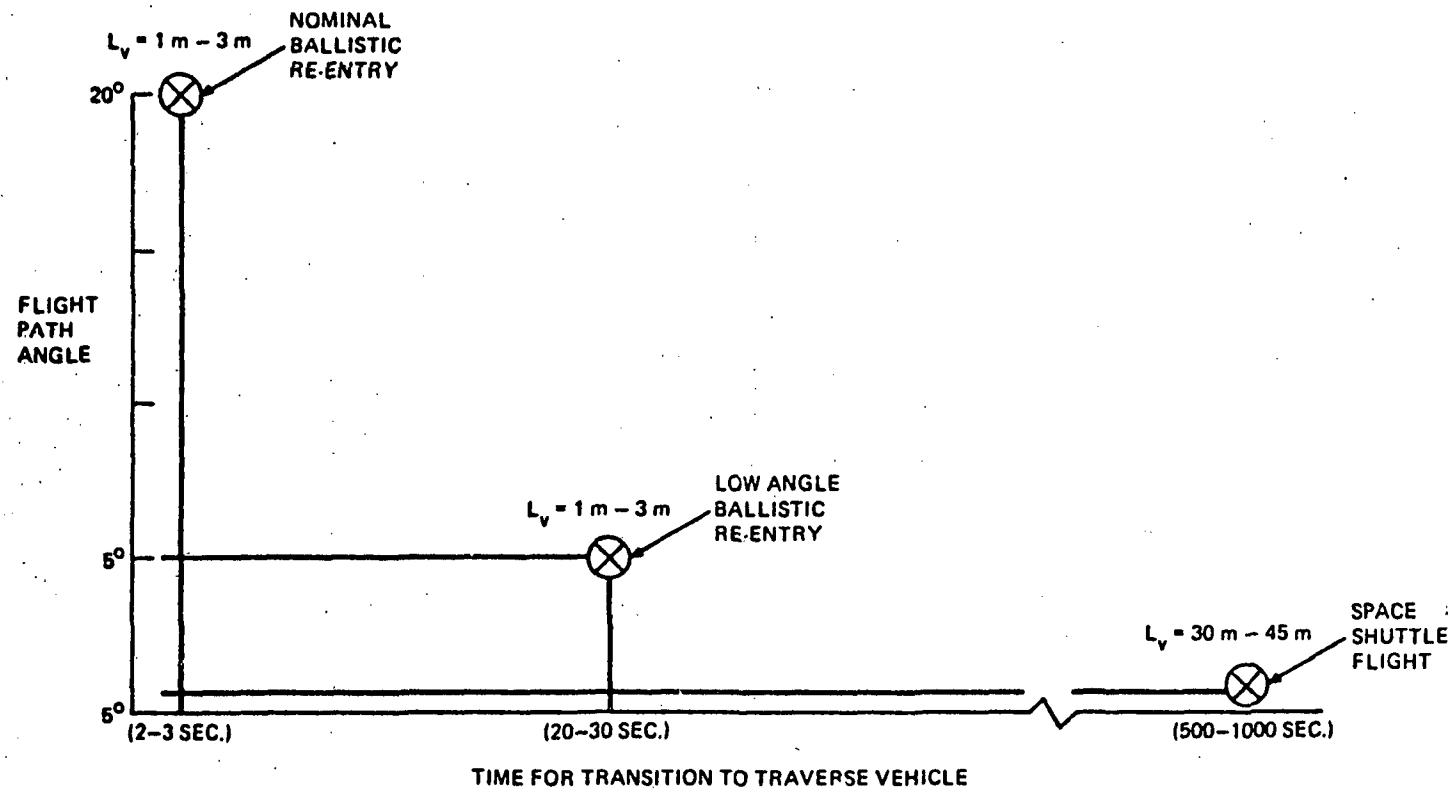

Figure 6. Variation of Transitional Flow Period with Path Angle

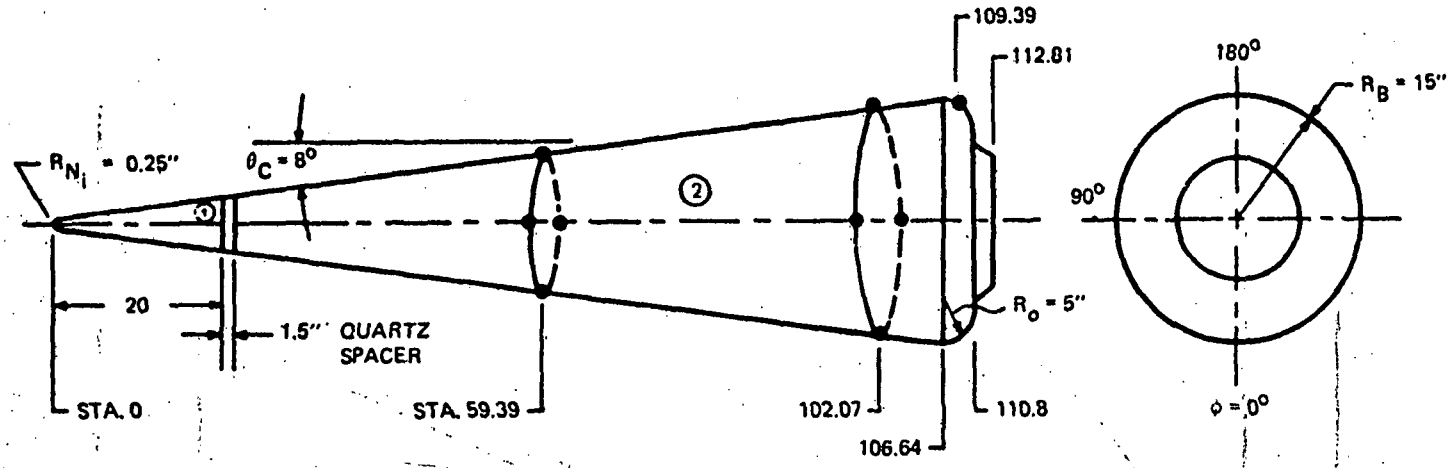

PRESSURE TAP LOCATIONS

CHAN.	STA.	RAD.°	RANGE
C-6	102.07	0	0-50 PSI
C-7	102.07	90	0-50
C-8	102.07	180	0-50
C-9	102.07	270	0-50
C-16	102.07	0	0-50
C-17	102.07	90	0-50
C-18	102.07	180	0-50
C-19	102.07	270	0-50
C-30	59.39	0	0-50
C-33	59.39	90	0-50
C-34	59.39	180	0-50
C-35	59.39	270	0-50

① ② TFE OVER CARBON IMPREGNATED PR

Figure 7. Geometric Details - Vehicle T03

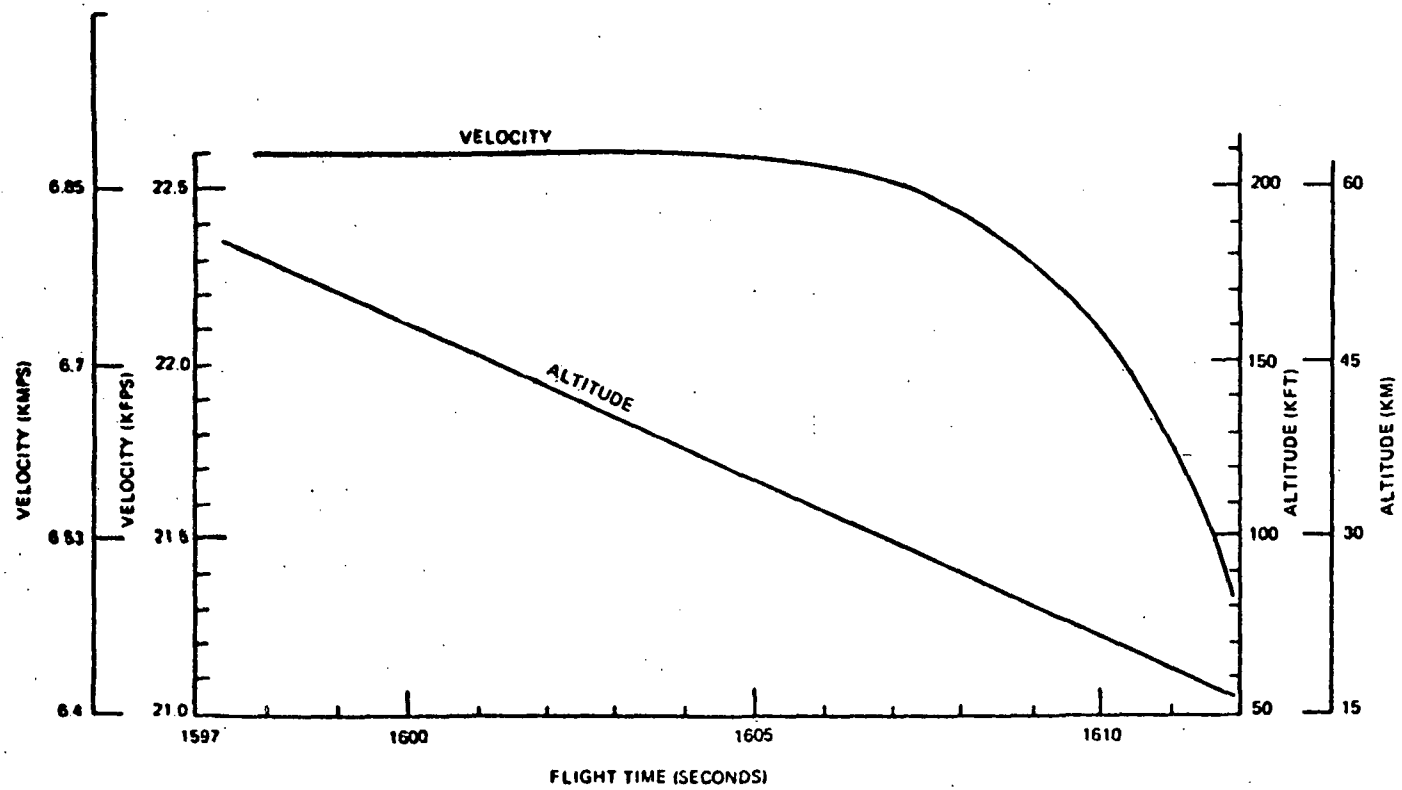

Figure 8. Post Flight Trajectory - Vehicle T03

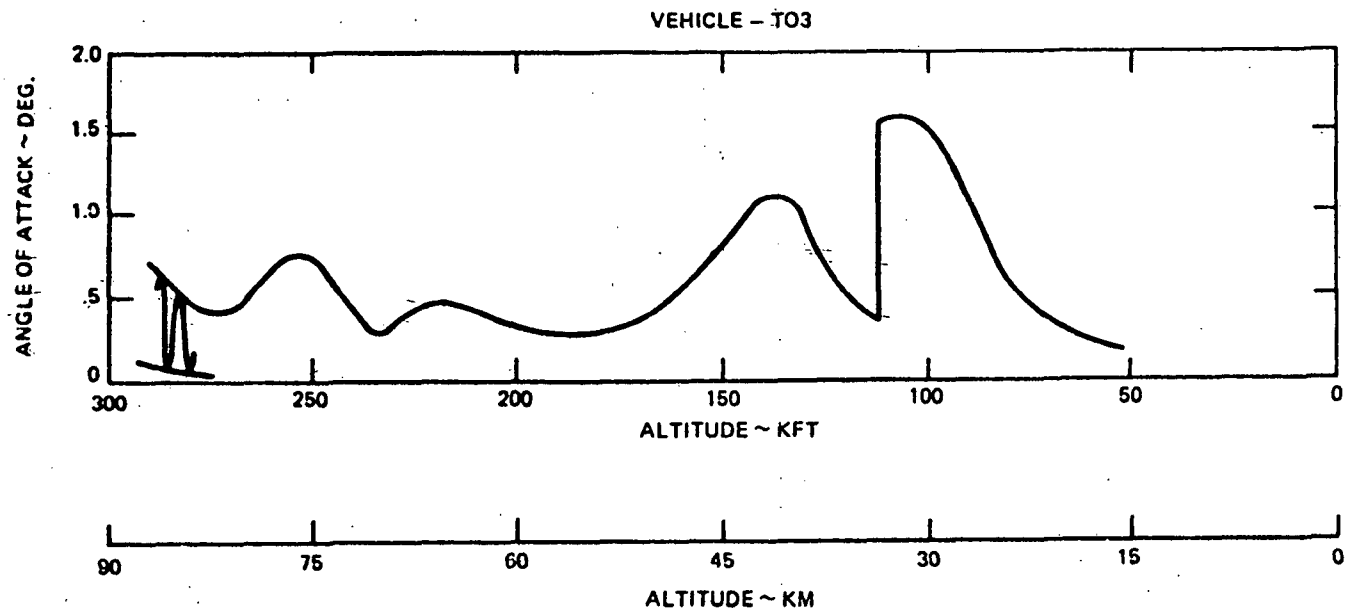

Figure 9. Angle of Attack Variation with Altitude

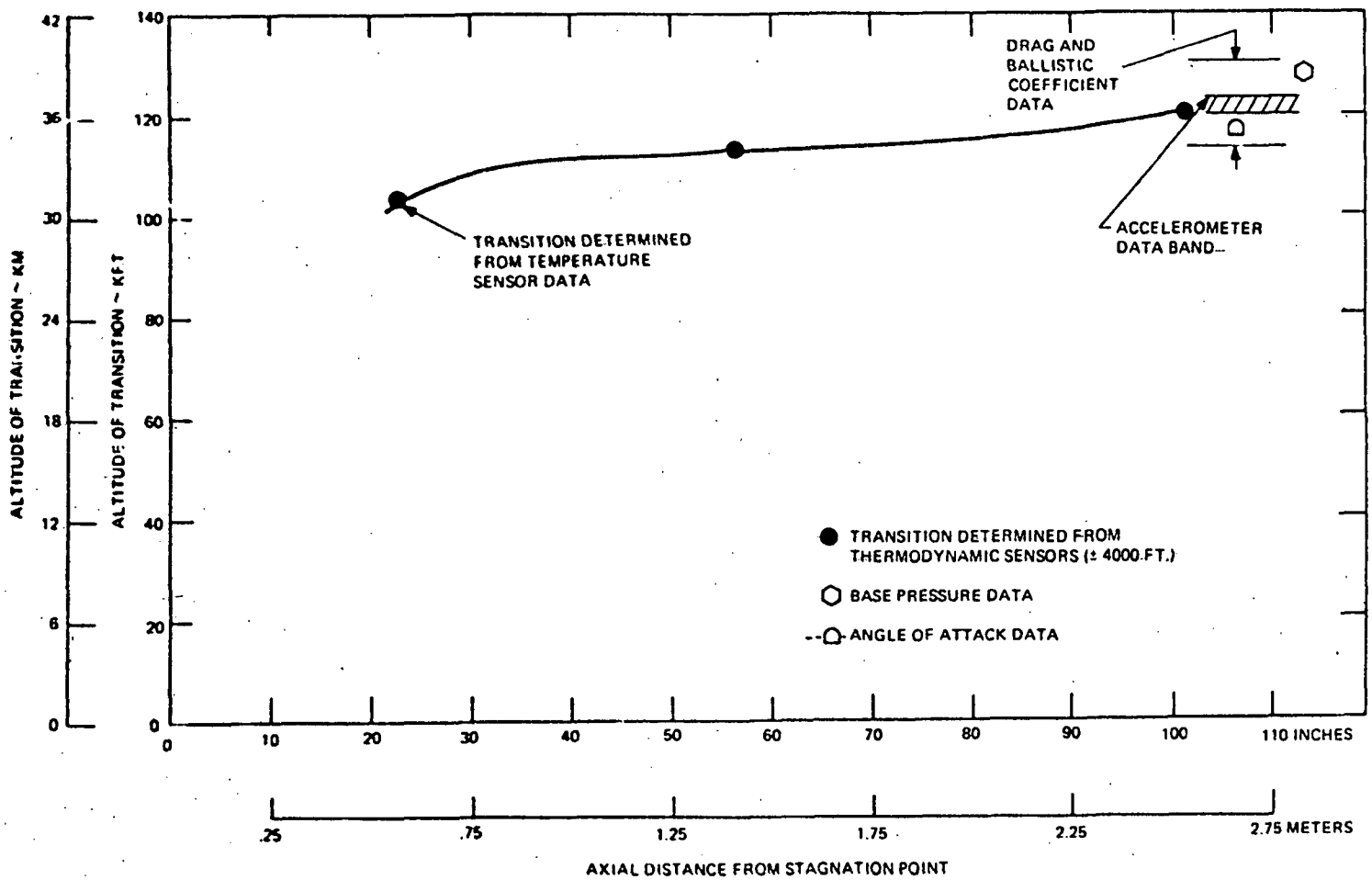

Figure 10. Boundary Layer Transition History - Vehicle T03

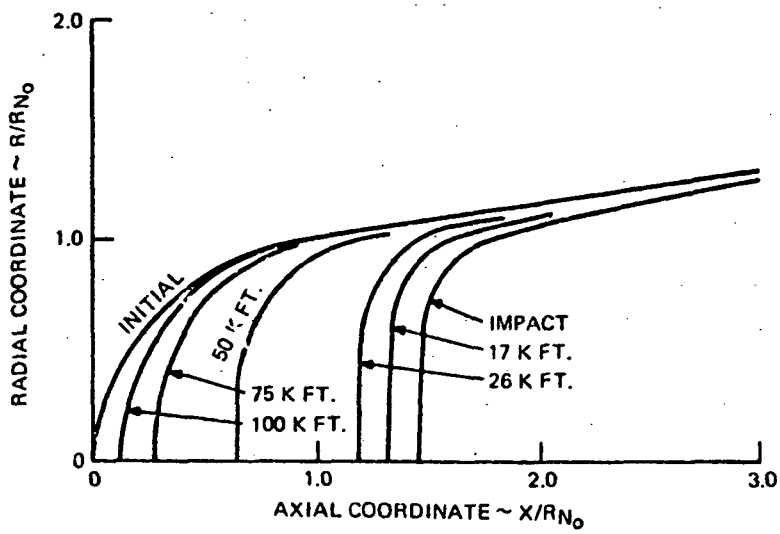

(A) VEHICLE C03

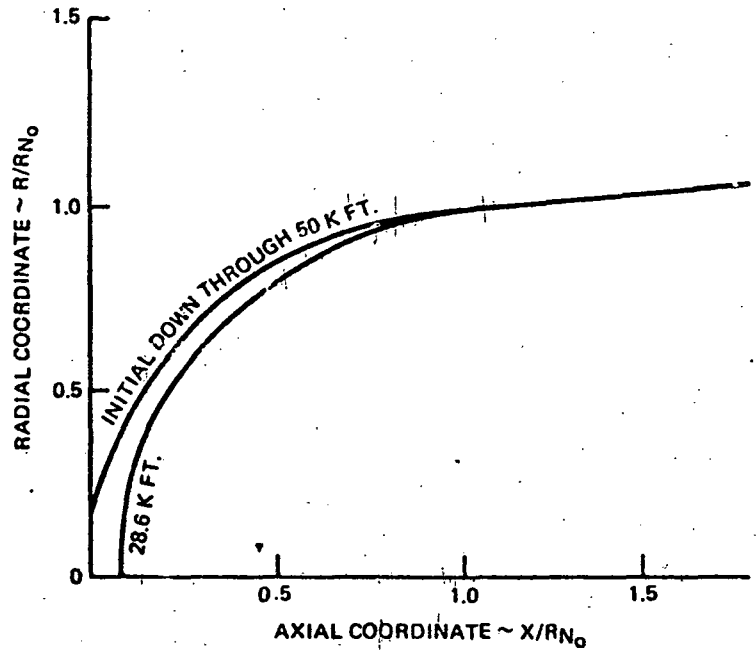

(B) VEHICLE B13

Figure 11. Computed Nose Tip Shapes During Re-entry

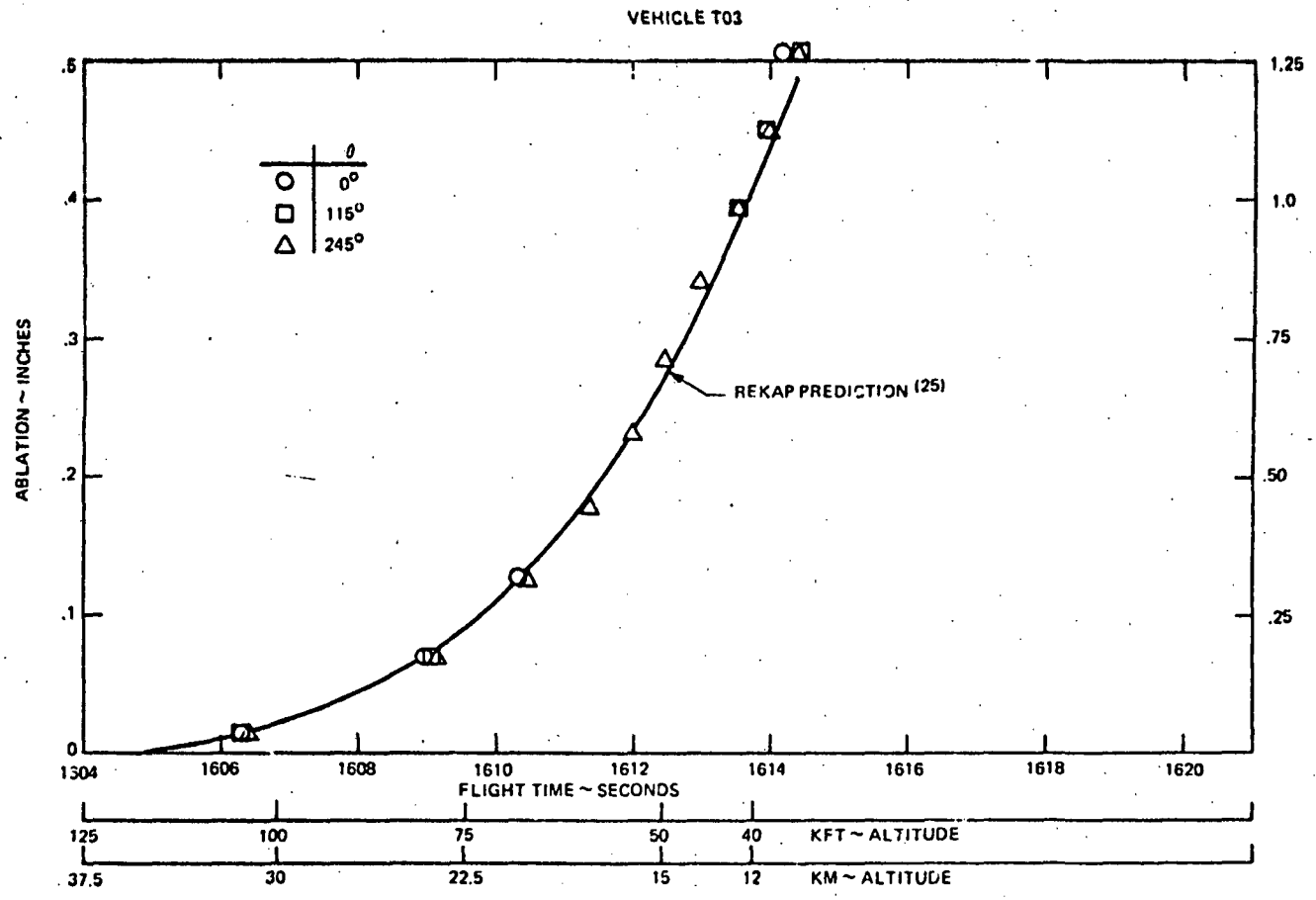

Figure 12. Measured and Predicted Ablation Histories (Sta. 55.86)

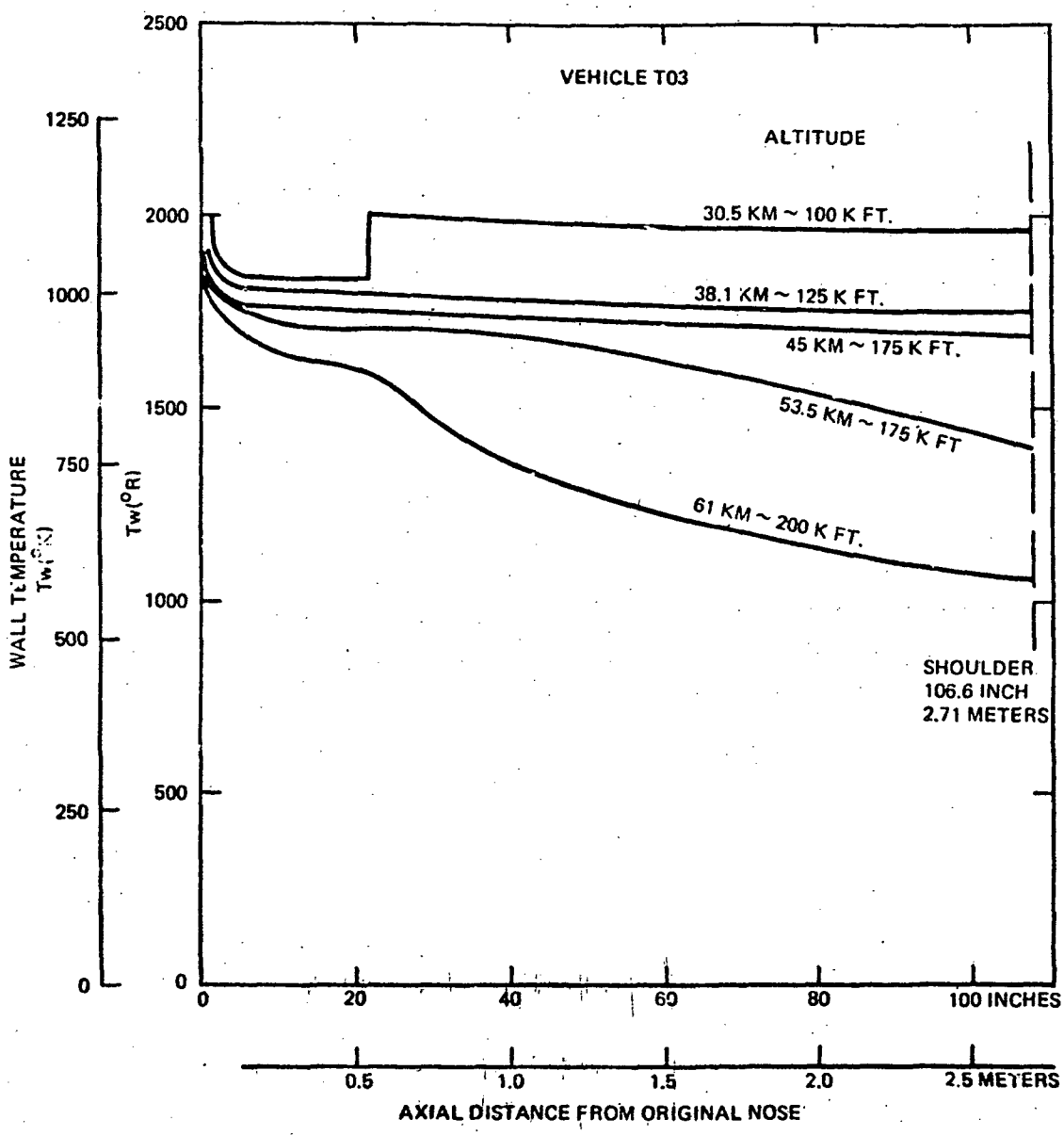

Figure 13. Axial Distribution of Vehicle Wall Temperature - Vehicle T03

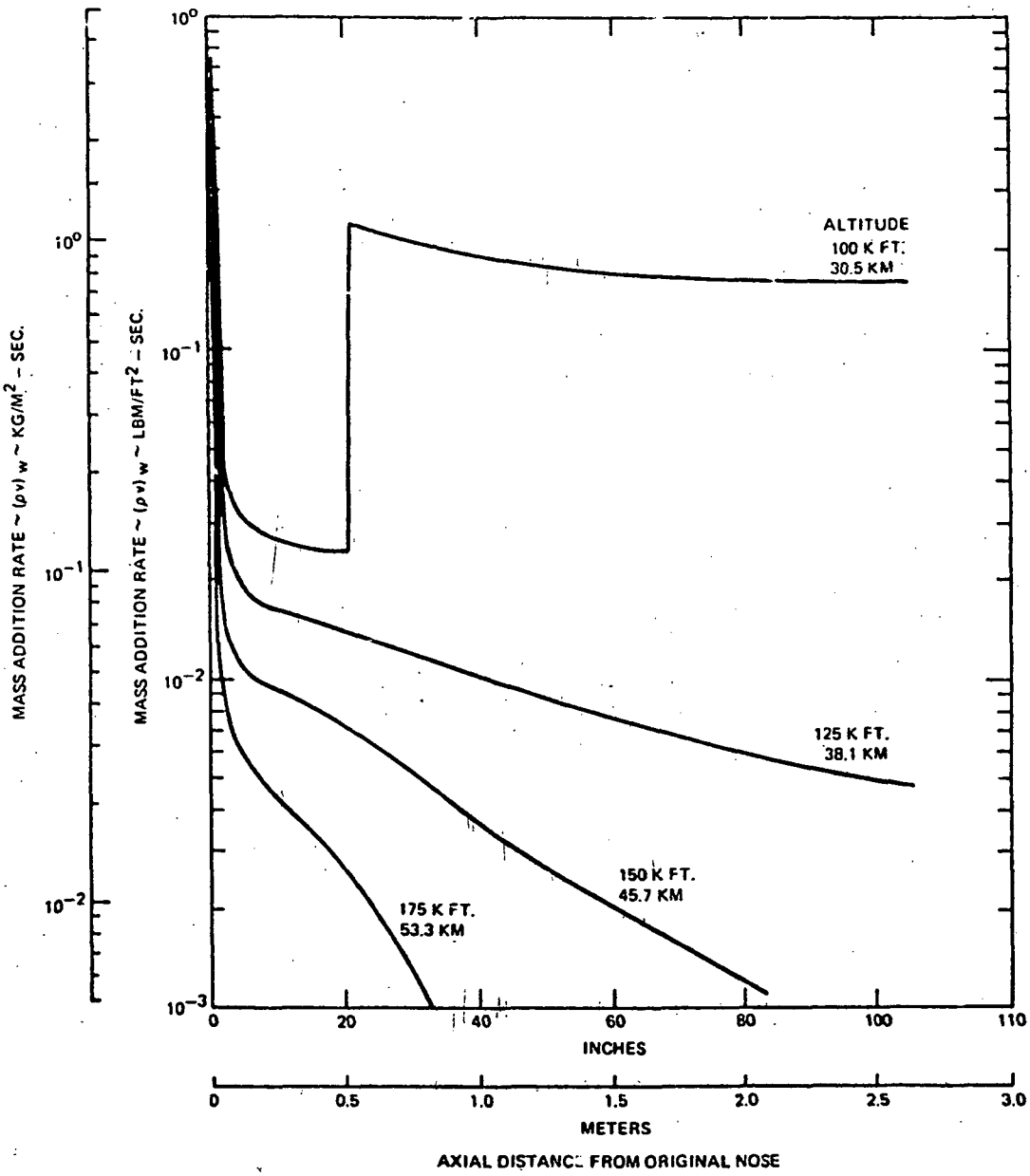

Figure 14. Axial Distribution of Mass Addition Rate - Vehicle T03

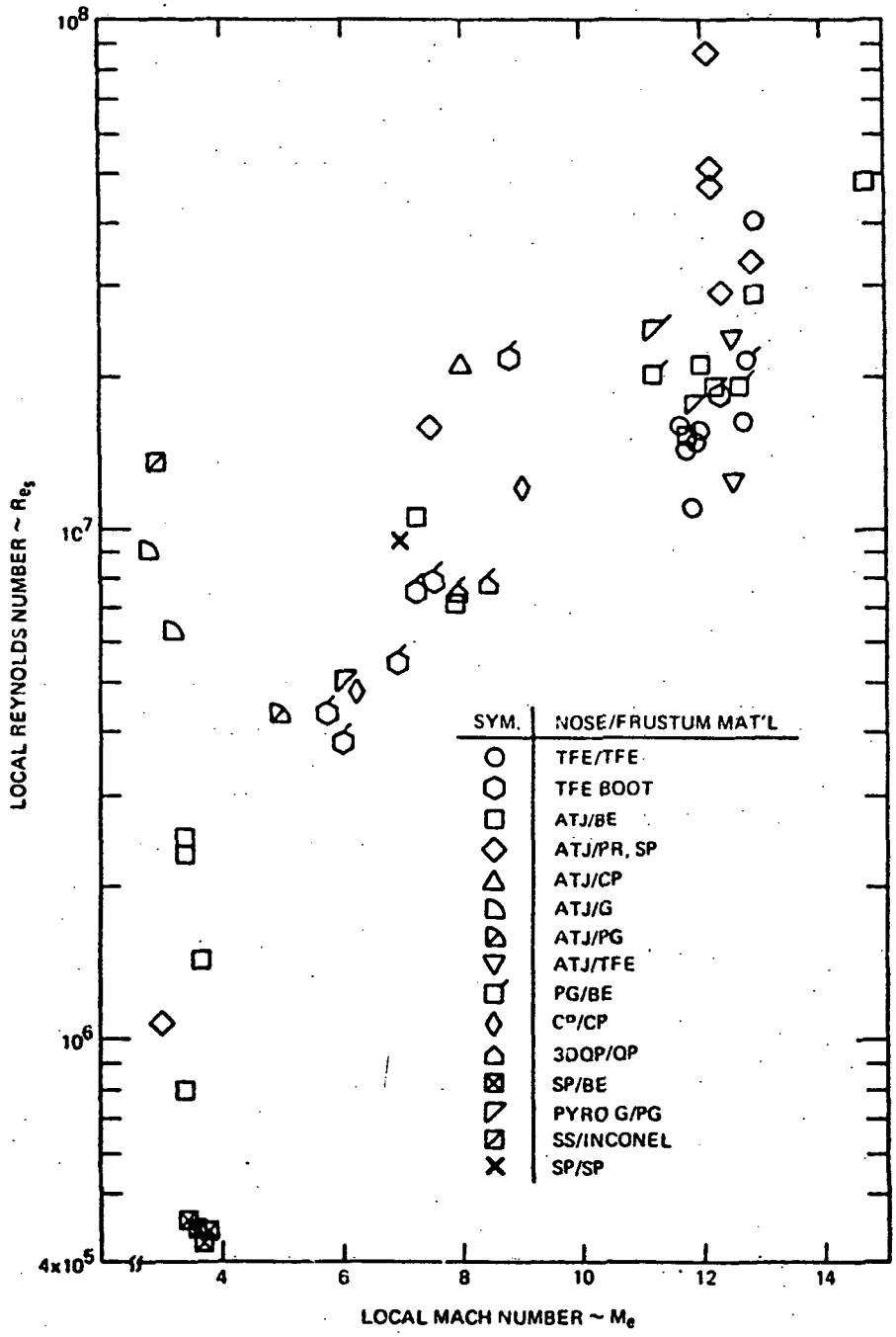

Figure 15. Flight Data Correlation Using Frustum Parameters; R_{e_s} vs. M_e

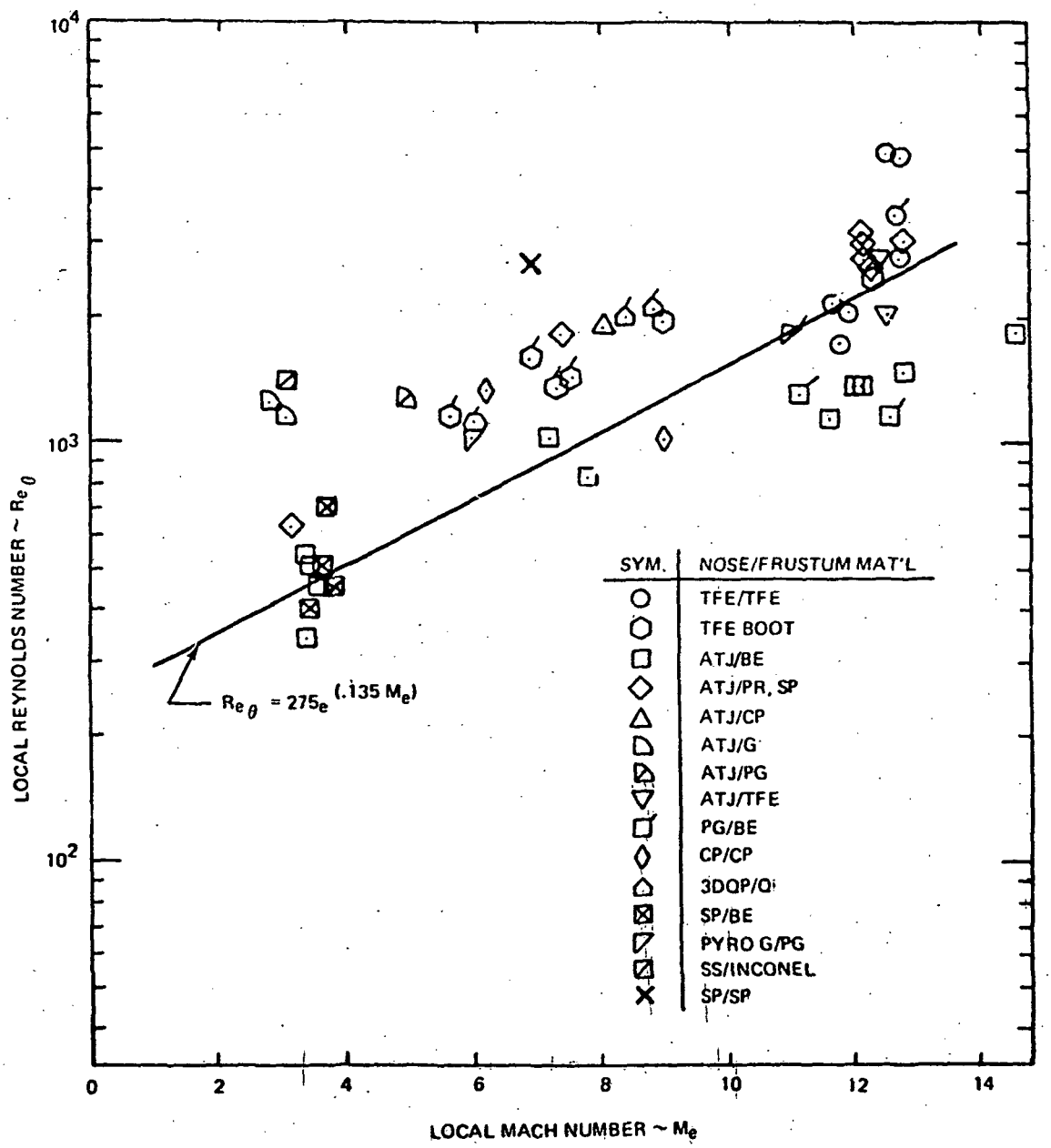

Figure 16. Flight Data Correlation Using Frustum Parameters (Re_θ vs M_e)

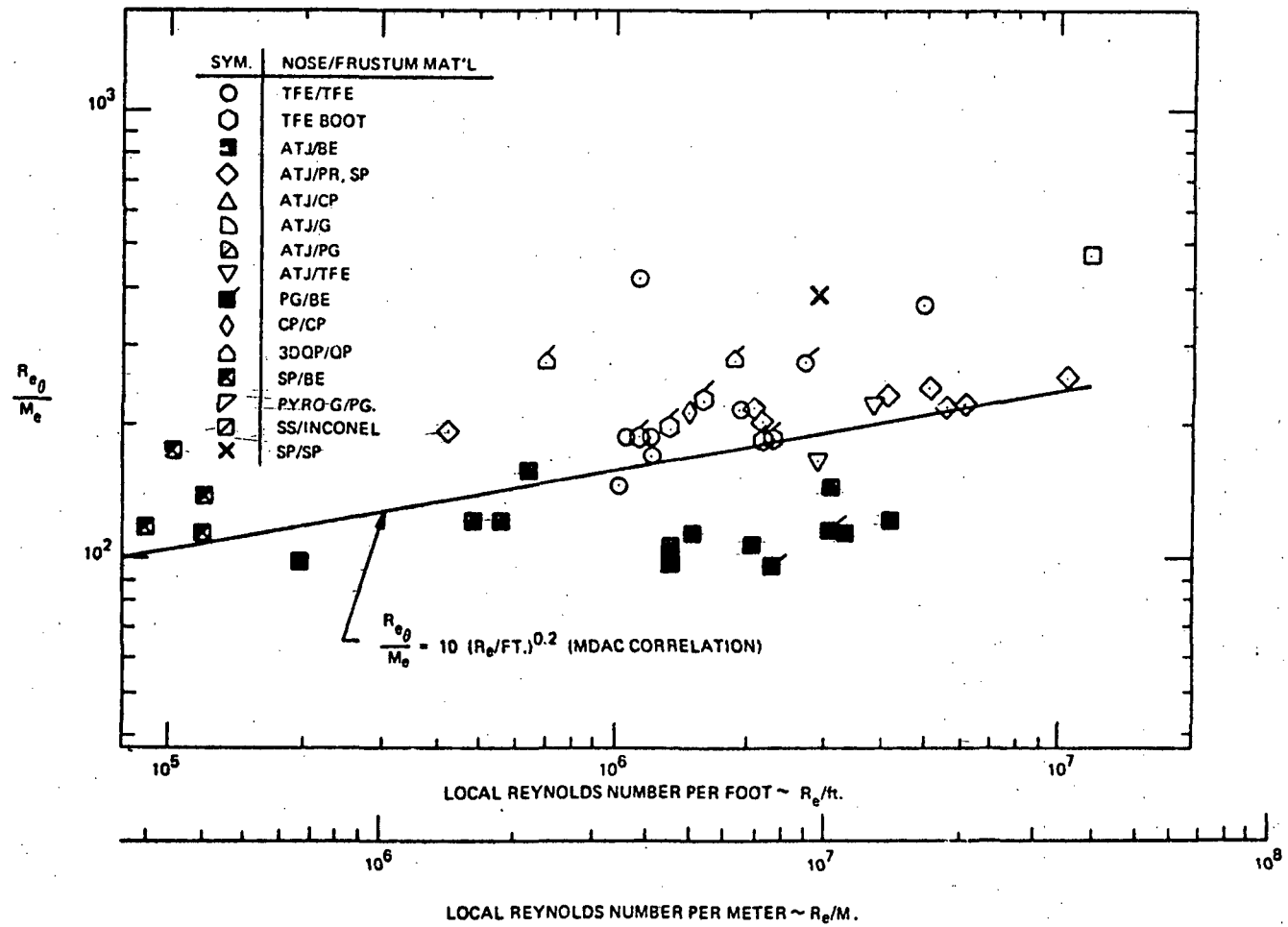

Figure 17. Effect of Unit Reynolds Number on Flight Vehicle Transition

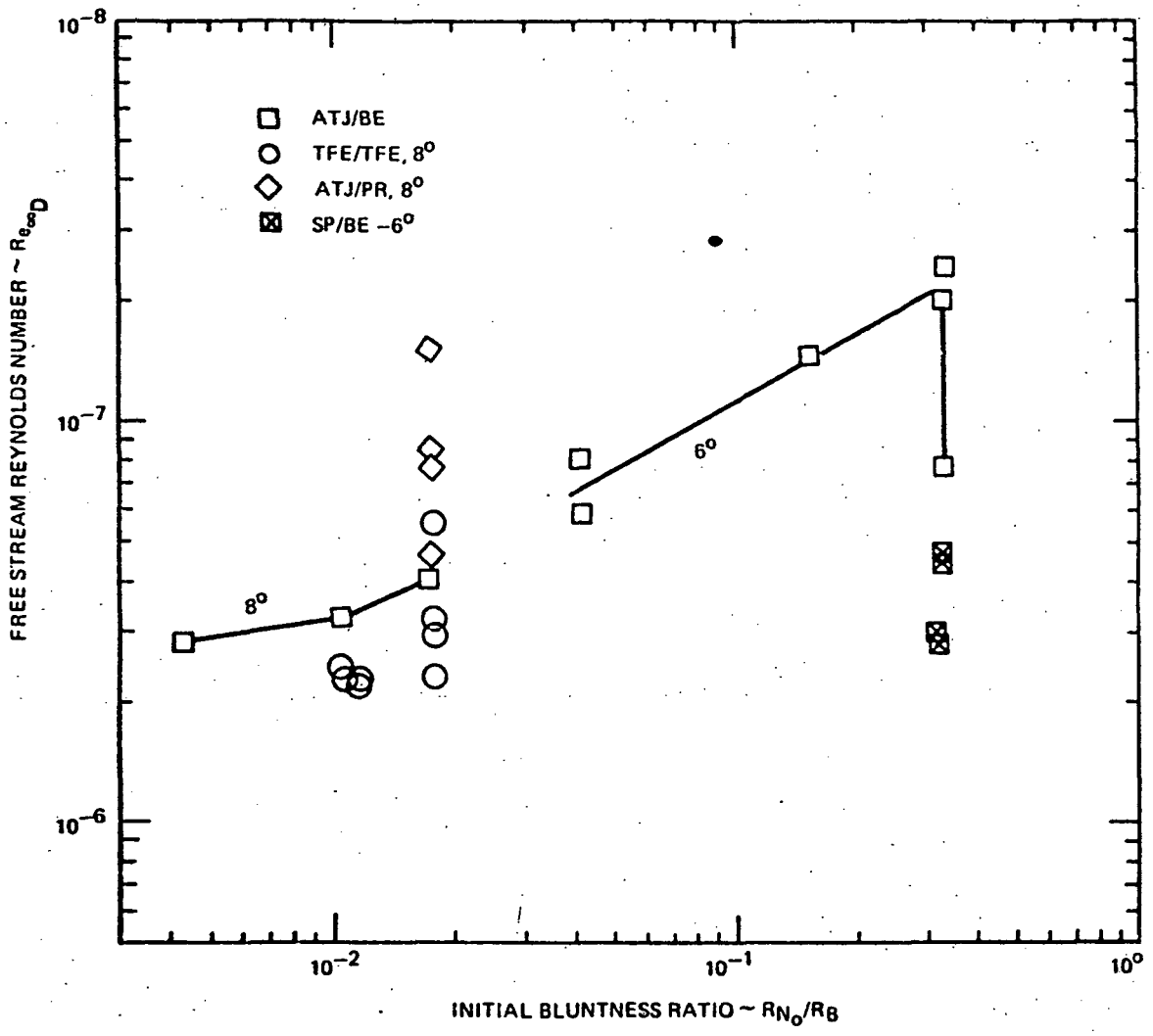

Figure 18. Summary Type Correlation; $R_{e_{\infty D}}$ vs. R_{N_0}/R_B

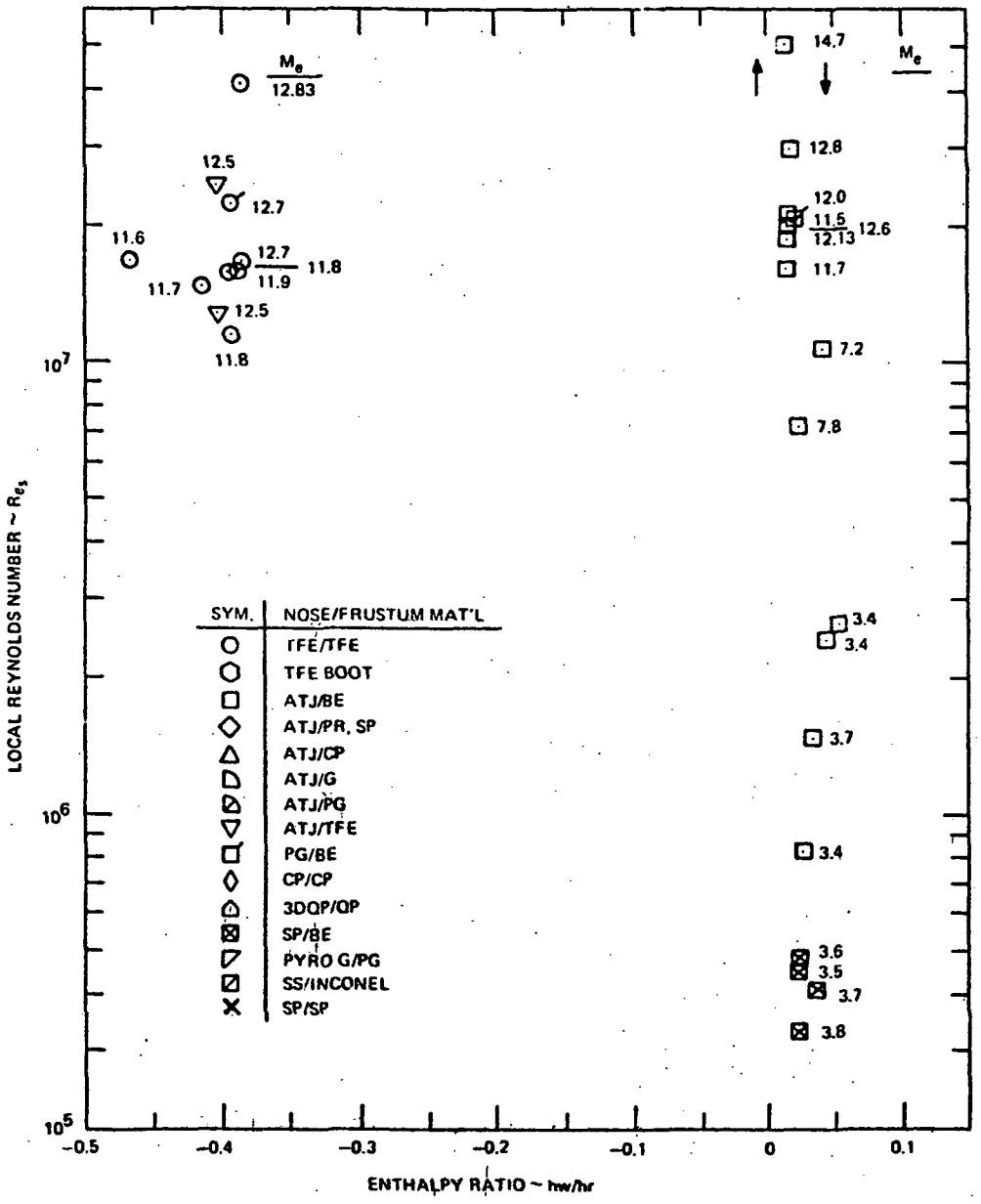

Figure 19. Flight Data Using Wall Gas Enthalpy Correlation Parameters

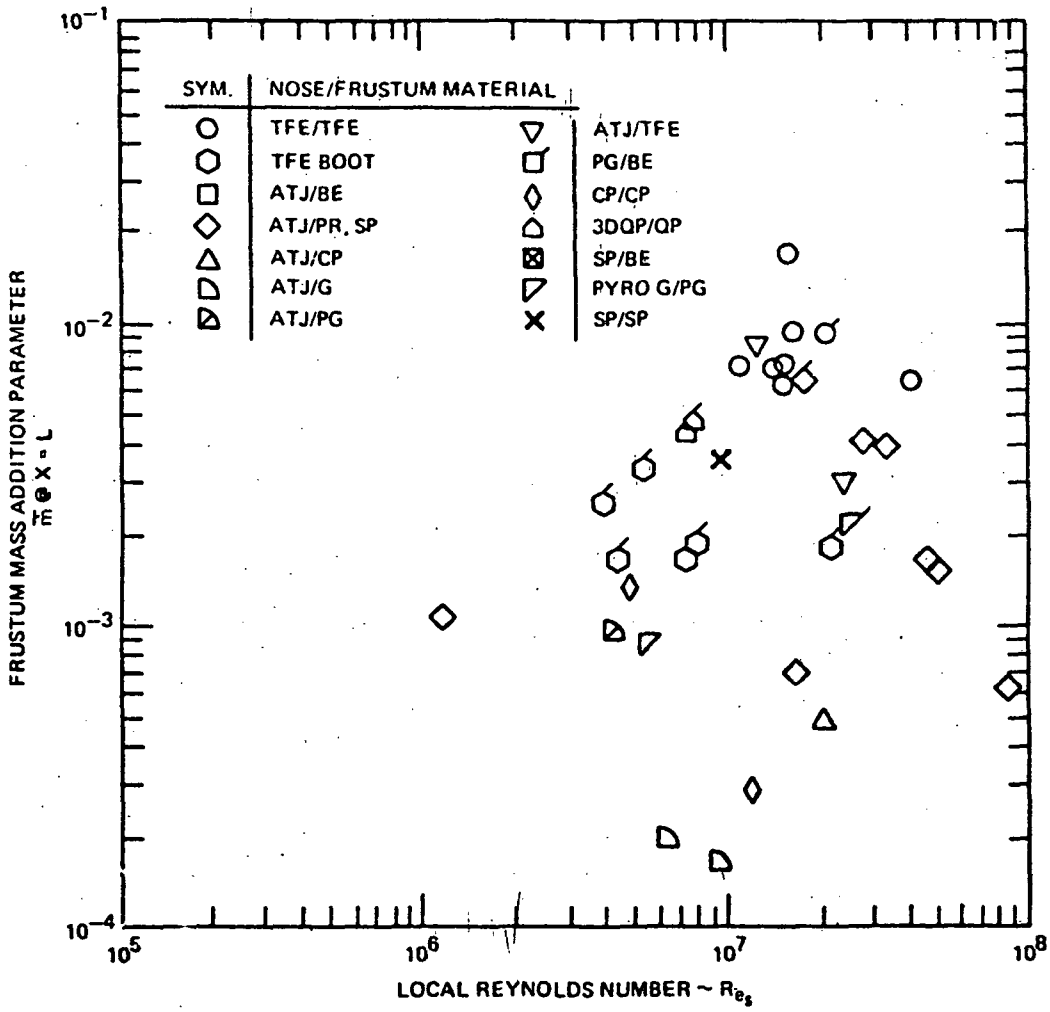

Figure 20. Flight Data Correlation Using Frustum Parameters; $\bar{m}_L$ vs. R_{e_s}

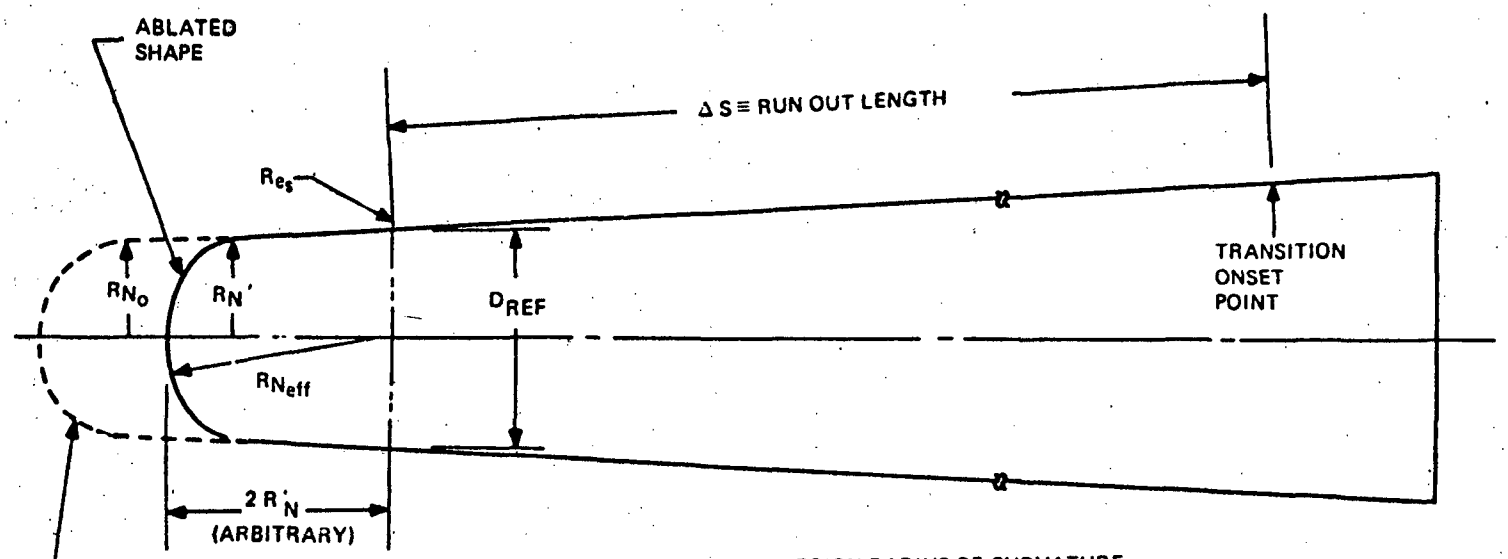

- $R_{N_{eff}}$ – STAGNATION REGION RADIUS OF CURVATURE
- $\int_{A_s} (\rho v)_w \, dA_s$ REPRESENTS THE MASS LOSS ON A $2 R_N'$ SEGMENT OF THE ABLATED NOSE
- $\bar{\dot{m}} \equiv \dfrac{\int (\rho v)_w \, dA_s}{(\rho u)_\infty \, A_{REF}}$

Figure 21. Definition of Terminology

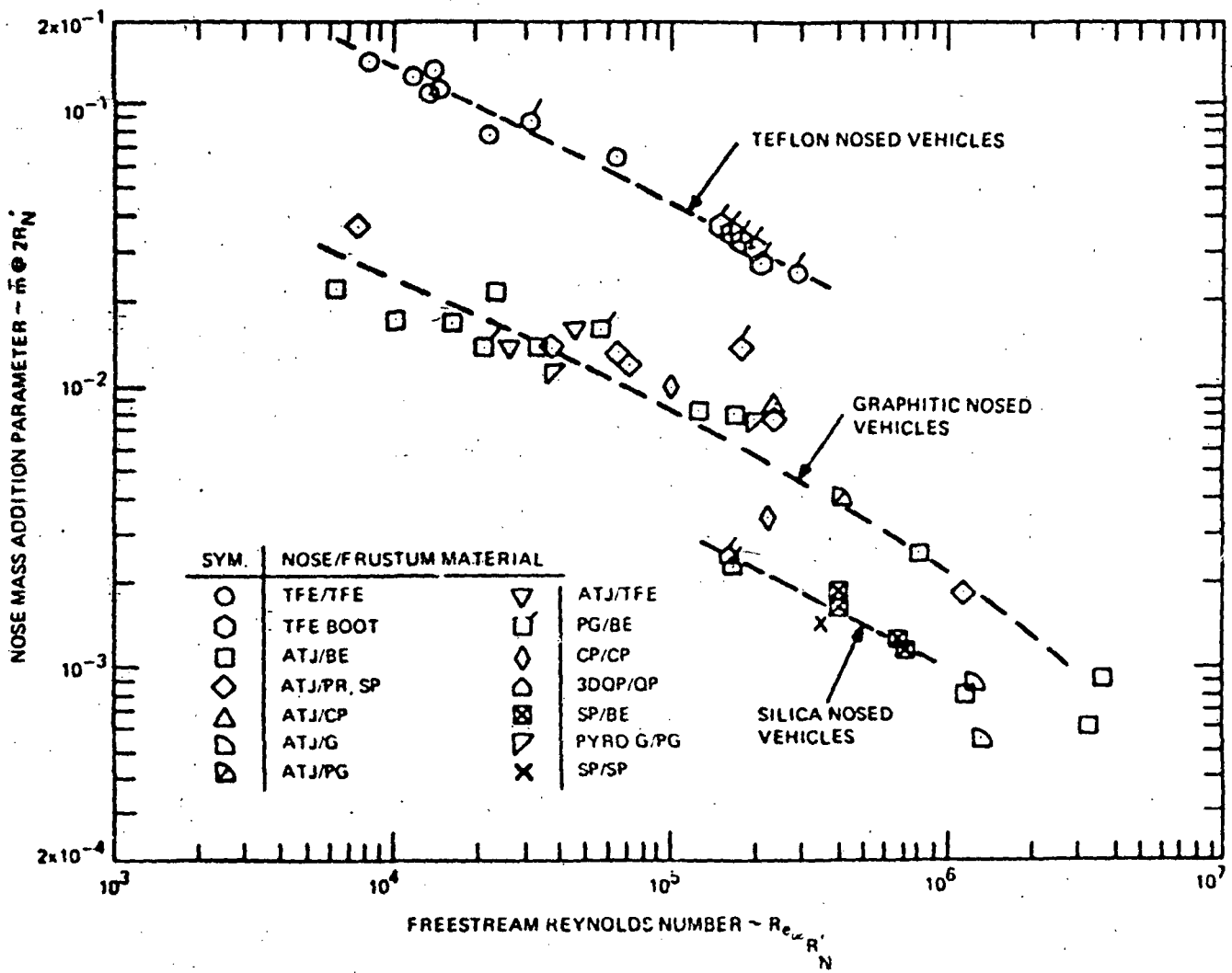

Figure 22. Flight Data Correlation Using Nose Parameters $\bar{m}_{2R_N'}$ vs. $R_{e_\infty R_N'}$

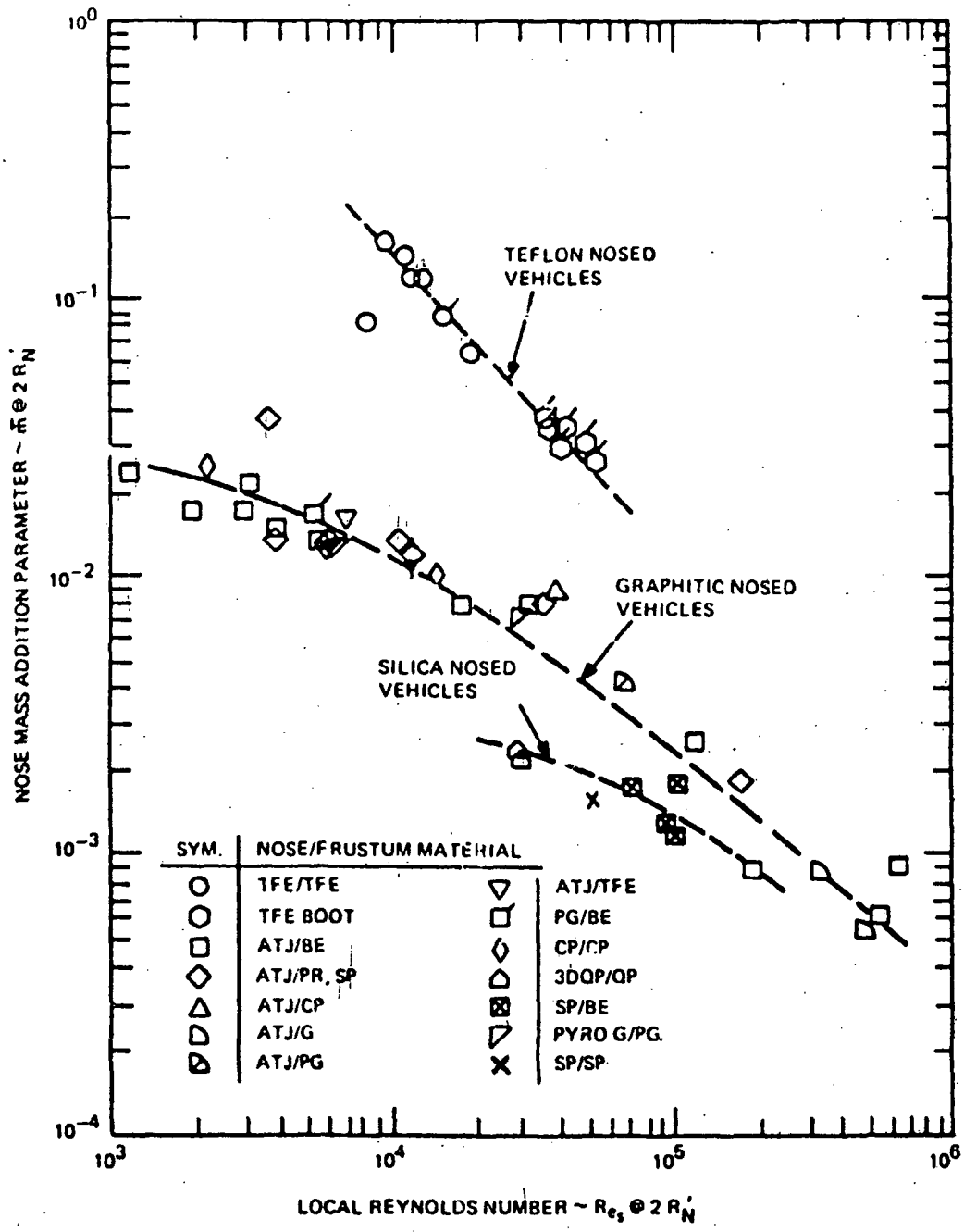

Figure 25. Flight Data Correlation Using Nose Parameters - $\bar{m}$ vs. R_{e_s} @ $2R_{N'}$

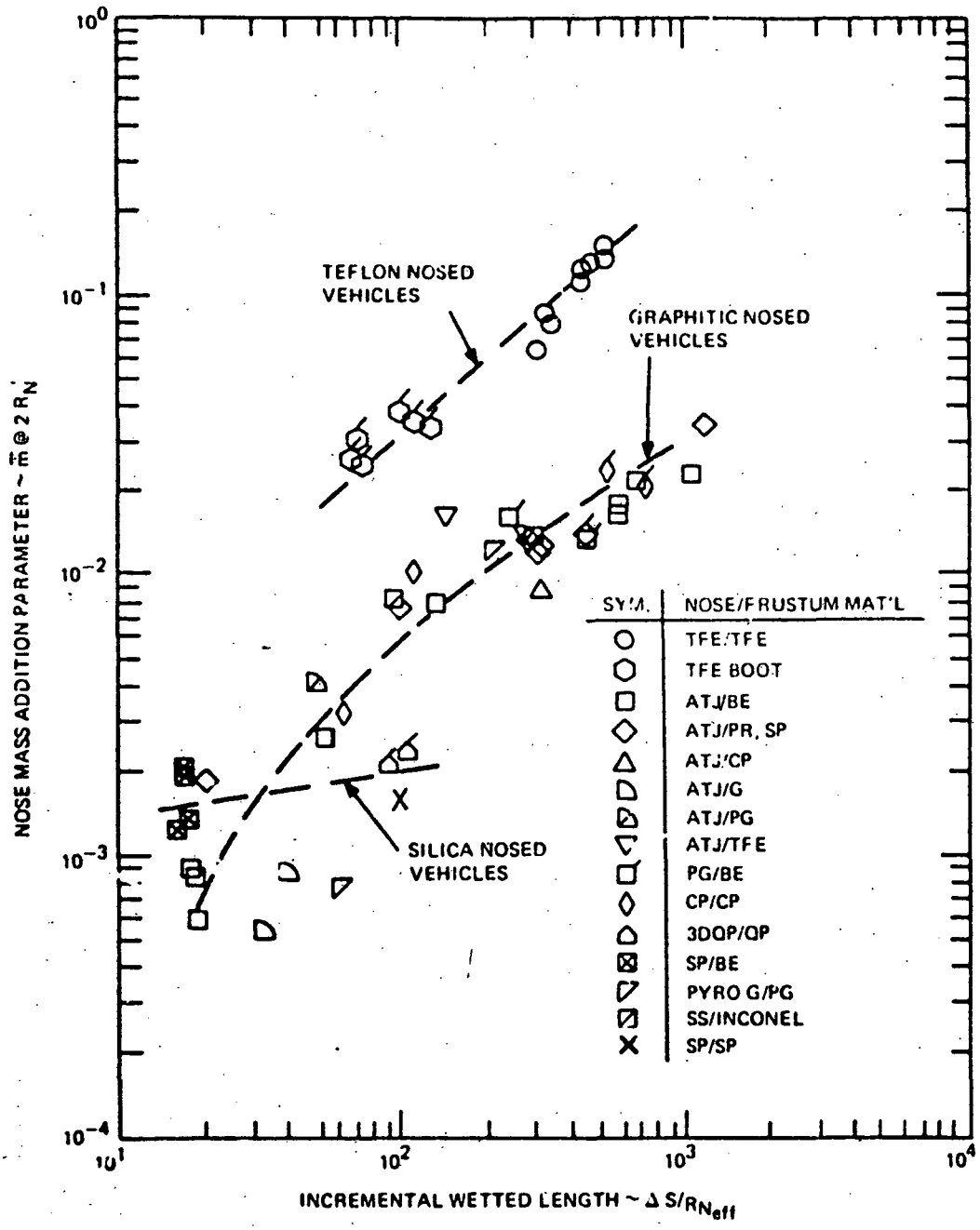

Figure 24. Flight Data Correlation Using Nose Parameters $\sim\bar{\dot{m}}_{2R_N}$, vs. $\Delta S/R_{N_{eff}}$

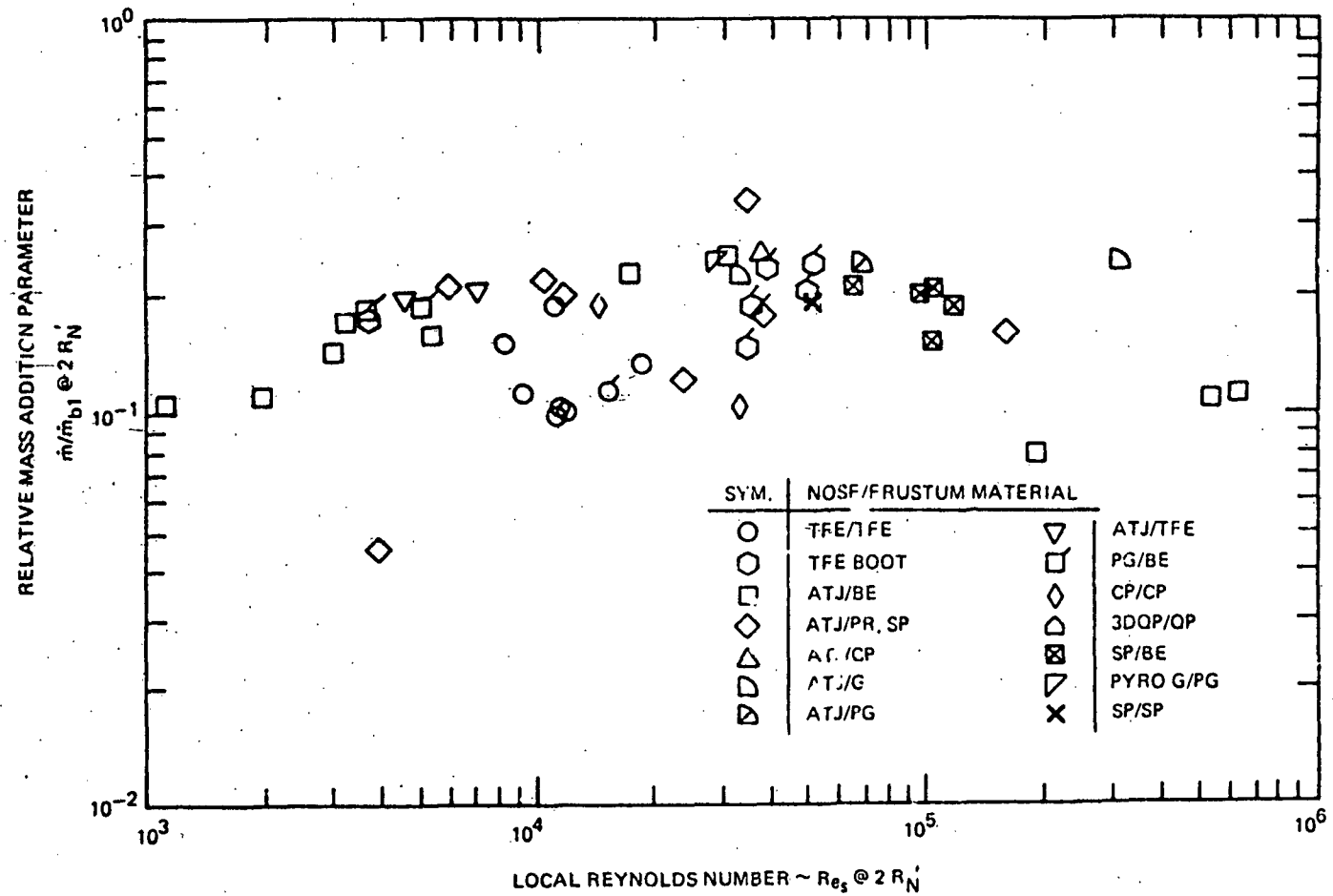

Figure 25. Flight Data Correlation Using Nose Parameters ~ $\dot{m}/\dot{m}_{b1}$ vs. $Re_{s_{2R_N'}}$

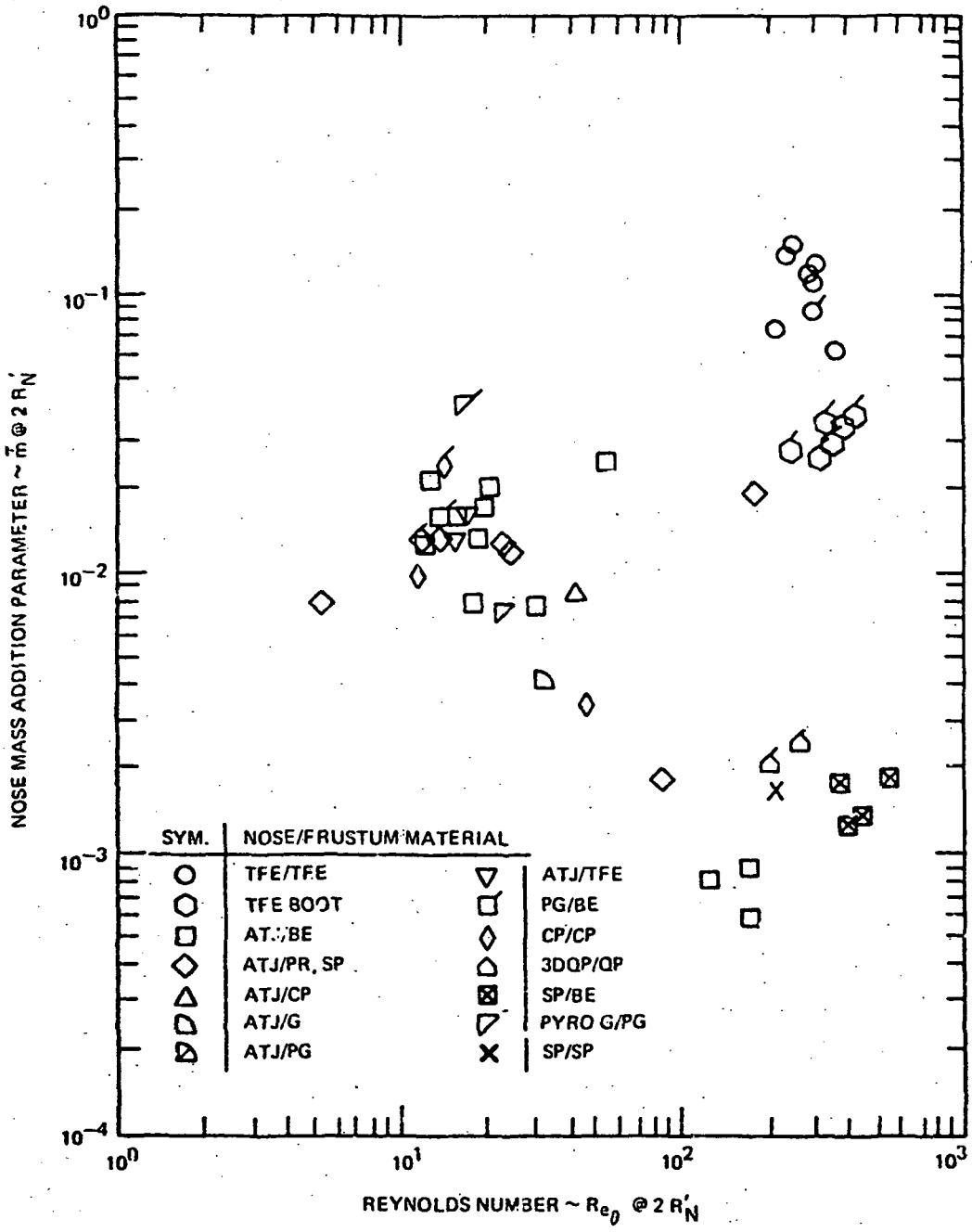

Figure 26. Flight Data Correlation Using Nose Parameters ~ $\bar{\dot{m}}$ vs. R_{e_θ} @ $2R_{N'}$

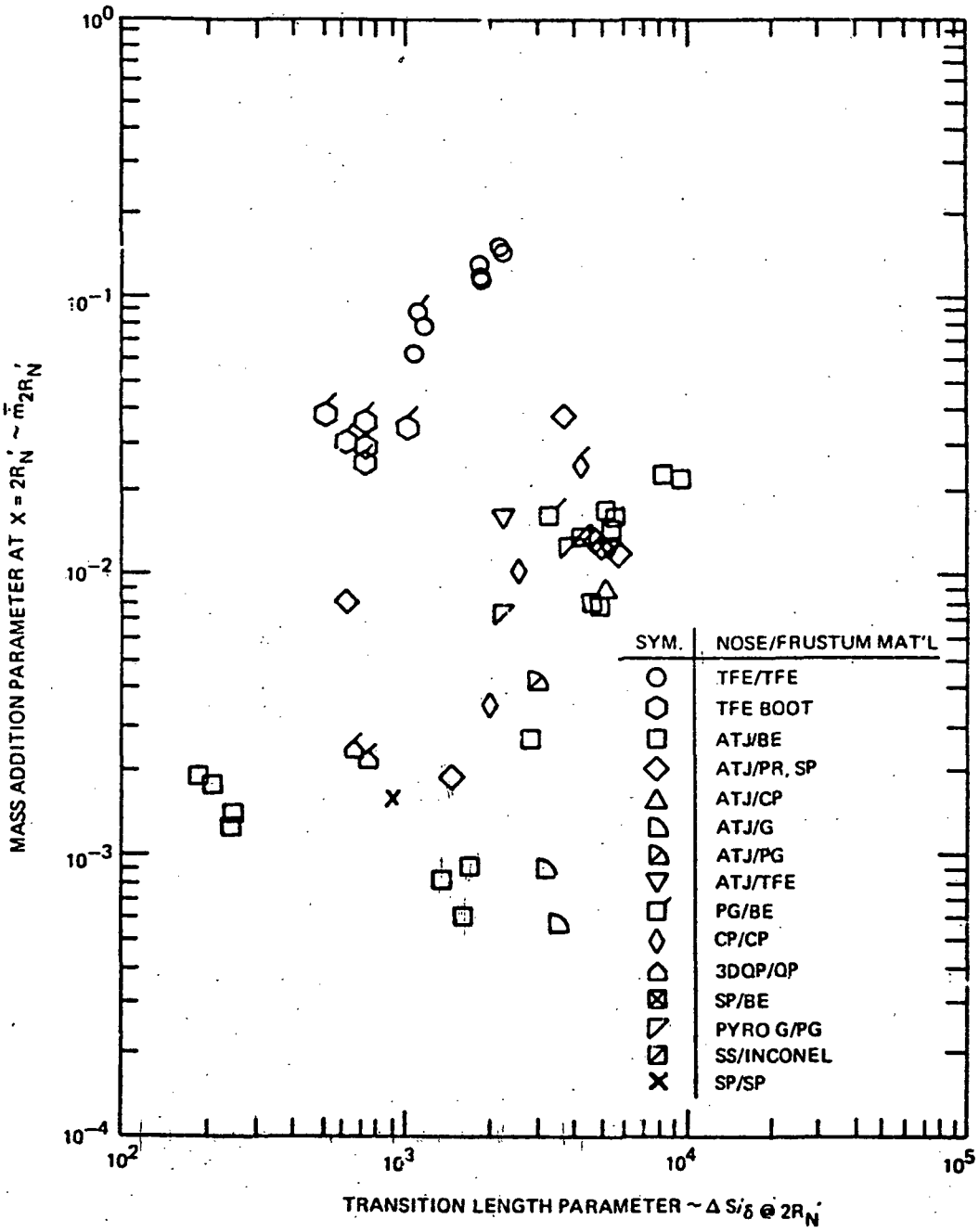

Figure 27. Flight Data Correlation Using Nose Parameters $\sim \dot{m}_{2R_{N'}}$ vs. $\Delta S/_{\delta\ 2R_{N'}}$

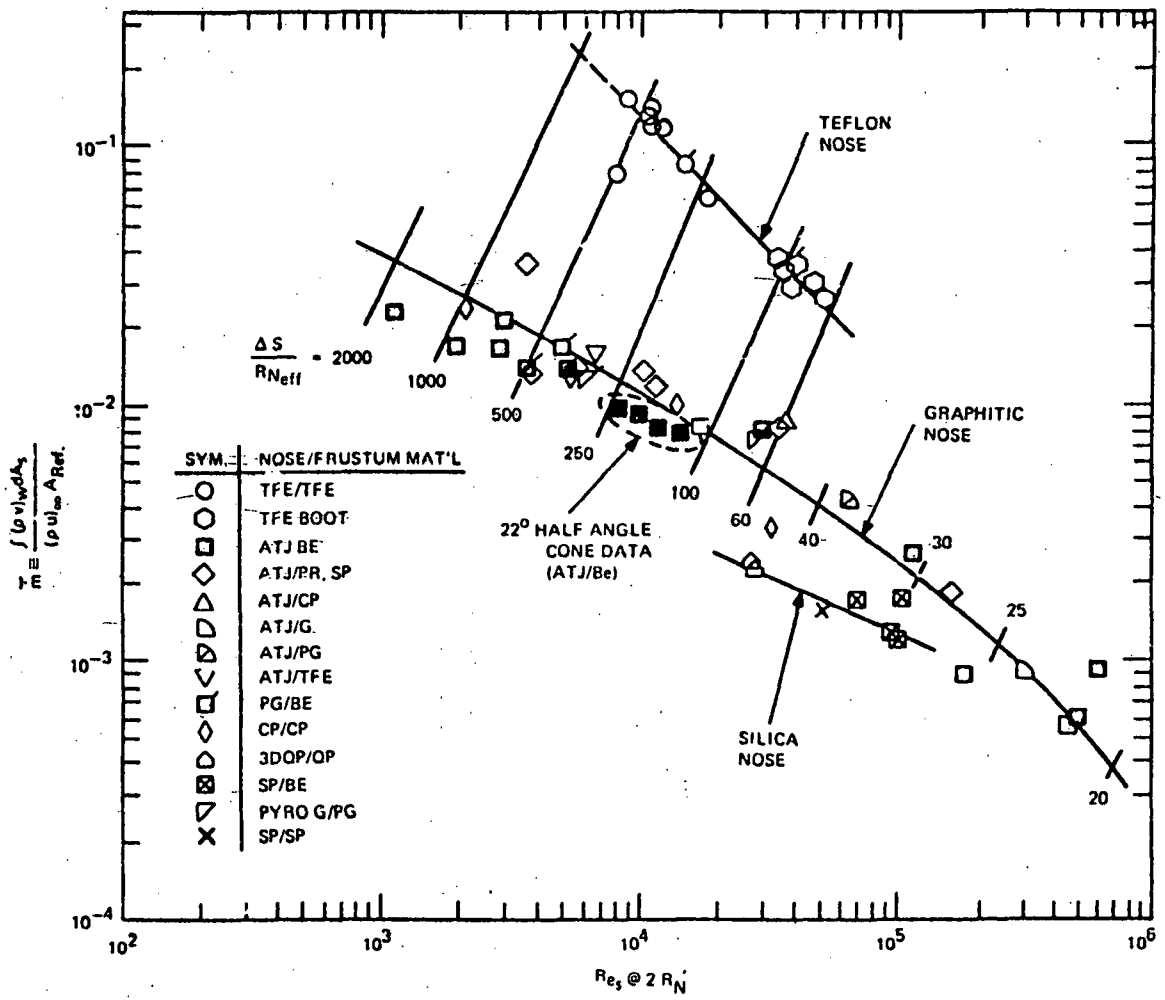

Figure 28. Effect of Nose Ablation on Flight Vehicle Transition

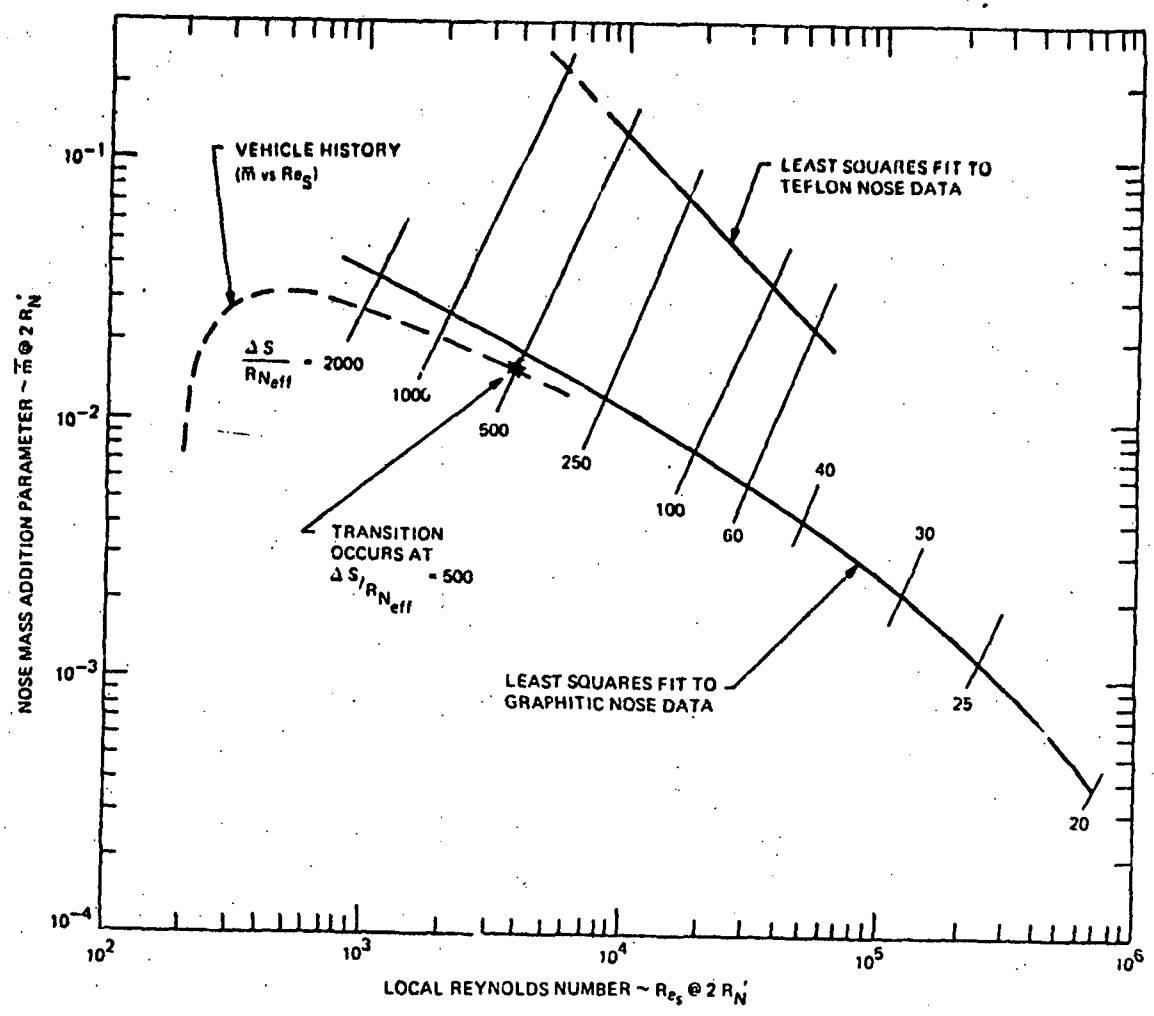

Figure 29. Typical Vehicle History of $\bar{m}$ vs. R_{e_s} @ $2R_{N'}$

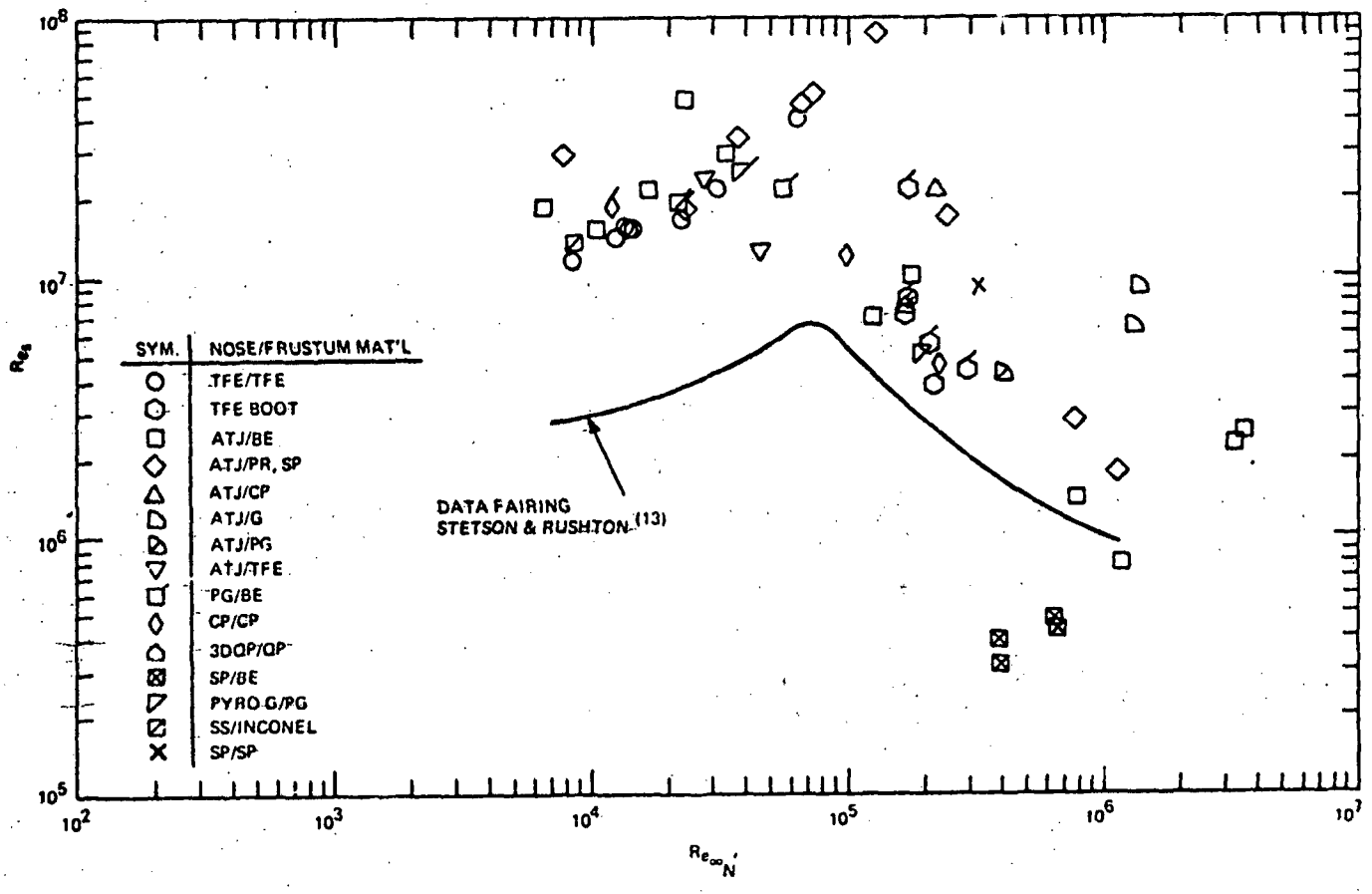

Figure 30. "Flight Transition Data" - Bluntness Effect

END

DATE

FILMED

FEB 2 1973

1. Report No.	2. Government Accession No.	3. Recipient's Catalog No.
NASA CR 129045		

4. Title and Subtitle	5. Report Date
Analysis of Flight Test Transition and Turbulent Heating Data Part I - Boundary Layer Transition Results	November 1972
	6. Performing Organization Code
7. Author(s) Anthony Martellucci Bernadette L. Maguire Robert S. Neff	8. Performing Organization Report No. GE TIS 72SD253
	10. Work Unit No.
9. Performing Organization Name and Address General Electric Co. Reentry and Environmental Systems Division Philadelphia, Pa. 19101	11. Contract or Grant No. NAS W-2234
	13. Type of Report and Period Covered
12. Sponsoring Agency Name and Address National Aeronautics and Space Administration Washington, D.C. 20546	14. Sponsoring Agency Code

15. Supplementary Notes

16. Abstract

The objective of the study documented in this report was to provide a detailed post flight evaluation of ballistic vehicle flight test boundary layer transition data. A total of fifty-five vehicles were selected for analysis. These vehicles were chosen from a data sampling of roughly two hundred flights and the criteria for vehicle selection is delineated herein. The results of the analysis indicate that frustum transition of re-entry vehicles appears to be nose tip dominated. Frustum related parameters and materials apparently have a second order effect on transition. This implies that local viscous parameters on the frustum should not correlate flight test transition data, and in fact they do not. Specific parameters relative to the nose tip have been identified as the apparent dominant factors that characterize the transition phenomena and a correlation of flight test data is presented.

17. Key Words (Suggested by Author(s))	18. Distribution Statement
Boundary Layer Transition Data Flight Test Boundary Layer Transition Correlations Cone Flight Reentry	UNCLASSIFIED - UNLIMITED

19. Security Classif. (of this report)	20. Security Classif. (of this page)	21. No. of Pages	22. Price*
UNCLASSIFIED	UNCLASSIFIED	82	

*For sale by the National Technical Information Service, Springfield, Virginia 22151